Bayesian Compressive Sampling applied to Microwave Imaging under the first Born Approximation as compared to Deterministic and Stocastic Techniques

L. Poli, G. Oliveri, A. Massa

Abstract

This report proposes a comparison of a Bayesian Compressive Sampling strategy applied to solve the inverse scattering problem under the first Born approximation, with deterministic (conjugate gradient method) and stocastic (genetic algorithms) approaches. The reconstruction errors has been evaluated and compared for different values of the dielectric permittivity.

Contents

1 TEST CASE: Square Cylinder $side = 0.16\lambda$

Goal: compare the performances of BCS, GA and CG

- Number of Views: V
- Number of Measurements: M
- Number of Cells for the Inversion: N
- Number of Cells for the Direct solver: D
- Side of the investigation domain: L

Test Case Description

Direct solver:

- Square domain divided in $\sqrt{D} \times \sqrt{D}$ cells
- Domain side: $L = 3\lambda$
- $D = 1296$ (discretization for the direct solver: $< \lambda/10$)

Investigation domain:

- Square domain divided in $\sqrt{N} \times \sqrt{N}$ cells
- $L = 3\lambda$
- $2ka = 2 \times \frac{2\pi}{\lambda} \times \frac{L\sqrt{2}}{2} = 6\pi\sqrt{2} = 26.65$
- $\#DOF = \frac{(2ka)^2}{2} = \frac{(2 \times \frac{2\pi}{\lambda} \times \frac{L\sqrt{2}}{2})^2}{2} = 4\pi^2 \left(\frac{L}{\lambda}\right)^2 = 4\pi^2 \times 9 \approx 355.3$
- N scelto in modo da essere vicino a $\#DOF$: $N = 324$ (18×18)

Measurement domain:

- Measurement points taken on a circle of radius $\rho = 3\lambda$
- Full-aspect measurements
- $M \approx 2ka \rightarrow M = 27$

Sources:

- Plane waves
- $V \approx 2ka \rightarrow V = 27$
- Amplitude $A = 1$
- Frequency: 300 MHz ($\lambda = 1$)

Object:

- Square cylinder of side $\frac{\lambda}{6} = 0.1667$
- $\varepsilon_r \in \{1.5, 2.0, 2.5, 3.0\}$
- $\sigma = 0$ [S/m]

BCS parameters:

- Initial estimate of the noise: $n_0 = 1.0 \times 10^{-3}$
- Convergenze parameter: $\tau = 1.0 \times 10^{-8}$

CG parameters:

- Iterations: 200
- Peso stato: 0
- Peso dati: 1

GA parameters:

- Iterations: 10000
- Tournament Selection: $TRUE$
- Prob. Crossover: 0.8
- Prob. Mutation: 0.4
- Prob. Bit Muation: 0.05
- Prob. New Generation: 0.01
- Elitism: $TRUE$
- Crossover Child: 1
- Population: 200
- Convergence Threshold: 0.001

RESULTS: $\varepsilon_r = 1.5$

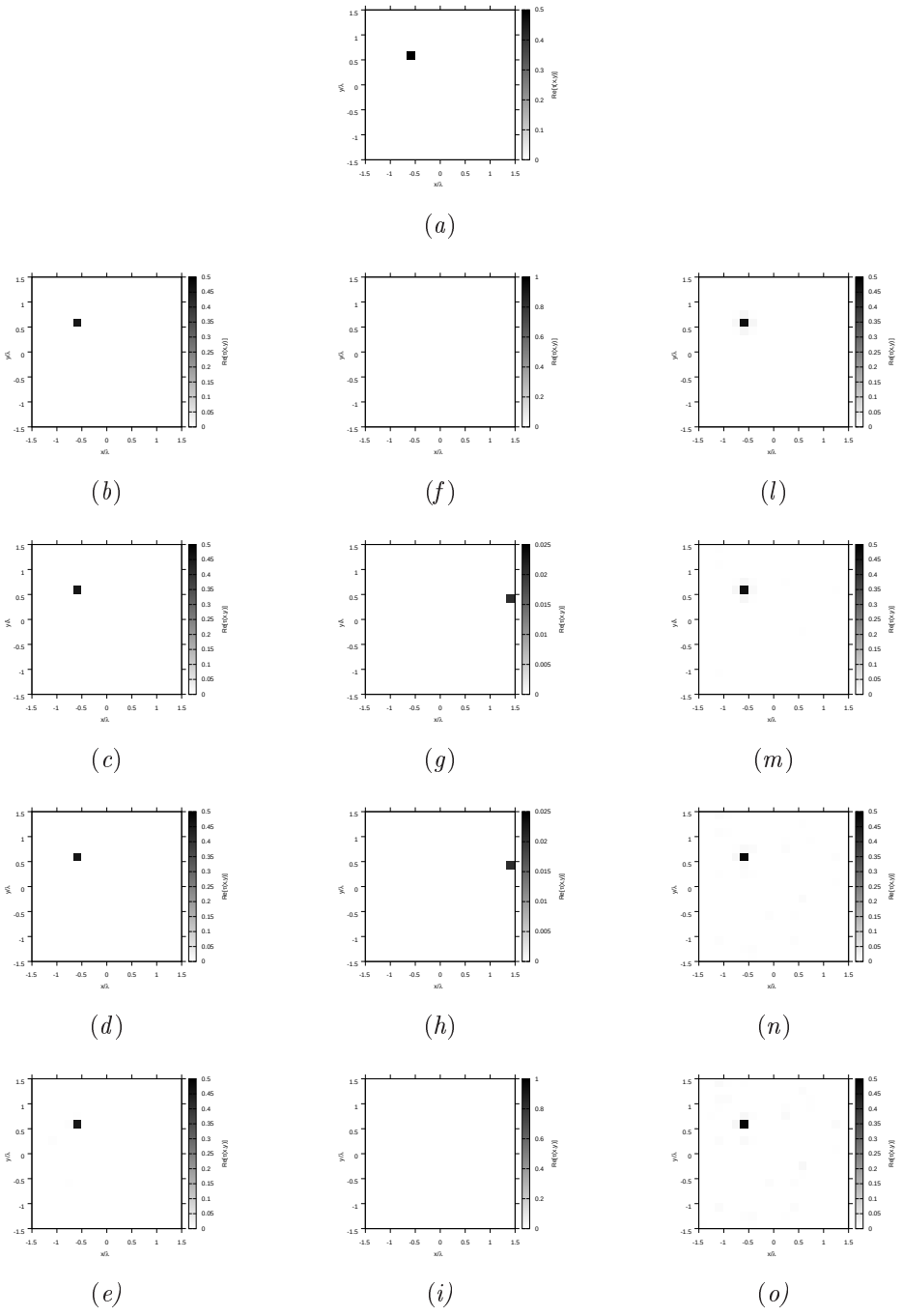

Figure 67. Actual object (a), (b)-(e) BCS reconstructed $(g)(i)$ GA-reconstructed, and (l)-(o) CG reconstructed object for $(b)(f)(l)$ Noiseless case, $(c)(g)(m)$ $SNR = 20$ [dB] , $(d)(h)(n)$ $SNR = 10$ [dB] , $(e)(i)(o)$ $SNR = 5$ [dB].

RESULTS: $\varepsilon_r = 1.5$

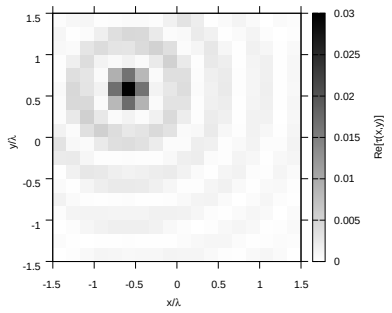

Figure 68. Actual object - Born approximation SVD-based approach reconstructed (Noiseless case)

SNR	Noiseless				20 [dB]			
	BCS	GA	CG	SVD	BCS	GA	CG	SVD
ξ_{tot}	1.55×10^{-4}	1.03×10^{-3}	3.18×10^{-4}	2.56×10^{-3}	1.55×10^{-4}	1.09×10^{-3}	3.57×10^{-4}	–
ξ_{int}	2.96×10^{-2}	0.3333	1.99×10^{-2}	0.3134	2.92×10^{-2}	0.3333	1.78×10^{-2}	–
ξ_{ext}	0.0000	0.0000	2.57×10^{-4}	1.60×10^{-3}	0.0000	6.39×10^{-5}	3.03×10^{-4}	–

SNR	10 [dB]				5 [dB]			
	BCS	GA	CG	SVD	BCS	GA	CG	SVD
ξ_{tot}	1.58×10^{-4}	1.09×10^{-3}	4.39×10^{-4}	–	2.42×10^{-4}	1.03×10^{-3}	6.10×10^{-4}	–
ξ_{int}	2.86×10^{-2}	0.3333	8.68×10^{-3}	–	3.12×10^{-2}	0.3333	7.13×10^{-3}	–
ξ_{ext}	4.38×10^{-6}	6.39×10^{-5}	4.14×10^{-4}	–	6.73×10^{-5}	0.0000	5.90×10^{-4}	–

Table I. Comparison of error figures for BCS, GA, CG and SVD-based approach.

Observations

- Le prestazioni del BCS sono sempre migliori rispetto a GA e CG.

RESULTS: $\varepsilon_r = 2.0$

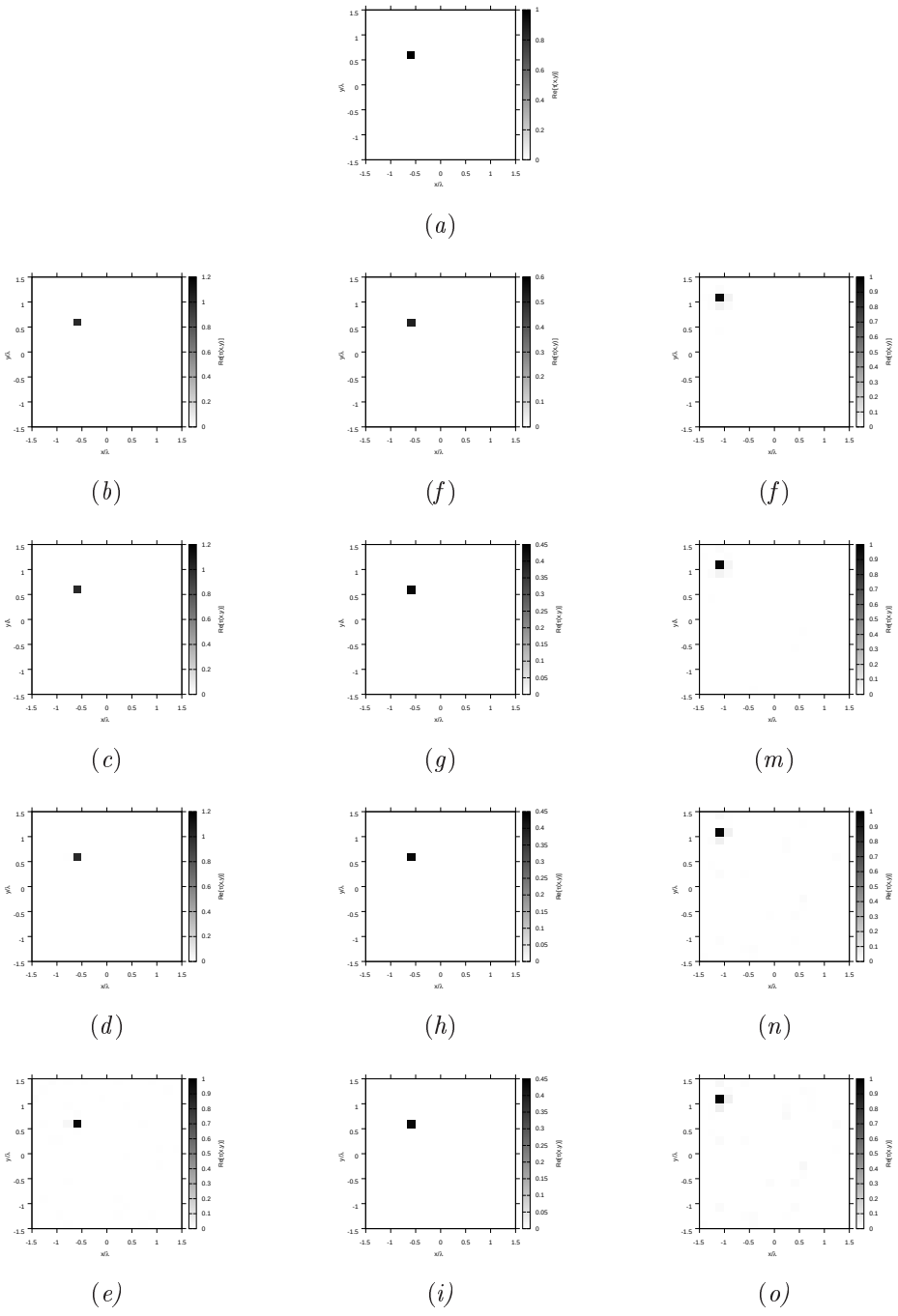

Figure 69. Actual object (a), (b)-(e) BCS reconstructed $(g)(i)$ GA-reconstructed, and (l)-(o) CG reconstructed object for $(b)(f)(l)$ Noiseless case, $(c)(g)(m)$ $SNR = 20$ [dB] , $(d)(h)(n)$ $SNR = 10$ [dB] , $(e)(i)(o)$ $SNR = 5$ [dB].

RESULTS: $\varepsilon_r = 2.0$

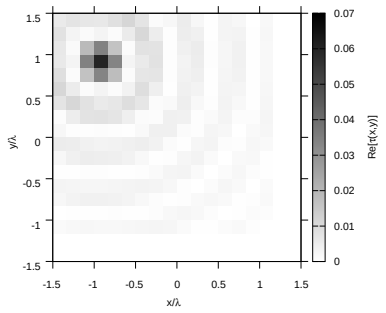

Figure 70. Actual object - Born approximation SVD-based approach reconstructed (Noiseless case)

SNR	Noiseless				20 [dB]			
	BCS	GA	CG	SVD	BCS	GA	CG	SVD
ξ_{tot}	4.73×10^{-4}	7.29×10^{-4}	6.31×10^{-4}	4.84×10^{-3}	4.81×10^{-4}	8.68×10^{-4}	6.51×10^{-4}	–
ξ_{int}	4.50×10^{-3}	0.2361	2.05×10^{-2}	0.4697	4.93×10^{-3}	0.2811	1.14×10^{-2}	–
ξ_{ext}	0.0000	0.0000	5.69×10^{-4}	3.26×10^{-3}	4.02×10^{-6}	0.0000	6.17×10^{-4}	–

SNR	10 [dB]				5 [dB]			
	BCS	GA	CG	SVD	BCS	GA	CG	SVD
ξ_{tot}	6.97×10^{-4}	8.68×10^{-4}	9.78×10^{-4}	–	2.47×10^{-3}	8.68×10^{-4}	1.34×10^{-3}	–
ξ_{int}	2.64×10^{-3}	0.2811	1.10×10^{-2}	–	1.52×10^{-2}	0.2811	6.54×10^{-3}	–
ξ_{ext}	1.52×10^{-4}	0.0000	9.47×10^{-4}	–	1.31×10^{-3}	3.25×10^{-5}	1.32×10^{-3}	–

Table II. Comparison of error figures for BCS, GA, CG and SVD-based approach.

Observations

- Le prestazioni del BCS sono in generale migliori rispetto a GA e CG. Nel caso $SNR = 5\,dB$ l'errore totale risulta però inferiore per GA e CG rispetto a BCS, questo perché la ricostruzione è più pulita con rumore esterno più basso: l'errore interno è però sempre di gran lunga inferiore per BCS rispetto a GA.

RESULTS: $\varepsilon_r = 2.5$

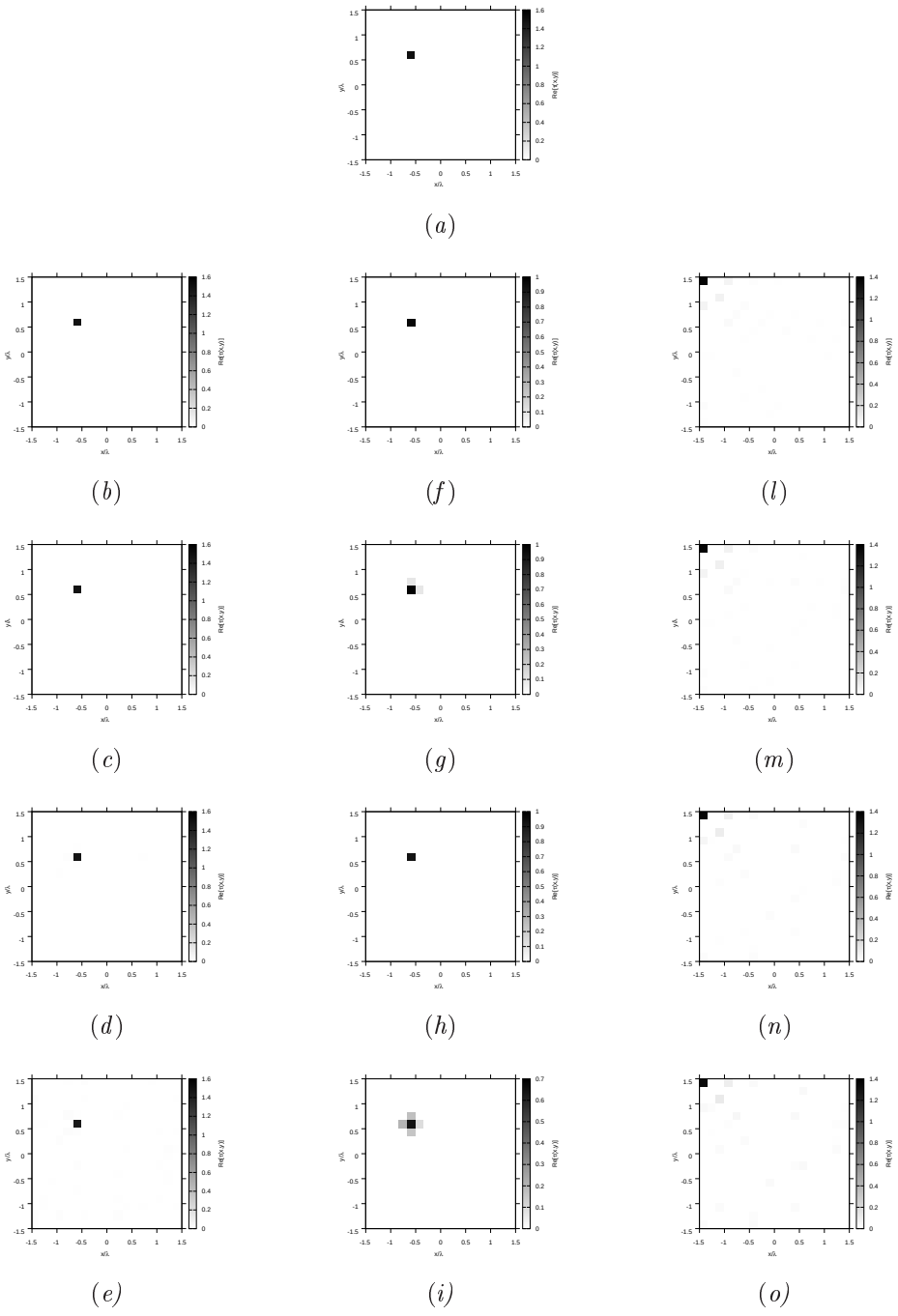

Figure 71. Actual object (a), (b)-(e) BCS reconstructed $(g)(i)$ GA-reconstructed, and (l)-(o) CG reconstructed object for $(b)(f)(l)$ Noiseless case, $(c)(g)(m)$ $SNR = 20$ [dB] , $(d)(h)(n)$ $SNR = 10$ [dB] , $(e)(i)(o)$ $SNR = 5$ [dB].

RESULTS: $\varepsilon_r = 2.5$

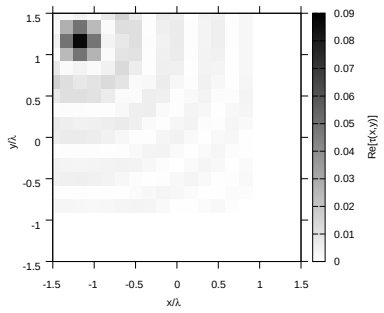

Figure 72. Actual object - Born approximation SVD-based approach reconstructed (Noiseless case)

SNR	Noiseless				20 [dB]			
	BCS	GA	CG	SVD	BCS	GA	CG	SVD
ξ_{tot}	8.83×10^{-4}	6.50×10^{-4}	3.74×10^{-3}	6.94×10^{-3}	9.18×10^{-4}	1.21×10^{-3}	3.75×10^{-3}	–
ξ_{int}	6.38×10^{-3}	0.2106	4.96×10^{-2}	0.5650	5.10×10^{-3}	0.2025	5.15×10^{-2}	–
ξ_{ext}	5.17×10^{-6}	0.0000	3.67×10^{-3}	4.72×10^{-3}	3.23×10^{-5}	5.91×10^{-4}	3.67×10^{-3}	–

SNR	10 [dB]				5 [dB]			
	BCS	GA	CG	SVD	BCS	GA	CG	SVD
ξ_{tot}	2.31×10^{-3}	7.09×10^{-4}	3.97×10^{-3}	–	5.55×10^{-3}	2.99×10^{-3}	4.43×10^{-3}	–
ξ_{int}	1.06×10^{-2}	0.2297	5.56×10^{-2}	–	2.30×10^{-2}	0.3401	6.09×10^{-2}	–
ξ_{ext}	9.27×10^{-4}	0.0000	3.89×10^{-3}	–	2.99×10^{-3}	1.95×10^{-3}	4.34×10^{-3}	–

Table III. Comparison of error figures for BCS, GA, CG and SVD-based approach.

Observations

- Le ricostruzioni ottenute mediante GA risultano in generale più pulite con errore esterno più basso; l'errore interno è però sempre di gran lunga inferiore per le ricostruzioni ottenute mediante BCS rispetto alle ricostruzioni con GA.

RESULTS: $\varepsilon_r = 3.0$

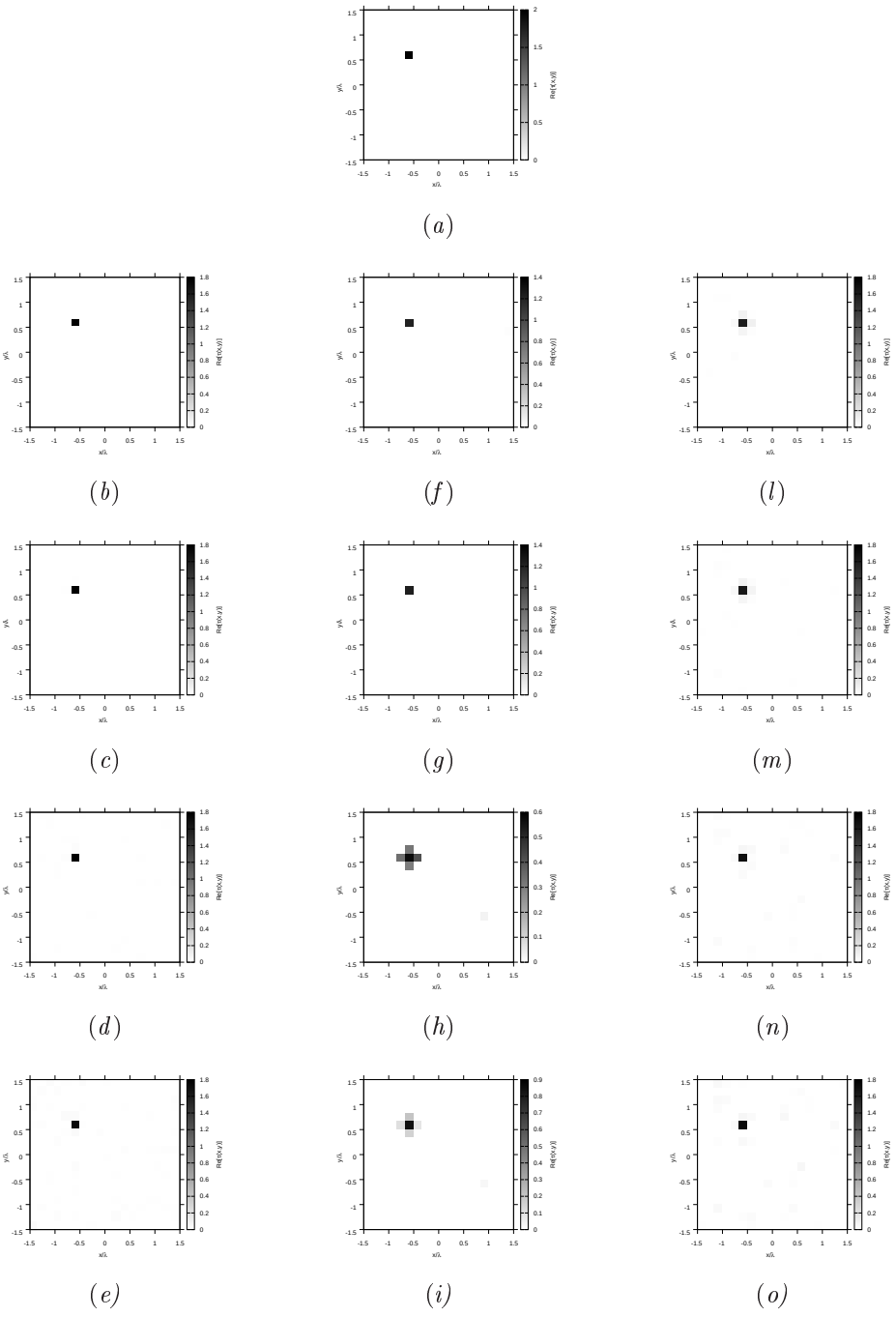

Figure 73. Actual object (a), (b)-(e) BCS reconstructed $(g)(i)$ GA-reconstructed, and (l)-(o) CG reconstructed object for $(b)(f)(l)$ Noiseless case, $(c)(g)(m)$ $SNR = 20$ [dB] , $(d)(h)(n)$ $SNR = 10$ [dB] , $(e)(i)(o)$ $SNR = 5$ [dB].

RESULTS: $\varepsilon_r = 3.0$

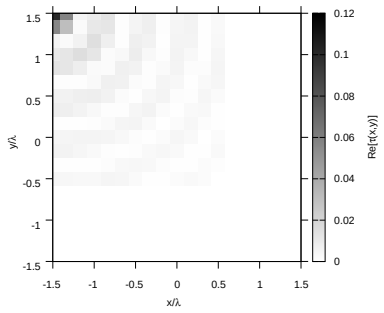

Figure 74. Actual object - Born approximation SVD-based approach reconstructed (Noiseless case)

SNR	Noiseless				20 [dB]			
	BCS	GA	CG	SVD	BCS	GA	CG	SVD
ξ_{tot}	1.35×10^{-3}	8.42×10^{-4}	1.85×10^{-3}	8.85×10^{-3}	1.40×10^{-3}	7.86×10^{-4}	1.91×10^{-3}	–
ξ_{int}	7.13×10^{-2}	0.2613	0.1317	0.6316	7.01×10^{-2}	0.2548	0.1258	–
ξ_{ext}	1.72×10^{-5}	3.61×10^{-5}	1.45×10^{-3}	5.75×10^{-3}	6.26×10^{-5}	0.0000	1.52×10^{-3}	–

SNR	10 [dB]				5 [dB]			
	BCS	GA	CG	SVD	BCS	GA	CG	SVD
ξ_{tot}	4.06×10^{-3}	5.82×10^{-3}	2.14×10^{-3}	–	9.07×10^{-3}	3.05×10^{-3}	2.79×10^{-3}	–
ξ_{int}	7.16×10^{-2}	0.4756	0.1001	–	9.06×10^{-2}	0.3849	9.18×10^{-2}	–
ξ_{ext}	1.82×10^{-3}	4.36×10^{-3}	1.84×10^{-3}	–	4.96×10^{-3}	1.87×10^{-3}	2.52×10^{-3}	–

Table IV. Comparison of error figures for BCS, GA, CG and SVD-based approach.

Observations

- Le ricostruzioni ottenute mediante GA risultano in generale più pulite con errore esterno più basso; l'errore interno è però sempre di gran lunga inferiore per le ricostruzioni ottenute mediante BCS rispetto alle ricostruzioni con GA.

2 TEST CASE: Square Cylinder $side = 0.33\lambda$

Goal: compare the performances of BCS, GA and CG

- Number of Views: V
- Number of Measurements: M
- Number of Cells for the Inversion: N
- Number of Cells for the Direct solver: D
- Side of the investigation domain: L

Test Case Description

Direct solver:

- Square domain divided in $\sqrt{D} \times \sqrt{D}$ cells
- Domain side: $L = 3\lambda$
- $D = 1296$ (discretization for the direct solver: $< \lambda/10$)

Investigation domain:

- Square domain divided in $\sqrt{N} \times \sqrt{N}$ cells
- $L = 3\lambda$
- $2ka = 2 \times \frac{2\pi}{\lambda} \times \frac{L\sqrt{2}}{2} = 6\pi\sqrt{2} = 26.65$
- $\#DOF = \frac{(2ka)^2}{2} = \frac{(2 \times \frac{2\pi}{\lambda} \times \frac{L\sqrt{2}}{2})^2}{2} = 4\pi^2 \left(\frac{L}{\lambda}\right)^2 = 4\pi^2 \times 9 \approx 355.3$
- N scelto in modo da essere vicino a $\#DOF$: $N = 324$ (18×18)

Measurement domain:

- Measurement points taken on a circle of radius $\rho = 3\lambda$
- Full-aspect measurements
- $M \approx 2ka \rightarrow M = 27$

Sources:

- Plane waves
- $V \approx 2ka \rightarrow V = 27$
- Amplitude $A = 1$
- Frequency: 300 MHz ($\lambda = 1$)

Object:

- Square cylinder of side $\frac{\lambda}{3} = 0.3333$
- $\varepsilon_r \in \{1.5, 2.0, 2.5, 3.0\}$
- $\sigma = 0$ [S/m]

BCS parameters:

- Initial estimate of the noise: $n_0 = 1.0 \times 10^{-3}$
- Convergenze parameter: $\tau = 1.0 \times 10^{-8}$

CG parameters:

- Iterations: 200
- Peso stato: 0
- Peso dati: 1

GA parameters:

- Iterations: 10000
- Tournament Selection: $TRUE$
- Prob. Crossover: 0.8
- Prob. Mutation: 0.4
- Prob. Bit Muation: 0.05
- Prob. New Generation: 0.01
- Elitism: $TRUE$
- Crossover Child: 1
- Population: 200
- Convergence Threshold: 0.001

RESULTS: $\varepsilon_r = 1.5$

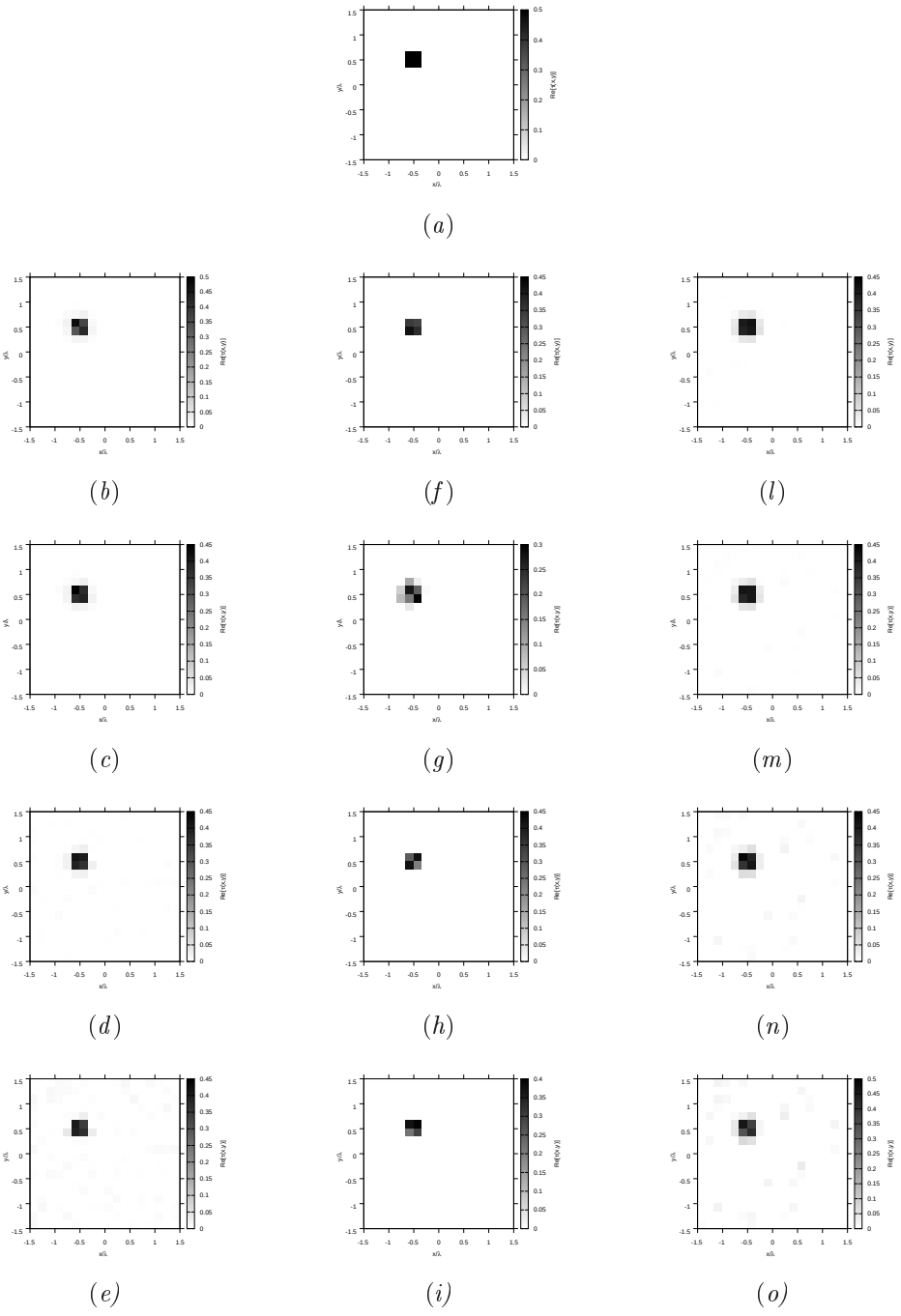

Figure 75. Actual object (a), (b)-(e) BCS reconstructed $(g)(i)$ GA-reconstructed, and (l)-(o) CG reconstructed object for $(b)(f)(l)$ Noiseless case, $(c)(g)(m)$ $SNR = 20$ [dB] , $(d)(h)(n)$ $SNR = 10$ [dB] , $(e)(i)(o)$ $SNR = 5$ [dB].

RESULTS: $\varepsilon_r = 1.5$

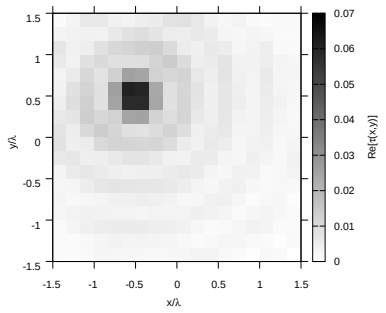

Figure 76. Actual object - Born approximation SVD-based approach reconstructed (Noiseless case)

SNR	Noiseless				20 [dB]			
	BCS	GA	CG	SVD	BCS	GA	CG	SVD
ξ_{tot}	1.85×10^{-3}	1.10×10^{-3}	2.01×10^{-3}	9.18×10^{-3}	1.85×10^{-3}	3.14×10^{-3}	2.16×10^{-3}	–
ξ_{int}	6.81×10^{-2}	8.87×10^{-2}	6.28×10^{-2}	0.2937	7.00×10^{-2}	0.1808	6.37×10^{-2}	–
ξ_{ext}	5.70×10^{-4}	0.0000	1.25×10^{-3}	5.39×10^{-3}	5.82×10^{-4}	9.19×10^{-4}	1.39×10^{-3}	–

SNR	10 [dB]				5 [dB]			
	BCS	GA	CG	SVD	BCS	GA	CG	SVD
ξ_{tot}	2.88×10^{-3}	1.33×10^{-3}	2.65×10^{-3}	–	5.76×10^{-3}	1.48×10^{-3}	3.23×10^{-3}	–
ξ_{int}	7.13×10^{-2}	0.1077	6.66×10^{-2}	–	8.16×10^{-2}	0.1200	7.00×10^{-2}	–
ξ_{ext}	1.22×10^{-3}	0.0000	1.85×10^{-3}	–	2.79×10^{-3}	0.0000	2.39×10^{-3}	–

Table V. Comparison of error figures for BCS, GA, CG and SVD-based approach.

Observations

- Le ricostruzioni ottenute mediante GA risultano in generale più pulite con errore esterno più basso; l'errore interno è però sempre di gran lunga inferiore per le ricostruzioni ottenute mediante BCS rispetto alle ricostruzioni con GA.

RESULTS: $\varepsilon_r = 2.0$

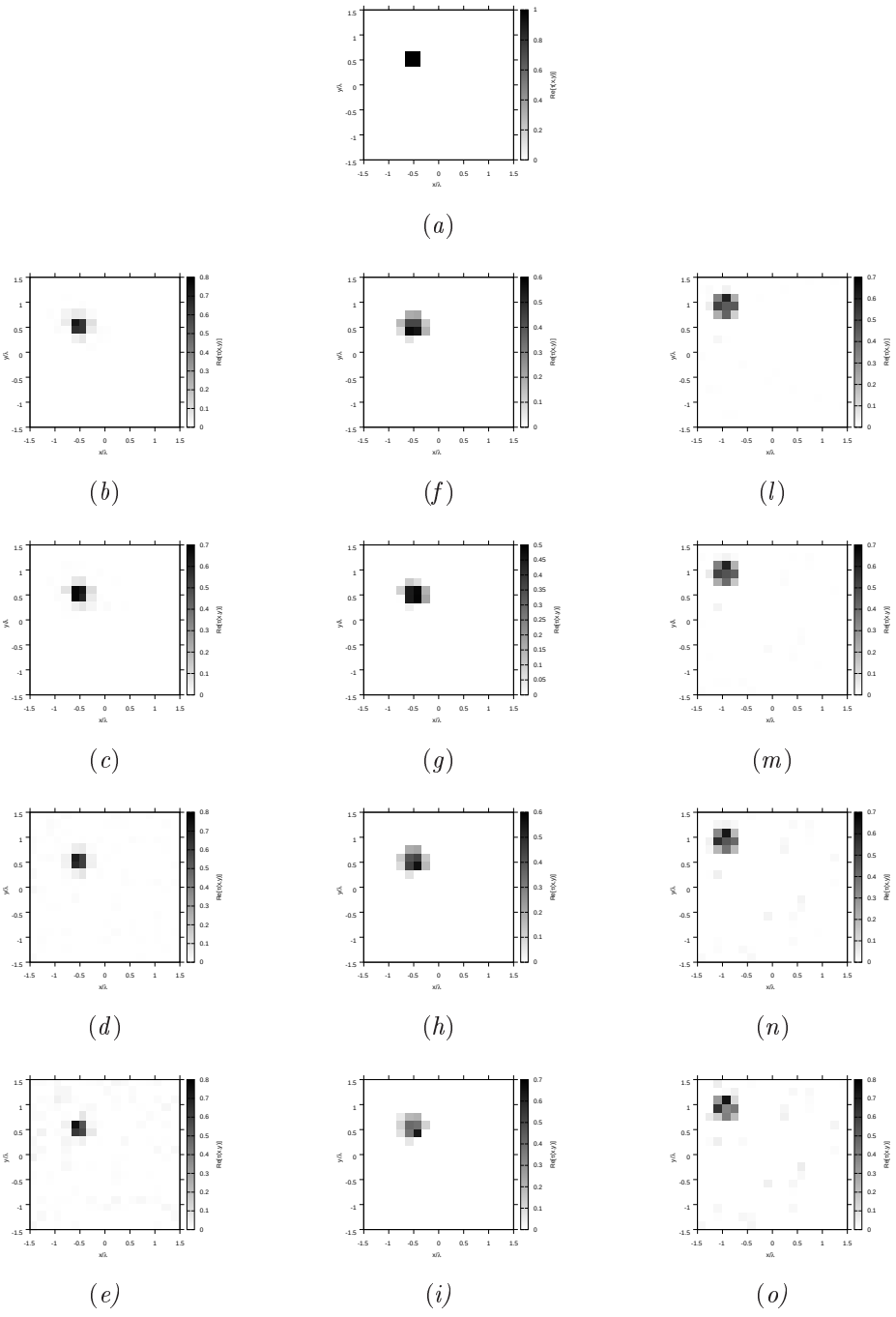

Figure 77. Actual object (a), (b)-(e) BCS reconstructed $(g)(i)$ GA-reconstructed, and (l)-(o) CG reconstructed object for $(b)(f)(l)$ Noiseless case, $(c)(g)(m)$ $SNR = 20$ [dB] , $(d)(h)(n)$ $SNR = 10$ [dB] , $(e)(i)(o)$ $SNR = 5$ [dB].

RESULTS: $\varepsilon_r = 2.0$

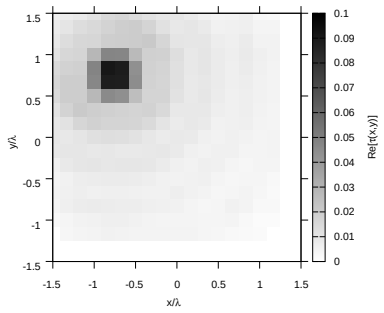

Figure 78. Actual object - Born approximation SVD-based approach reconstructed (Noiseless case)

SNR	Noiseless				20 [dB]			
	BCS	GA	CG	SVD	BCS	GA	CG	SVD
ξ_{tot}	5.22×10^{-3}	6.26×10^{-3}	9.45×10^{-3}	1.62×10^{-2}	5.42×10^{-3}	5.18×10^{-3}	9.61×10^{-3}	–
ξ_{int}	0.1668	0.2500	0.2891	0.4554	0.1735	0.2662	0.2884	–
ξ_{ext}	1.96×10^{-3}	3.22×10^{-3}	5.95×10^{-3}	9.52×10^{-3}	2.05×10^{-3}	1.92×10^{-3}	6.12×10^{-3}	–

SNR	10 [dB]				5 [dB]			
	BCS	GA	CG	SVD	BCS	GA	CG	SVD
ξ_{tot}	8.36×10^{-3}	6.33×10^{-3}	1.03×10^{-2}	–	1.37×10^{-2}	6.05×10^{-3}	1.12×10^{-2}	–
ξ_{int}	0.1759	0.2678	0.2882	–	0.1892	0.2738	0.2895	–
ξ_{ext}	3.87×10^{-3}	3.06×10^{-3}	6.79×10^{-3}	–	7.08×10^{-3}	2.71×10^{-3}	7.71×10^{-3}	–

Table VI. Comparison of error figures for BCS, GA, CG and SVD-based approach.

Observations

- Le ricostruzioni ottenute mediante BCS e GA sono in questo caso paragonabili; l'errore interno è però sempre inferiore per le ricostruzioni ottenute mediante BCS rispetto alle ricostruzioni con GA.

3 TEST CASE: Two Square Cylinders

Goal: compare the performances of BCS, GA and CG

- Number of Views: V
- Number of Measurements: M
- Number of Cells for the Inversion: N
- Number of Cells for the Direct solver: D
- Side of the investigation domain: L

Test Case Description

Direct solver:

- Square domain divided in $\sqrt{D} \times \sqrt{D}$ cells
- Domain side: $L = 3\lambda$
- $D = 1296$ (discretization for the direct solver: $< \lambda/10$)

Investigation domain:

- Square domain divided in $\sqrt{N} \times \sqrt{N}$ cells
- $L = 3\lambda$
- $2ka = 2 \times \frac{2\pi}{\lambda} \times \frac{L\sqrt{2}}{2} = 6\pi\sqrt{2} = 26.65$
- $\#DOF = \frac{(2ka)^2}{2} = \frac{(2 \times \frac{2\pi}{\lambda} \times \frac{L\sqrt{2}}{2})^2}{2} = 4\pi^2 \left(\frac{L}{\lambda}\right)^2 = 4\pi^2 \times 9 \approx 355.3$
- N scelto in modo da essere vicino a $\#DOF$: $N = 324$ (18×18)

Measurement domain:

- Measurement points taken on a circle of radius $\rho = 3\lambda$
- Full-aspect measurements
- $M \approx 2ka \rightarrow M = 27$

Sources:

- Plane waves
- $V \approx 2ka \rightarrow V = 27$
- Amplitude $A = 1$
- Frequency: 300 MHz ($\lambda = 1$)

Object:

- Square cylinder of side $\frac{\lambda}{6} = 0.1667$
- $\varepsilon_r \in \{1.5, 2.0, 2.5, 3.0\}$ (one square), $\varepsilon_r = 1.9$ (one square)
- $\sigma = 0$ [S/m]

BCS parameters:

- Initial estimate of the noise: $n_0 = 1.0 \times 10^{-3}$
- Convergenze parameter: $\tau = 1.0 \times 10^{-8}$

CG parameters:

- Iterations: 200
- Peso stato: 0
- Peso dati: 1

GA parameters:

- Iterations: 10000
- Tournament Selection: $TRUE$
- Prob. Crossover: 0.8
- Prob. Mutation: 0.4
- Prob. Bit Muation: 0.05
- Prob. New Generation: 0.01
- Elitism: $TRUE$
- Crossover Child: 1
- Population: 200
- Convergence Threshold: 0.001

RESULTS: $\varepsilon_r = 1.5$

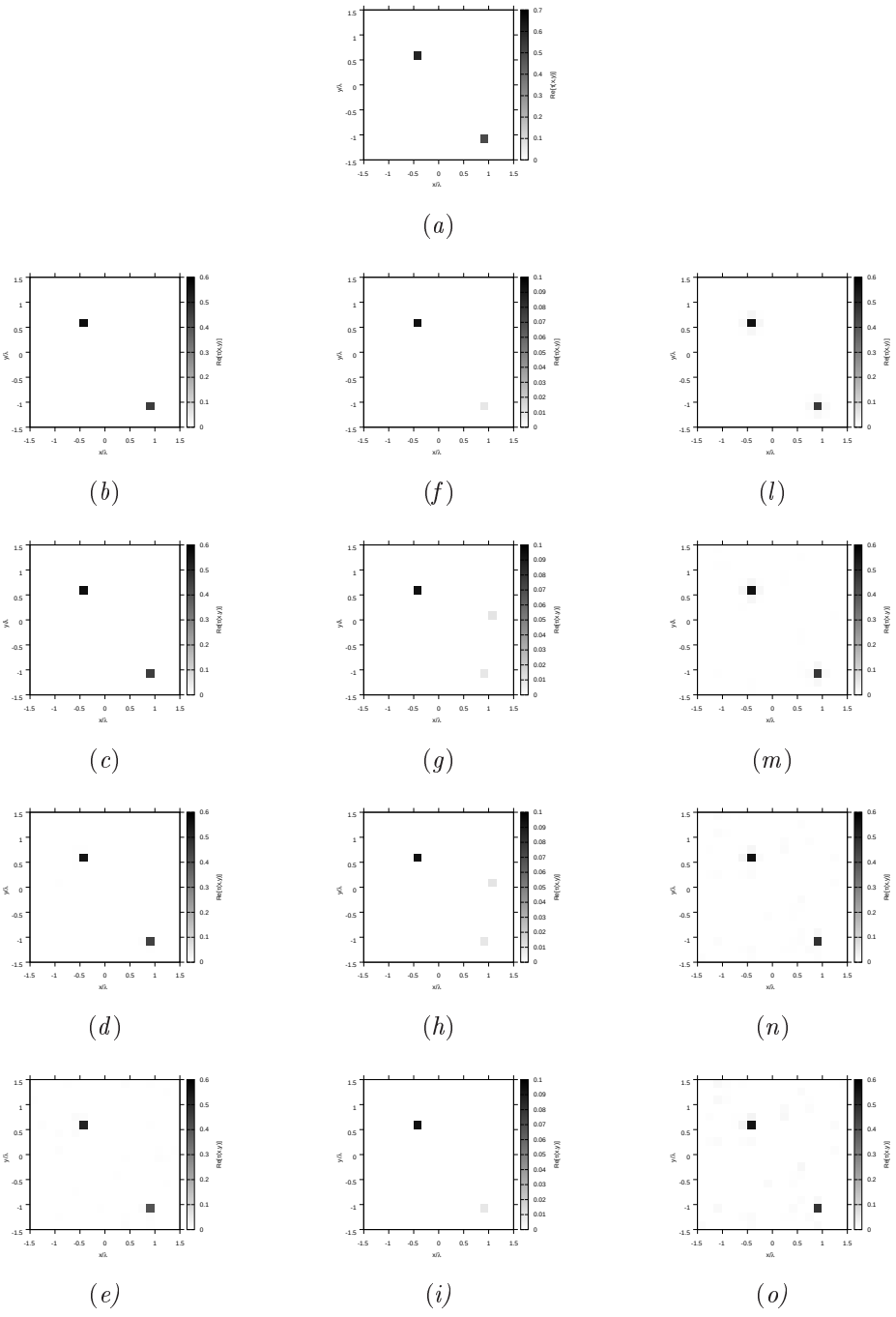

(a)

(b) (f) (l)

(c) (g) (m)

(d) (h) (n)

(e) (i) (o)

Figure 79. Actual object (a), (b)-(e) BCS reconstructed $(g)(i)$ GA-reconstructed, and (l)-(o) CG reconstructed object for $(b)(f)(l)$ Noiseless case, $(c)(g)(m)$ $SNR = 20$ [dB] , $(d)(h)(n)$ $SNR = 10$ [dB] , $(e)(i)(o)$ $SNR = 5$ [dB].

RESULTS: $\varepsilon_r = 1.5$

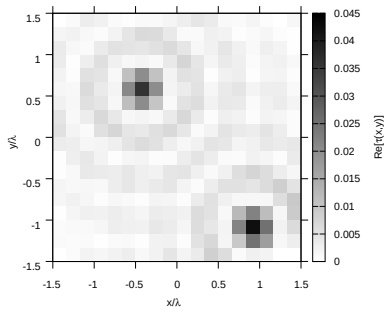

Figure 80. Actual object - Born approximation SVD-based approach reconstructed (Noiseless case)

SNR	Noiseless				20 [dB]			
	BCS	GA	CG	SVD	BCS	GA	CG	SVD
ξ_{tot}	3.56×10^{-4}	1.99×10^{-3}	7.12×10^{-4}	5.50×10^{-3}	3.54×10^{-4}	2.02×10^{-3}	7.72×10^{-4}	–
ξ_{int}	2.34×10^{-2}	0.3218	2.24×10^{-2}	0.3288	2.50×10^{-2}	0.3218	2.18×10^{-2}	–
ξ_{ext}	0.0000	0.0000	5.78×10^{-4}	3.49×10^{-3}	0.0000	3.26×10^{-5}	6.41×10^{-4}	–

SNR	10 [dB]				5 [dB]			
	BCS	GA	CG	SVD	BCS	GA	CG	SVD
ξ_{tot}	4.60×10^{-4}	2.02×10^{-3}	9.17×10^{-4}	–	1.49×10^{-3}	1.99×10^{-3}	1.24×10^{-3}	–
ξ_{int}	3.24×10^{-2}	0.3218	1.70×10^{-2}	–	5.55×10^{-2}	0.3218	2.06×10^{-2}	–
ξ_{ext}	8.51×10^{-5}	3.26×10^{-5}	8.17×10^{-4}	–	6.67×10^{-4}	0.0000	1.12×10^{-3}	–

Table VII. Comparison of error figures for BCS, GA, CG and SVD-based approach.

Observations

- Le prestazioni del BCS risultano in questo caso sempre migliori rispetto ai GA.

RESULTS: $\varepsilon_r = 2.0$

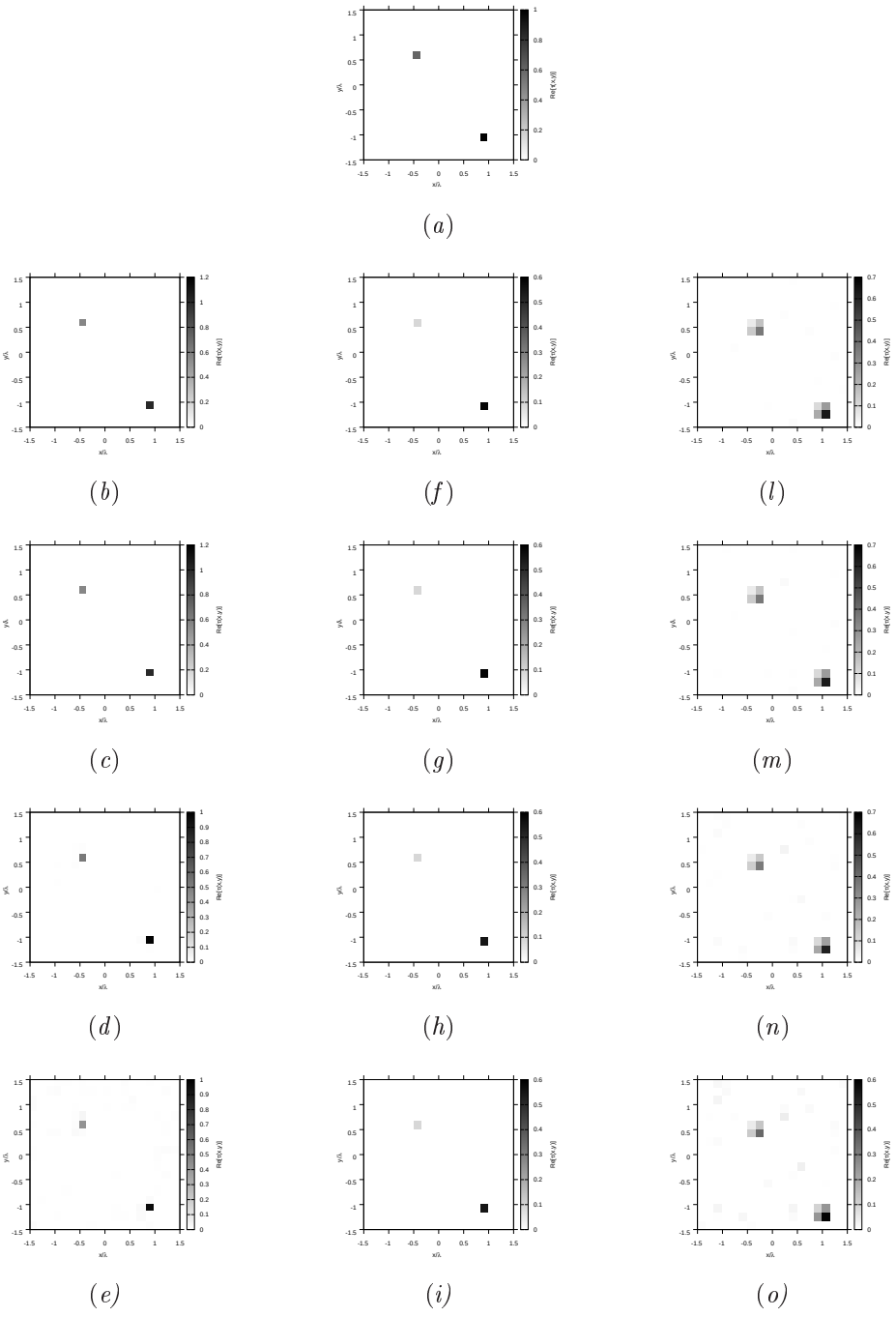

Figure 81. Actual object (a), (b)-(e) BCS reconstructed $(g)(i)$ GA-reconstructed, and (l)-(o) CG reconstructed object for $(b)(f)(l)$ Noiseless case, $(c)(g)(m)$ $SNR = 20$ [dB] , $(d)(h)(n)$ $SNR = 10$ [dB] , $(e)(i)(o)$ $SNR = 5$ [dB].

RESULTS: $\varepsilon_r = 2.0$

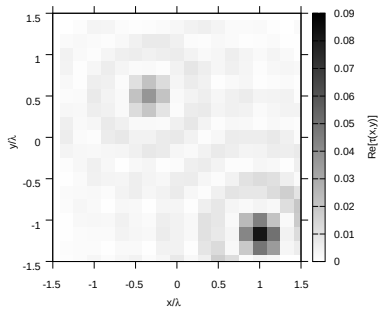

Figure 82. Actual object - Born approximation SVD-based approach reconstructed (Noiseless case)

SNR	Noiseless				20 [dB]			
	BCS	GA	CG	SVD	BCS	GA	CG	SVD
ξ_{tot}	6.72×10^{-4}	1.61×10^{-3}	6.62×10^{-3}	7.75×10^{-3}	6.69×10^{-4}	1.61×10^{-3}	6.64×10^{-3}	–
ξ_{int}	1.25×10^{-2}	0.2615	0.3020	0.4049	1.33×10^{-2}	0.2604	0.3033	–
ξ_{ext}	0.0000	0.0000	4.79×10^{-3}	5.12×10^{-3}	1.37×10^{-6}	0.0000	4.80×10^{-3}	–

SNR	10 [dB]				5 [dB]			
	BCS	GA	CG	SVD	BCS	GA	CG	SVD
ξ_{tot}	1.34×10^{-3}	1.67×10^{-3}	6.88×10^{-3}	–	3.90×10^{-3}	1.67×10^{-3}	7.28×10^{-3}	–
ξ_{int}	2.50×10^{-2}	0.2709	0.3068	–	6.58×10^{-2}	0.2709	0.3113	–
ξ_{ext}	4.73×10^{-4}	0.0000	5.01×10^{-3}	–	2.24×10^{-3}	0.0000	5.39×10^{-3}	–

Table VIII. Comparison of error figures for BCS, GA, CG and SVD-based approach.

Observations

- In questo caso ricostruzioni migliori ottenute mediante BCS per i casi $Noiseless$ e $SNR = 20\,dB$, ricostuzioni invece più pulite ottenute mediante GA per i casi con maggiore rumore, ma con errore interno sempre inferiore per le ricostruzioni ottenute mediante BCS rispetto alle ricostruzioni con GA.

RESULTS: $\varepsilon_r = 2.5$

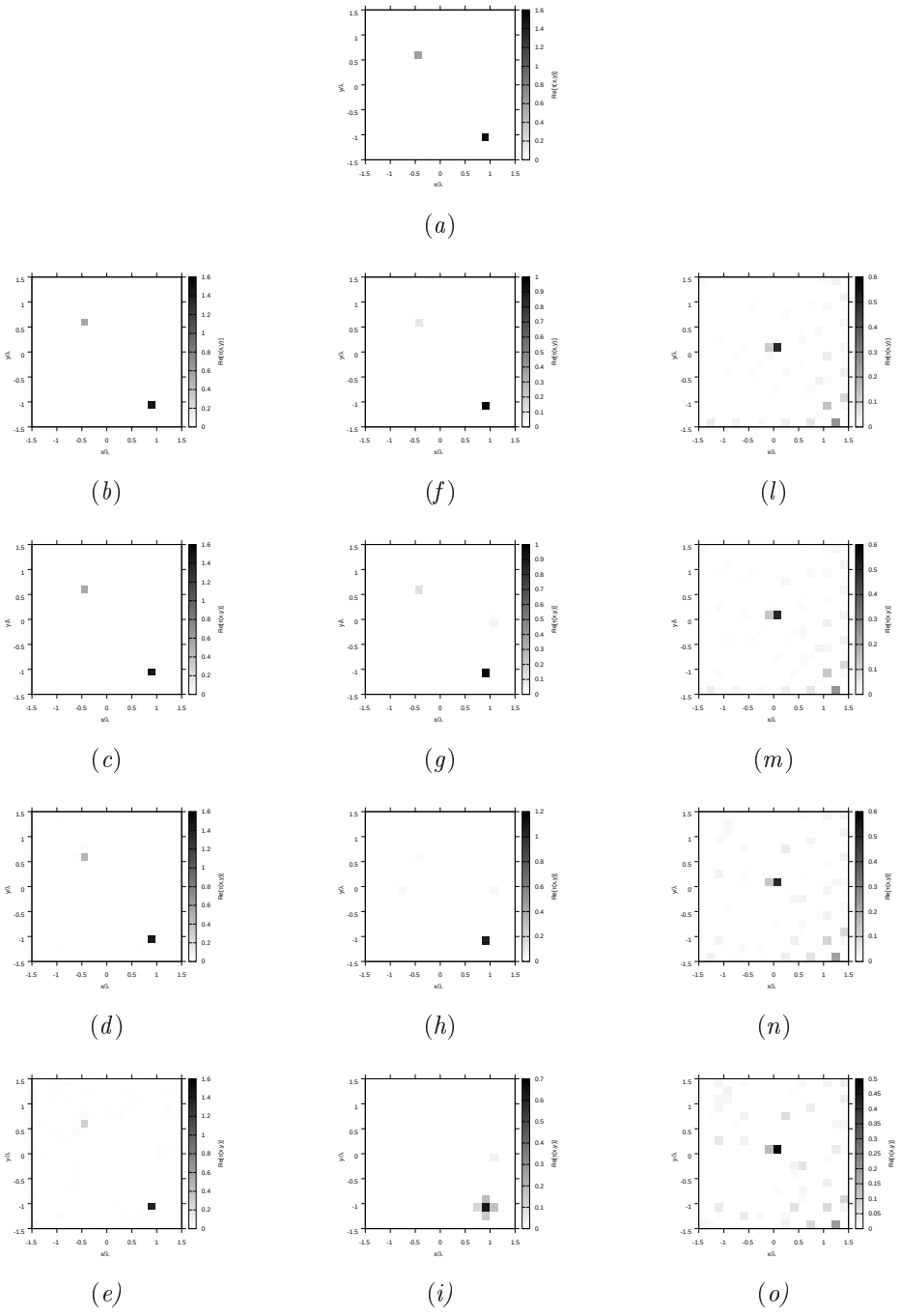

Figure 83. Actual object (a), (b)-(e) BCS reconstructed $(g)(i)$ GA-reconstructed, and (l)-(o) CG reconstructed object for $(b)(f)(l)$ Noiseless case, $(c)(g)(m)$ $SNR = 20$ [dB] , $(d)(h)(n)$ $SNR = 10$ [dB] , $(e)(i)(o)$ $SNR = 5$ [dB].

RESULTS: $\varepsilon_r = 2.5$

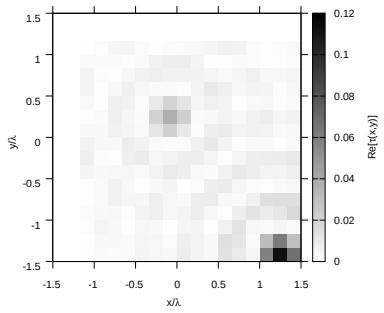

Figure 84. Actual object - Born approximation SVD-based approach reconstructed (Noiseless case)

SNR	Noiseless				20 [dB]			
	BCS	GA	CG	SVD	BCS	GA	CG	SVD
ξ_{tot}	1.11×10^{-3}	1.60×10^{-3}	5.20×10^{-3}	9.79×10^{-3}	1.12×10^{-3}	1.69×10^{-3}	5.16×10^{-3}	–
ξ_{int}	1.86×10^{-2}	0.2596	0.1794	0.4517	2.16×10^{-2}	0.2489	0.1760	–
ξ_{ext}	3.67×10^{-6}	0.0000	4.66×10^{-3}	6.56×10^{-3}	9.07×10^{-6}	1.51×10^{-4}	4.63×10^{-3}	–

SNR	10 [dB]				5 [dB]			
	BCS	GA	CG	SVD	BCS	GA	CG	SVD
ξ_{tot}	3.08×10^{-3}	1.85×10^{-3}	5.27×10^{-3}	–	7.01×10^{-3}	4.26×10^{-3}	5.60×10^{-3}	–
ξ_{int}	5.33×10^{-2}	0.2660	0.1749	–	0.1093	0.3597	0.1767	–
ξ_{ext}	1.34×10^{-3}	2.13×10^{-4}	4.75×10^{-3}	–	4.05×10^{-3}	2.06×10^{-3}	5.07×10^{-3}	–

Table IX. Comparison of error figures for BCS, GA, CG and SVD-based approach.

Observations

- In questo caso ricostruzioni migliori ottenute mediante BCS per i casi $Noiseless$ e $SNR = 20\,dB$, ricostuzioni invece più pulite ottenute mediante GA per i casi con maggiore rumore, ma con errore interno sempre inferiore per le ricostruzioni ottenute mediante BCS rispetto alle ricostruzioni con GA.

RESULTS: $\varepsilon_r = 3.0$

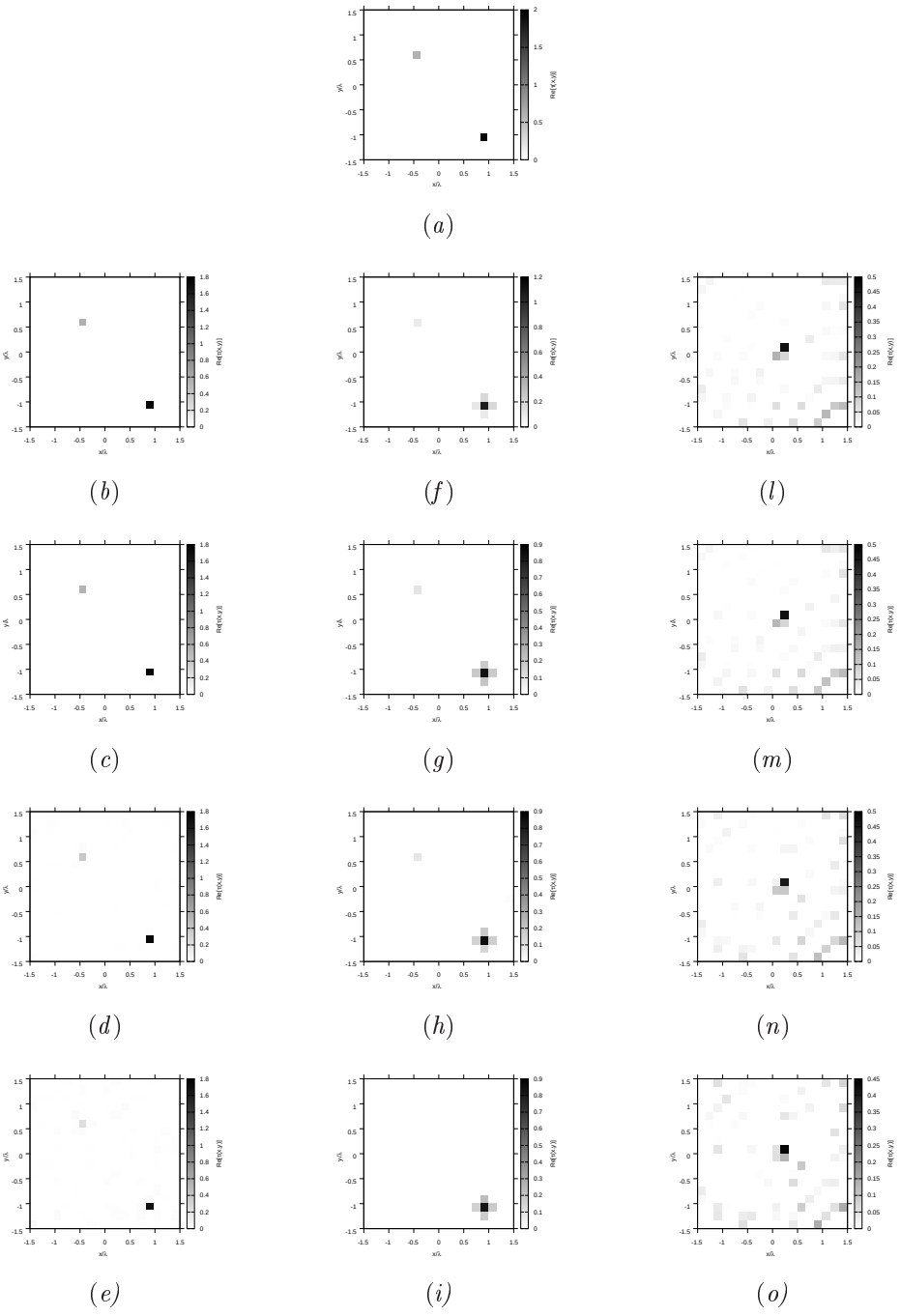

Figure 85. Actual object (a), (b)-(e) BCS reconstructed $(g)(i)$ GA-reconstructed, and (l)-(o) CG reconstructed object for $(b)(f)(l)$ Noiseless case, $(c)(g)(m)$ $SNR = 20$ [dB] , $(d)(h)(n)$ $SNR = 10$ [dB] , $(e)(i)(o)$ $SNR = 5$ [dB].

RESULTS: $\varepsilon_r = 3.0$

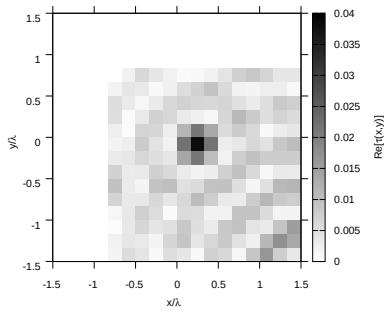

Figure 86. Actual object - Born approximation SVD-based approach reconstructed (Noiseless case)

SNR	Noiseless				20 [dB]			
	BCS	GA	CG	SVD	BCS	GA	CG	SVD
ξ_{tot}	1.57×10^{-3}	3.75×10^{-3}	6.63×10^{-3}	1.16×10^{-2}	1.69×10^{-3}	4.54×10^{-3}	6.59×10^{-3}	–
ξ_{int}	5.13×10^{-2}	0.3143	0.2042	0.4851	5.66×10^{-2}	0.3521	0.2024	–
ξ_{ext}	2.10×10^{-5}	1.82×10^{-3}	6.01×10^{-3}	7.54×10^{-3}	1.14×10^{-4}	2.38×10^{-3}	5.98×10^{-3}	–

SNR	10 [dB]				5 [dB]			
	BCS	GA	CG	SVD	BCS	GA	CG	SVD
ξ_{tot}	4.99×10^{-3}	4.27×10^{-3}	6.80×10^{-3}	–	1.01×10^{-2}	4.72×10^{-3}	7.29×10^{-3}	–
ξ_{int}	0.1070	0.3493	0.1995	–	0.1689	0.3831	0.1968	–
ξ_{ext}	2.29×10^{-3}	2.12×10^{-3}	6.20×10^{-3}	–	5.25×10^{-3}	2.37×10^{-3}	6.70×10^{-3}	–

Table X. Comparison of error figures for BCS, GA, CG and SVD-based approach.

Observations

- In questo caso ricostruzioni migliori ottenute mediante BCS per i casi $Noiseless$ e $SNR = 20\,dB$, ricostuzioni invece più pulite ottenute mediante GA per i casi con maggiore rumore, ma con errore interno sempre inferiore per le ricostruzioni ottenute mediante BCS rispetto alle ricostruzioni con GA.

4 TEST CASE: Three Square Cylinders

Goal: compare the performances of BCS, GA and CG

- Number of Views: V
- Number of Measurements: M
- Number of Cells for the Inversion: N
- Number of Cells for the Direct solver: D
- Side of the investigation domain: L

Test Case Description

Direct solver:

- Square domain divided in $\sqrt{D} \times \sqrt{D}$ cells
- Domain side: $L = 3\lambda$
- $D = 1296$ (discretization for the direct solver: $< \lambda/10$)

Investigation domain:

- Square domain divided in $\sqrt{N} \times \sqrt{N}$ cells
- $L = 3\lambda$
- $2ka = 2 \times \frac{2\pi}{\lambda} \times \frac{L\sqrt{2}}{2} = 6\pi\sqrt{2} = 26.65$
- $\#DOF = \frac{(2ka)^2}{2} = \frac{(2\times\frac{2\pi}{\lambda}\times\frac{L\sqrt{2}}{2})^2}{2} = 4\pi^2\left(\frac{L}{\lambda}\right)^2 = 4\pi^2 \times 9 \approx 355.3$
- N scelto in modo da essere vicino a $\#DOF$: $N = 324$ (18×18)

Measurement domain:

- Measurement points taken on a circle of radius $\rho = 3\lambda$
- Full-aspect measurements
- $M \approx 2ka \rightarrow M = 27$

Sources:

- Plane waves
- $V \approx 2ka \rightarrow V = 27$
- Amplitude $A = 1$
- Frequency: 300 MHz ($\lambda = 1$)

Object:

- Square cylinder of side $\frac{\lambda}{6} = 0.1667$
- $\varepsilon_r \in \{1.5, 2.0, 2.5, 3.0\}$ (two squares), $\varepsilon_r = 1.9$ (one square)
- $\sigma = 0$ [S/m]

BCS parameters:

- Initial estimate of the noise: $n_0 = 1.0 \times 10^{-3}$
- Convergenze parameter: $\tau = 1.0 \times 10^{-8}$

CG parameters:

- Iterations: 200
- Peso stato: 0
- Peso dati: 1

GA parameters:

- Iterations: 10000
- Tournament Selection: $TRUE$
- Prob. Crossover: 0.8
- Prob. Mutation: 0.4
- Prob. Bit Muation: 0.05
- Prob. New Generation: 0.01
- Elitism: $TRUE$
- Crossover Child: 1
- Population: 200
- Convergence Threshold: 0.001

RESULTS: $\varepsilon_r = 1.5$

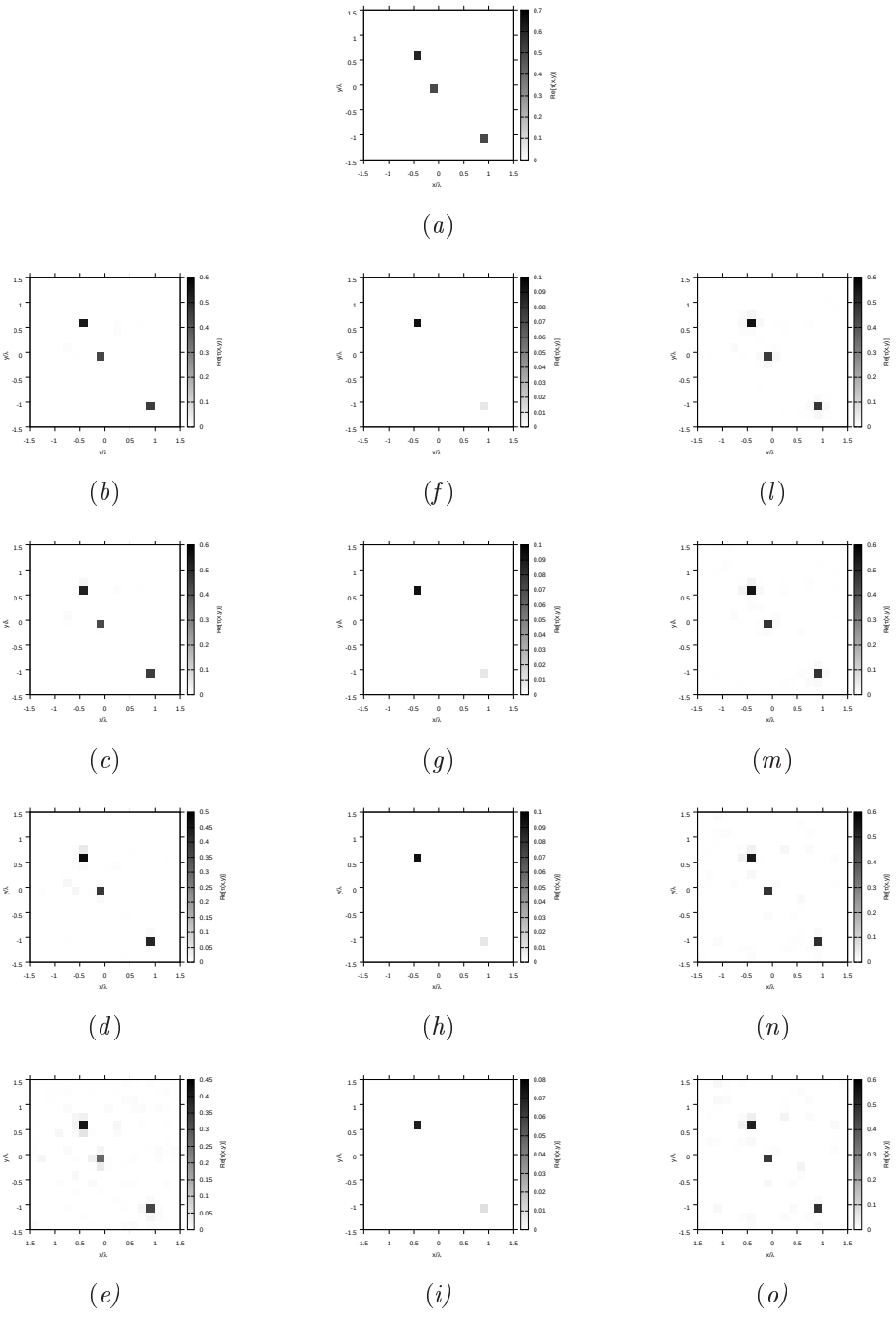

Figure 87. Actual object (a), (b)-(e) BCS reconstructed $(g)(i)$ GA-reconstructed, and (l)-(o) CG reconstructed object for $(b)(f)(l)$ Noiseless case, $(c)(g)(m)$ $SNR = 20$ [dB] , $(d)(h)(n)$ $SNR = 10$ [dB] , $(e)(i)(o)$ $SNR = 5$ [dB].

RESULTS: $\varepsilon_r = 1.5$

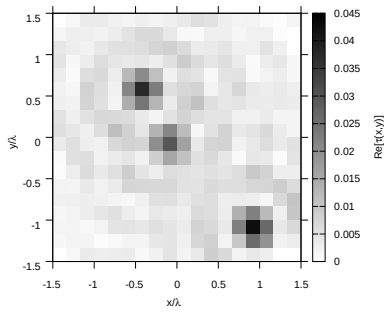

Figure 88. Actual object - Born approximation SVD-based approach reconstructed (Noiseless case)

SNR	Noiseless				20 [dB]			
	BCS	GA	CG	SVD	BCS	GA	CG	SVD
ξ_{tot}	7.85×10^{-4}	3.02×10^{-3}	1.10×10^{-3}	8.02×10^{-3}	8.80×10^{-4}	3.02×10^{-3}	1.04×10^{-3}	–
ξ_{int}	3.65×10^{-2}	0.3257	2.36×10^{-2}	0.3233	4.25×10^{-2}	0.3257	1.96×10^{-2}	–
ξ_{ext}	1.30×10^{-4}	0.0000	8.88×10^{-4}	5.07×10^{-3}	1.75×10^{-4}	0.0000	8.70×10^{-4}	–

SNR	10 [dB]				5 [dB]			
	BCS	GA	CG	SVD	BCS	GA	CG	SVD
ξ_{tot}	1.46×10^{-3}	3.02×10^{-3}	1.24×10^{-3}	–	3.91×10^{-3}	3.06×10^{-3}	1.71×10^{-3}	–
ξ_{int}	6.53×10^{-2}	0.3257	1.84×10^{-2}	–	0.1290	0.3305	2.62×10^{-2}	–
ξ_{ext}	6.02×10^{-4}	0.0000	1.07×10^{-3}	–	2.07×10^{-3}	0.0000	1.48×10^{-3}	–

Table XI. Comparison of error figures for BCS, GA, CG and SVD-based approach.

Observations

- In questo caso ricostruzioni migliori ottenute mediante BCS per i casi *Noiseless*, $SNR = 20\,dB$ e $SNR = 10\,dB$ ricostuzioni invece più pulite ottenute mediante GA per i casi con maggiore rumore, ma con errore interno sempre inferiore per le ricostruzioni ottenute mediante BCS rispetto alle ricostruzioni con GA.

RESULTS: $\varepsilon_r = 2.0$

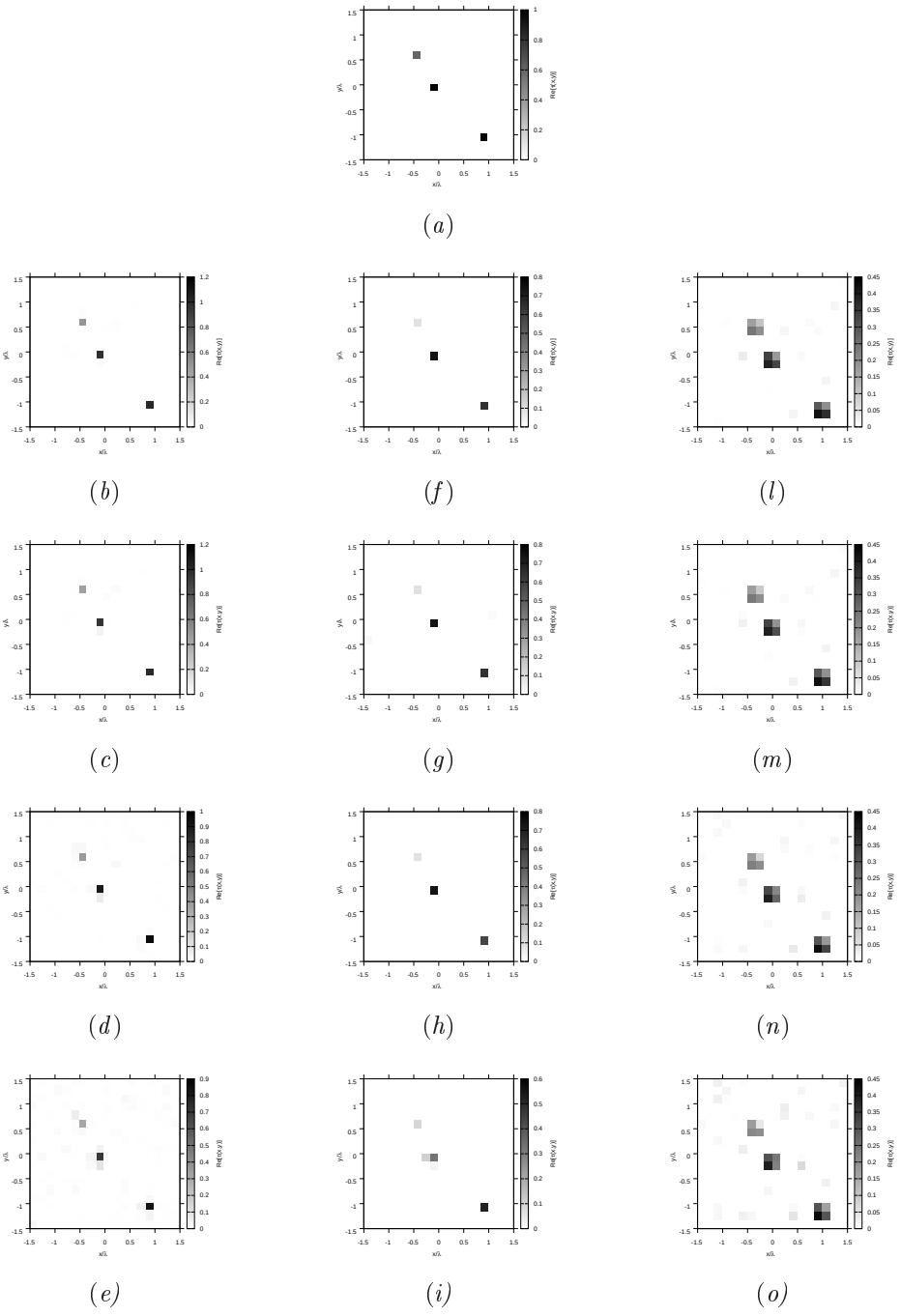

Figure 89. Actual object (a), (b)-(e) BCS reconstructed $(g)(i)$ GA-reconstructed, and (l)-(o) CG reconstructed object for $(b)(f)(l)$ Noiseless case, $(c)(g)(m)$ $SNR = 20$ [dB] , $(d)(h)(n)$ $SNR = 10$ [dB] , $(e)(i)(o)$ $SNR = 5$ [dB].

RESULTS: $\varepsilon_r = 2.0$

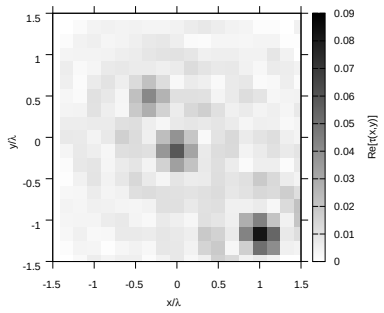

Figure 90. Actual object - Born approximation SVD-based approach reconstructed (Noiseless case)

SNR	Noiseless				20 [dB]			
	BCS	GA	CG	SVD	BCS	GA	CG	SVD
ξ_{tot}	1.61×10^{-3}	1.92×10^{-3}	1.09×10^{-2}	1.25×10^{-2}	1.94×10^{-3}	2.04×10^{-3}	1.08×10^{-2}	–
ξ_{int}	2.73×10^{-2}	0.2078	0.3164	0.4263	3.86×10^{-2}	0.2078	0.3179	–
ξ_{ext}	3.05×10^{-4}	0.0000	8.00×10^{-3}	8.33×10^{-3}	5.27×10^{-4}	1.19×10^{-4}	7.98×10^{-3}	–

SNR	10 [dB]				5 [dB]			
	BCS	GA	CG	SVD	BCS	GA	CG	SVD
ξ_{tot}	3.78×10^{-3}	2.02×10^{-3}	1.11×10^{-2}	–	8.20×10^{-3}	3.17×10^{-3}	1.15×10^{-2}	–
ξ_{int}	6.69×10^{-2}	0.2186	0.3220	–	0.1378	0.2971	0.3273	–
ξ_{ext}	1.99×10^{-3}	0.0000	8.18×10^{-3}	–	4.43×10^{-3}	4.28×10^{-4}	8.57×10^{-3}	–

Table XII. Comparison of error figures for BCS, GA, CG and SVD-based approach.

Observations

- In questo caso ricostruzioni migliori ottenute mediante BCS per i casi $Noiseless$ e $SNR = 20\,dB$, ricostuzioni invece più pulite ottenute mediante GA per i casi con maggiore rumore, ma con errore interno sempre inferiore per le ricostruzioni ottenute mediante BCS rispetto alle ricostruzioni con GA.

RESULTS: $\varepsilon_r = 2.5$

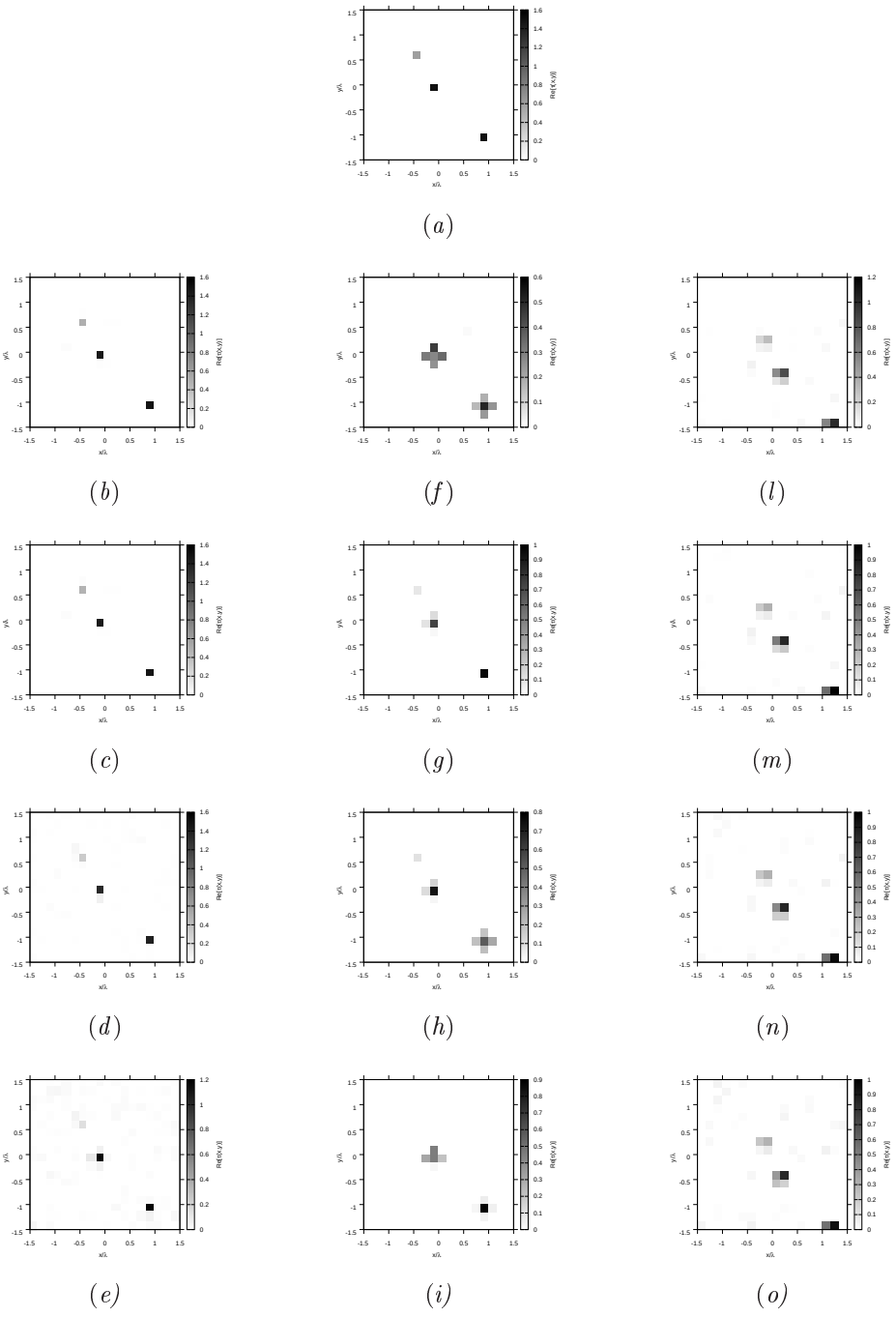

Figure 91. Actual object (a), (b)-(e) BCS reconstructed $(g)(i)$ GA-reconstructed, and (l)-(o) CG reconstructed object for $(b)(f)(l)$ Noiseless case, $(c)(g)(m)$ $SNR = 20$ [dB] , $(d)(h)(n)$ $SNR = 10$ [dB] , $(e)(i)(o)$ $SNR = 5$ [dB].

RESULTS: $\varepsilon_r = 2.5$

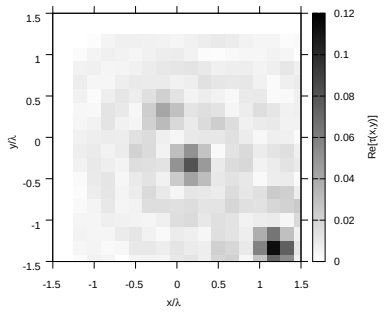

Figure 92. Actual object - Born approximation SVD-based approach reconstructed (Noiseless case)

SNR	Noiseless				20 [dB]			
	BCS	GA	CG	SVD	BCS	GA	CG	SVD
ξ_{tot}	2.43×10^{-3}	1.08×10^{-2}	1.04×10^{-2}	1.66×10^{-2}	2.59×10^{-3}	3.42×10^{-3}	1.04×10^{-2}	–
ξ_{int}	3.10×10^{-2}	0.4191	0.2751	0.4895	3.71×10^{-2}	0.2772	0.2758	–
ξ_{ext}	2.28×10^{-4}	6.96×10^{-3}	7.92×10^{-3}	1.12×10^{-2}	3.45×10^{-4}	8.62×10^{-4}	7.93×10^{-3}	–

SNR	10 [dB]				5 [dB]			
	BCS	GA	CG	SVD	BCS	GA	CG	SVD
ξ_{tot}	6.59×10^{-3}	6.66×10^{-3}	1.09×10^{-2}	–	1.37×10^{-2}	6.92×10^{-3}	1.16×10^{-2}	–
ξ_{int}	8.97×10^{-2}	0.3386	0.2809	–	0.1825	0.3452	0.2877	–
ξ_{ext}	3.10×10^{-3}	3.55×10^{-3}	8.33×10^{-3}	–	7.60×10^{-3}	3.76×10^{-3}	9.01×10^{-3}	–

Table XIII. Comparison of error figures for BCS, GA, CG and SVD-based approach.

Observations

- In questo caso ricostruzioni migliori ottenute mediante BCS per i casi $Noiseless$ e $SNR = 20\,dB$, ricostuzioni invece più pulite ottenute mediante GA per i casi con maggiore rumore, ma con errore interno sempre inferiore per le ricostruzioni ottenute mediante BCS rispetto alle ricostruzioni con GA.

RESULTS: $\varepsilon_r = 3.0$

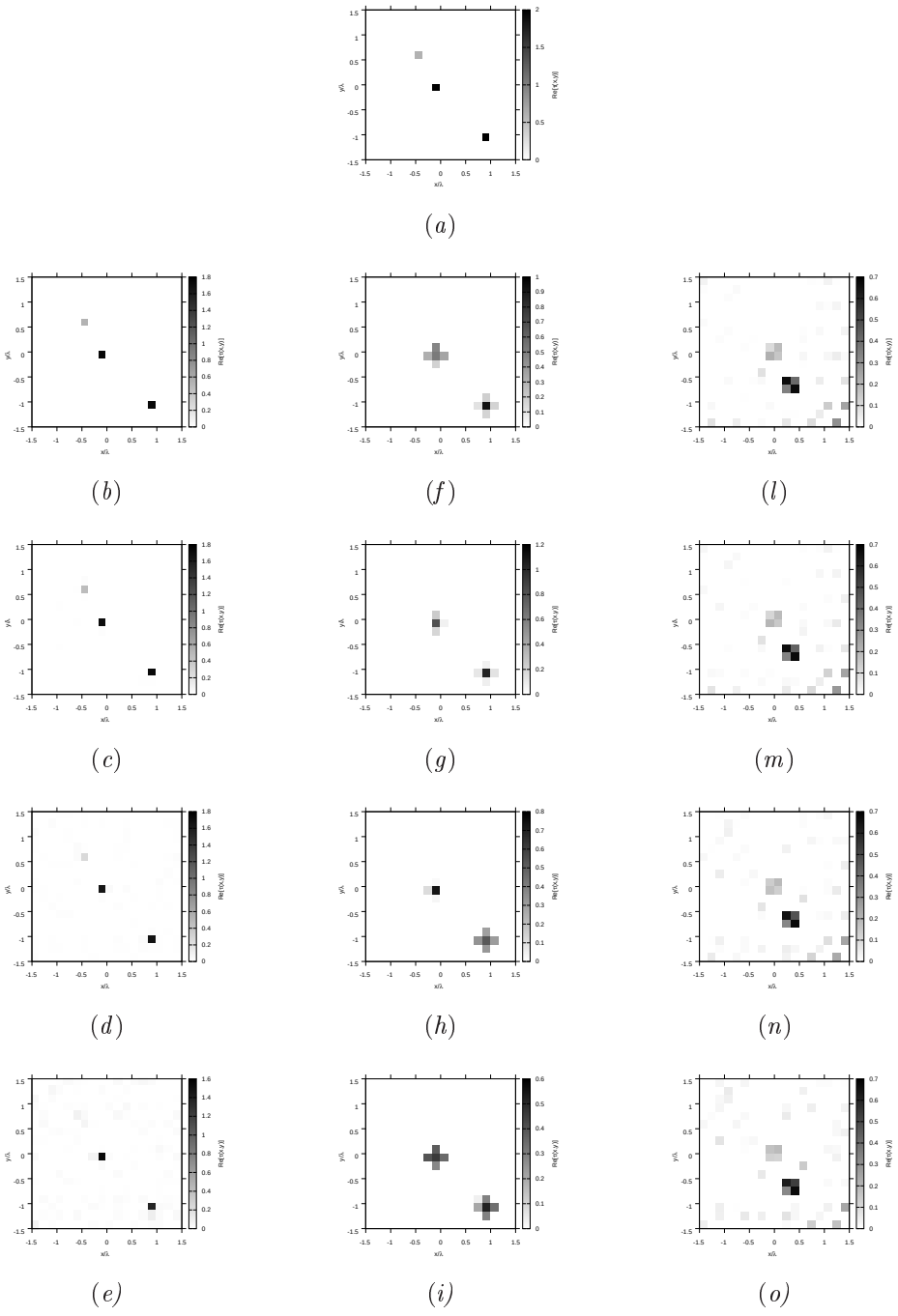

Figure 93. Actual object (a), (b)-(e) BCS reconstructed $(g)(i)$ GA-reconstructed, and (l)-(o) CG reconstructed object for $(b)(f)(l)$ Noiseless case, $(c)(g)(m)$ $SNR = 20$ [dB] , $(d)(h)(n)$ $SNR = 10$ [dB] , $(e)(i)(o)$ $SNR = 5$ [dB].

RESULTS: $\varepsilon_r = 3.0$

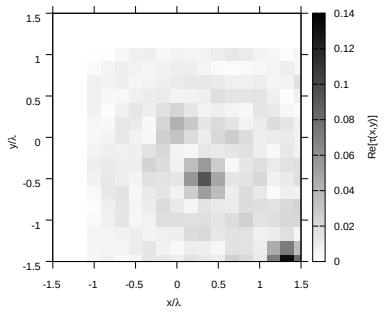

Figure 94. Actual object - Born approximation SVD-based approach reconstructed (Noiseless case)

SNR	Noiseless				20 [dB]			
	BCS	GA	CG	SVD	BCS	GA	CG	SVD
ξ_{tot}	3.10×10^{-3}	9.83×10^{-3}	1.40×10^{-2}	2.03×10^{-2}	3.80×10^{-3}	6.11×10^{-3}	1.40×10^{-2}	–
ξ_{int}	7.16×10^{-2}	0.4082	0.3822	0.5345	8.75×10^{-2}	0.3626	0.3823	–
ξ_{ext}	6.07×10^{-5}	6.11×10^{-3}	1.76×10^{-2}	1.30×10^{-2}	5.52×10^{-4}	2.78×10^{-3}	1.71×10^{-2}	–

SNR	10 [dB]				5 [dB]			
	BCS	GA	CG	SVD	BCS	GA	CG	SVD
ξ_{tot}	9.73×10^{-3}	8.38×10^{-3}	1.42×10^{-2}	–	1.84×10^{-2}	1.22×10^{-2}	1.48×10^{-2}	–
ξ_{int}	0.1453	0.4292	0.3830	–	0.2315	0.4600	0.3847	–
ξ_{ext}	4.39×10^{-3}	4.44×10^{-3}	1.19×10^{-2}	–	1.03×10^{-2}	8.06×10^{-3}	1.25×10^{-2}	–

Table XIV. Comparison of error figures for BCS, GA, CG and SVD-based approach.

Observations

- In questo caso ricostruzioni migliori ottenute mediante BCS per i casi $Noiseless$ e $SNR = 20\,dB$, ricostuzioni invece più pulite ottenute mediante GA per i casi con maggiore rumore, ma con errore interno sempre inferiore per le ricostruzioni ottenute mediante BCS rispetto alle ricostruzioni con GA.

5 TEST CASE: Four Square Cylinders

Goal: compare the performances of BCS, GA and CG

- Number of Views: V
- Number of Measurements: M
- Number of Cells for the Inversion: N
- Number of Cells for the Direct solver: D
- Side of the investigation domain: L

Test Case Description

Direct solver:

- Square domain divided in $\sqrt{D} \times \sqrt{D}$ cells
- Domain side: $L = 3\lambda$
- $D = 1296$ (discretization for the direct solver: $< \lambda/10$)

Investigation domain:

- Square domain divided in $\sqrt{N} \times \sqrt{N}$ cells
- $L = 3\lambda$
- $2ka = 2 \times \frac{2\pi}{\lambda} \times \frac{L\sqrt{2}}{2} = 6\pi\sqrt{2} = 26.65$
- $\#DOF = \frac{(2ka)^2}{2} = \frac{(2 \times \frac{2\pi}{\lambda} \times \frac{L\sqrt{2}}{2})^2}{2} = 4\pi^2 \left(\frac{L}{\lambda}\right)^2 = 4\pi^2 \times 9 \approx 355.3$
- N scelto in modo da essere vicino a $\#DOF$: $N = 324$ (18×18)

Measurement domain:

- Measurement points taken on a circle of radius $\rho = 3\lambda$
- Full-aspect measurements
- $M \approx 2ka \rightarrow M = 27$

Sources:

- Plane waves
- $V \approx 2ka \rightarrow V = 27$
- Amplitude $A = 1$
- Frequency: 300 MHz ($\lambda = 1$)

Object:

- Square cylinder of side $\frac{\lambda}{6} = 0.1667$
- $\varepsilon_r \in \{1.5, 2.0, 2.5, 3.0\}$ (two squares), $\varepsilon_r = 1.9$ (two square)
- $\sigma = 0$ [S/m]

BCS parameters:

- Initial estimate of the noise: $n_0 = 1.0 \times 10^{-3}$
- Convergenze parameter: $\tau = 1.0 \times 10^{-8}$

CG parameters:

- Iterations: 200
- Peso stato: 0
- Peso dati: 1

GA parameters:

- Iterations: 10000
- Tournament Selection: $TRUE$
- Prob. Crossover: 0.8
- Prob. Mutation: 0.4
- Prob. Bit Muation: 0.05
- Prob. New Generation: 0.01
- Elitism: $TRUE$
- Crossover Child: 1
- Population: 200
- Convergence Threshold: 0.001

RESULTS: $\varepsilon_r = 1.5$

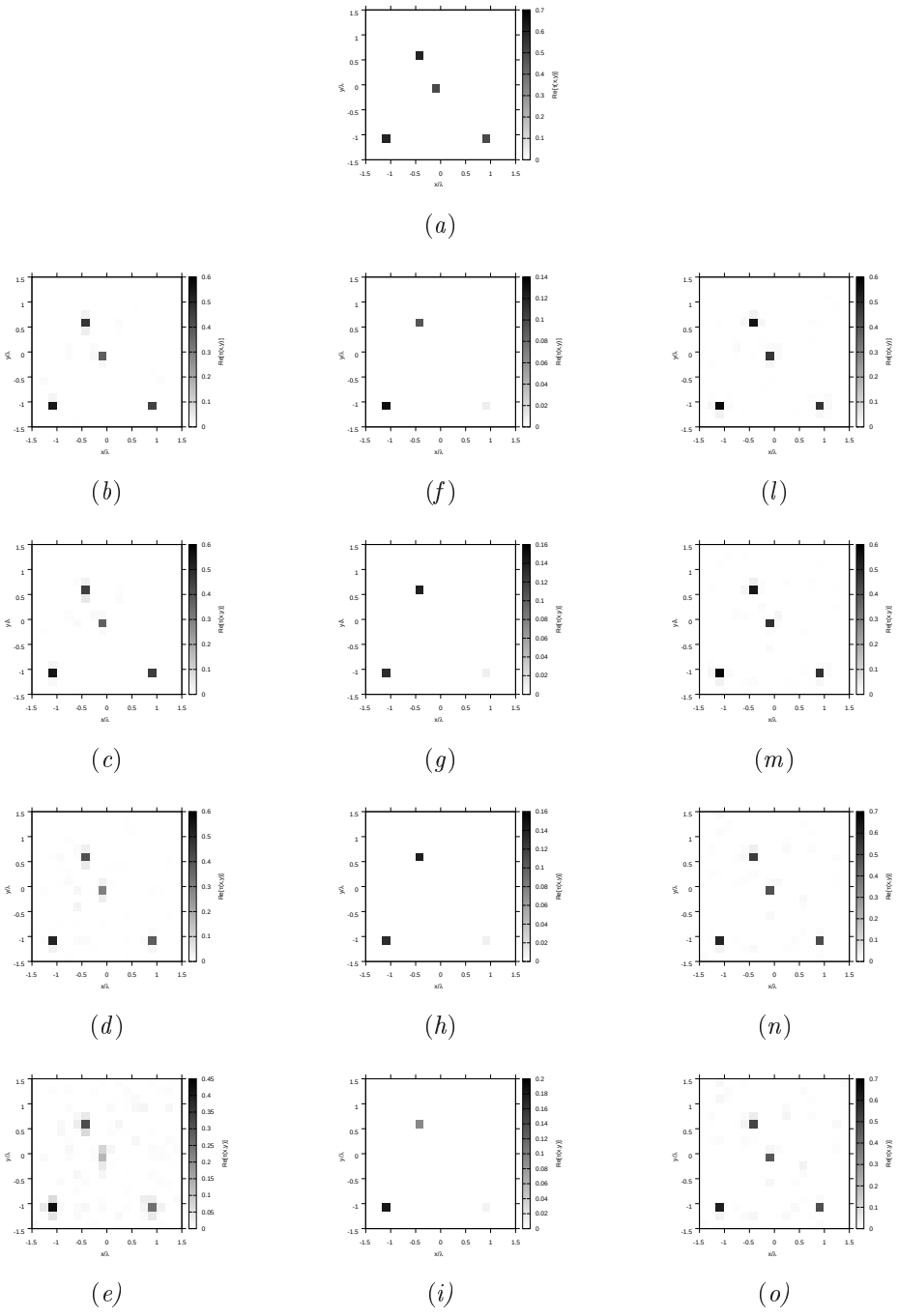

Figure 95. Actual object (a), (b)-(e) BCS reconstructed $(g)(i)$ GA-reconstructed, and (l)-(o) CG reconstructed object for $(b)(f)(l)$ Noiseless case, $(c)(g)(m)$ $SNR = 20$ [dB] , $(d)(h)(n)$ $SNR = 10$ [dB] , $(e)(i)(o)$ $SNR = 5$ [dB].

RESULTS: $\varepsilon_r = 1.5$

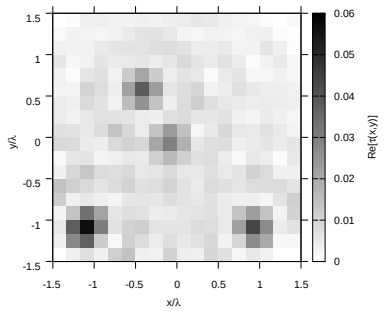

Figure 96. Actual object - Born approximation SVD-based approach reconstructed (Noiseless case)

SNR	Noiseless				20 [dB]			
	BCS	GA	CG	SVD	BCS	GA	CG	SVD
ξ_{tot}	1.72×10^{-3}	3.92×10^{-3}	1.38×10^{-3}	1.10×10^{-2}	1.77×10^{-3}	3.83×10^{-3}	1.31×10^{-3}	–
ξ_{int}	5.72×10^{-2}	0.3173	1.93×10^{-2}	0.3271	5.83×10^{-2}	0.3099	1.60×10^{-2}	–
ξ_{ext}	6.38×10^{-4}	0.0000	1.56×10^{-3}	7.00×10^{-3}	7.16×10^{-4}	0.0000	1.13×10^{-3}	–

SNR	10 [dB]				5 [dB]			
	BCS	GA	CG	SVD	BCS	GA	CG	SVD
ξ_{tot}	3.13×10^{-3}	3.83×10^{-3}	1.56×10^{-3}	–	6.96×10^{-3}	3.82×10^{-3}	2.16×10^{-3}	–
ξ_{int}	9.45×10^{-2}	0.3099	1.63×10^{-2}	–	0.1749	0.3097	2.67×10^{-2}	–
ξ_{ext}	1.50×10^{-3}	0.0000	1.37×10^{-3}	–	3.79×10^{-3}	0.0000	1.86×10^{-3}	–

Table XV. Comparison of error figures for BCS, GA, CG and SVD-based approach.

Observations

- In questo caso ricostruzioni migliori ottenute mediante BCS per i casi *Noiseless*, $SNR = 20\,dB$ e $SNR = 10\,dB$ ricostuzioni invece più pulite ottenute mediante GA per i casi con maggiore rumore, ma con errore interno sempre inferiore per le ricostruzioni ottenute mediante BCS rispetto alle ricostruzioni con GA.

RESULTS: $\varepsilon_r = 2.0$

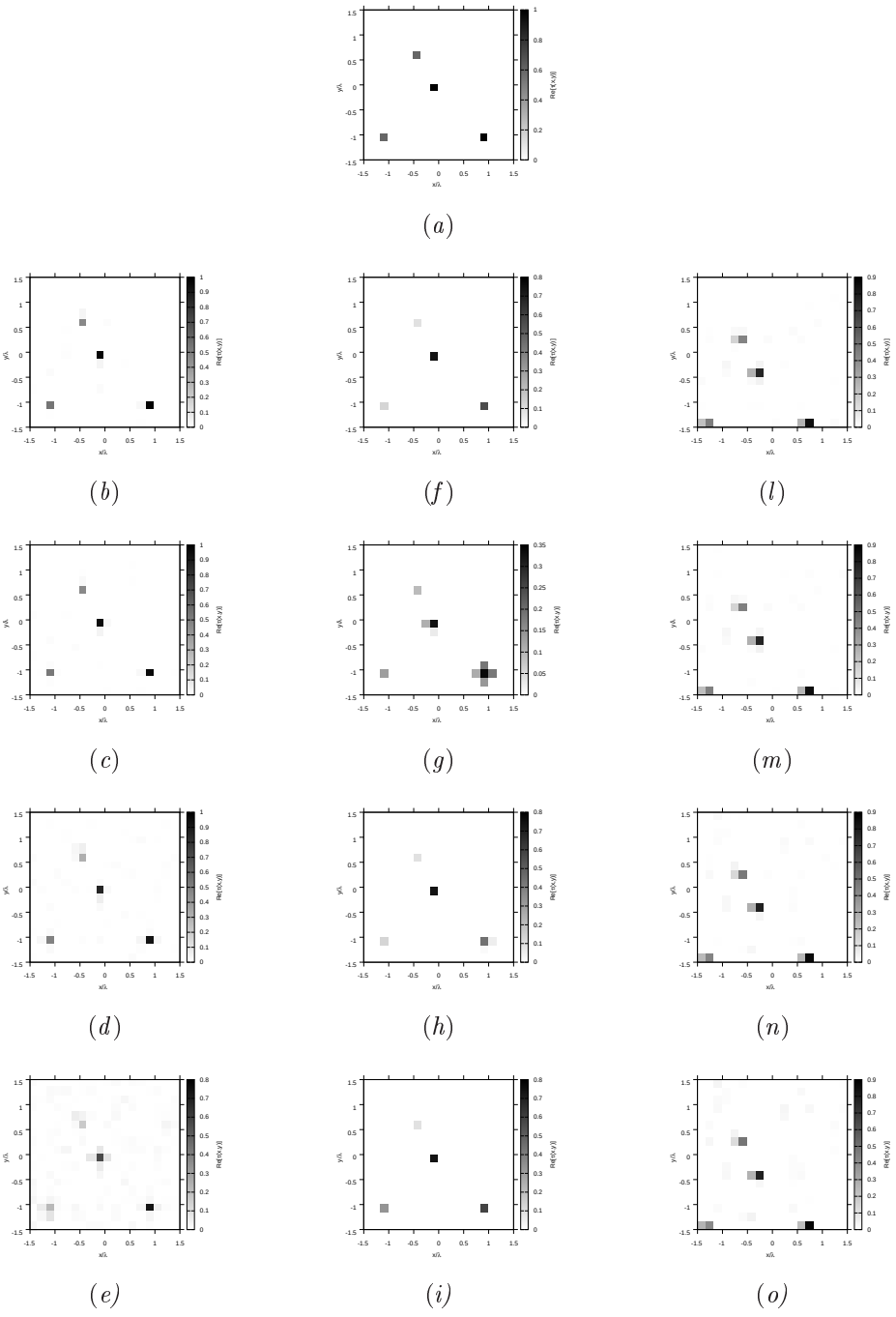

(a)

(b) (f) (l)

(c) (g) (m)

(d) (h) (n)

(e) (i) (o)

Figure 97. Actual object (a), (b)-(e) BCS reconstructed $(g)(i)$ GA-reconstructed, and (l)-(o) CG reconstructed object for $(b)(f)(l)$ Noiseless case, $(c)(g)(m)$ $SNR = 20$ [dB] , $(d)(h)(n)$ $SNR = 10$ [dB] , $(e)(i)(o)$ $SNR = 5$ [dB].

RESULTS: $\varepsilon_r = 2.0$

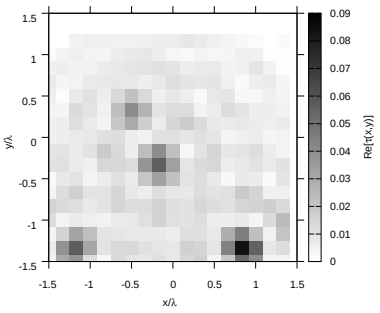

Figure 98. Actual object - Born approximation SVD-based approach reconstructed (Noiseless case)

SNR	Noiseless				20 [dB]			
	BCS	GA	CG	SVD	BCS	GA	CG	SVD
ξ_{tot}	2.32×10^{-3}	2.96×10^{-3}	8.89×10^{-3}	1.55×10^{-2}	2.60×10^{-3}	6.30×10^{-3}	8.84×10^{-3}	–
ξ_{int}	3.50×10^{-2}	0.2395	0.2034	0.4043	4.29×10^{-2}	0.3189	0.2023	–
ξ_{ext}	6.46×10^{-4}	0.0000	6.46×10^{-3}	1.03×10^{-2}	7.80×10^{-4}	2.39×10^{-3}	6.42×10^{-3}	–

SNR	10 [dB]				5 [dB]			
	BCS	GA	CG	SVD	BCS	GA	CG	SVD
ξ_{tot}	5.40×10^{-3}	3.36×10^{-3}	9.06×10^{-3}	–	1.21×10^{-2}	2.52×10^{-3}	9.63×10^{-3}	–
ξ_{int}	8.94×10^{-2}	0.2543	0.2005	–	0.2140	0.2045	0.2017	–
ξ_{ext}	2.74×10^{-3}	2.19×10^{-4}	6.66×10^{-3}	–	6.85×10^{-3}	0.0000	7.23×10^{-3}	–

Table XVI. Comparison of error figures for BCS, GA, CG and SVD-based approach.

Observations

- In questo caso ricostruzioni migliori ottenute mediante BCS per i casi $Noiseless$ e $SNR = 20\,dB$, ricostuzioni invece più pulite ottenute mediante GA per i casi con maggiore rumore, ma con errore interno sempre inferiore per le ricostruzioni ottenute mediante BCS rispetto alle ricostruzioni con GA.

RESULTS: $\varepsilon_r = 2.5$

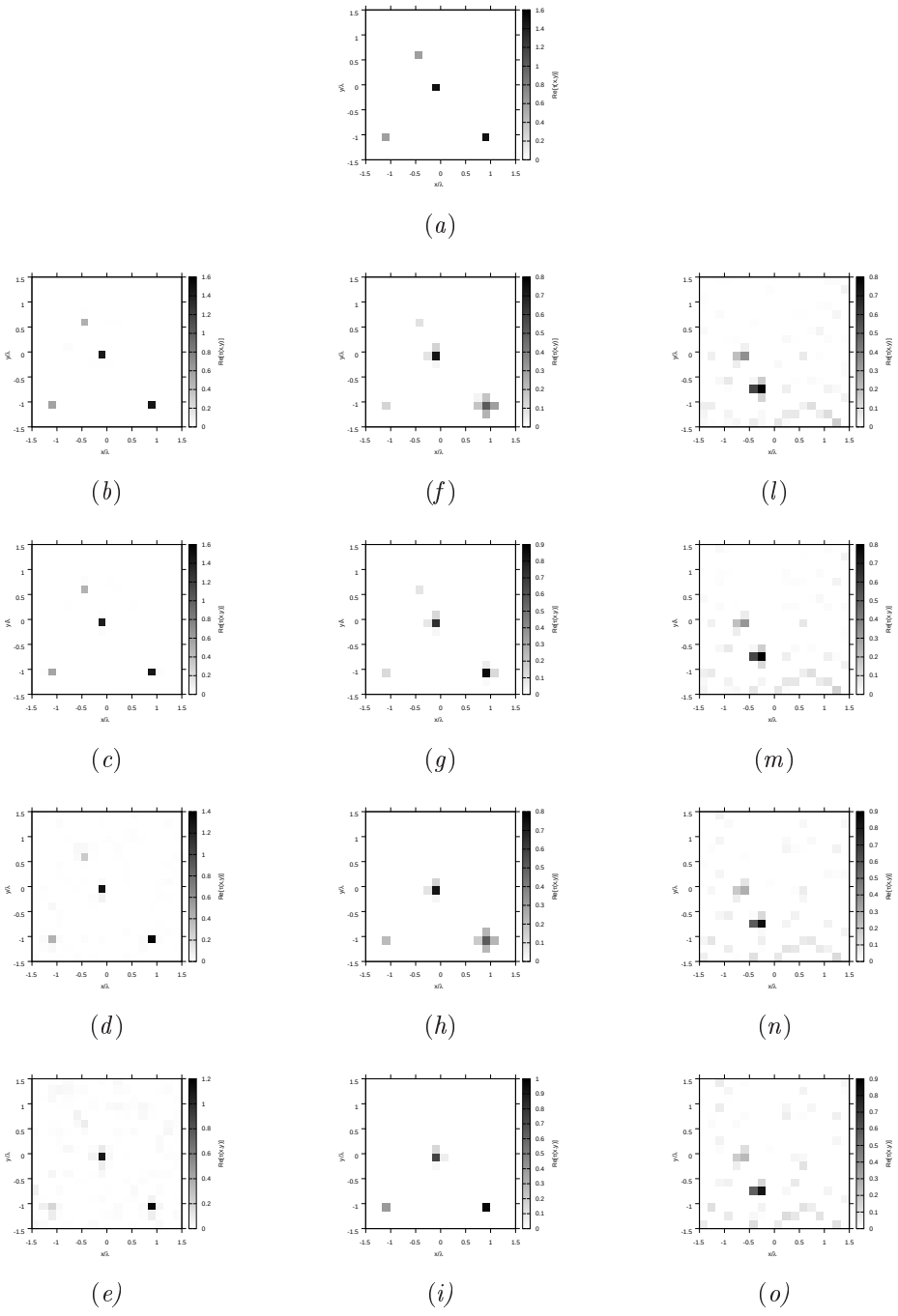

Figure 99. Actual object (a), (b)-(e) BCS reconstructed $(g)(i)$ GA-reconstructed, and (l)-(o) CG reconstructed object for $(b)(f)(l)$ Noiseless case, $(c)(g)(m)$ $SNR = 20$ [dB] , $(d)(h)(n)$ $SNR = 10$ [dB] , $(e)(i)(o)$ $SNR = 5$ [dB].

RESULTS: $\varepsilon_r = 2.5$

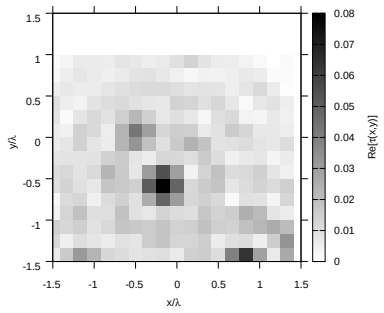

Figure 100. Actual object - Born approximation SVD-based approach reconstructed (Noiseless case)

SNR	Noiseless				20 [dB]			
	BCS	GA	CG	SVD	BCS	GA	CG	SVD
ξ_{tot}	2.75×10^{-3}	7.74×10^{-3}	1.13×10^{-2}	1.96×10^{-2}	3.08×10^{-3}	5.05×10^{-3}	1.13×10^{-2}	–
ξ_{int}	2.85×10^{-2}	0.3270	0.2645	0.4517	3.57×10^{-2}	0.2920	0.2672	–
ξ_{ext}	2.81×10^{-4}	3.75×10^{-3}	9.78×10^{-3}	1.31×10^{-2}	5.42×10^{-4}	1.46×10^{-3}	9.73×10^{-3}	–

SNR	10 [dB]				5 [dB]			
	BCS	GA	CG	SVD	BCS	GA	CG	SVD
ξ_{tot}	8.13×10^{-3}	7.48×10^{-3}	1.15×10^{-2}	–	1.62×10^{-2}	3.92×10^{-3}	1.21×10^{-2}	–
ξ_{int}	0.1087	0.3289	0.2712	–	0.2182	0.2542	0.2813	–
ξ_{ext}	3.78×10^{-3}	3.46×10^{-3}	9.92×10^{-3}	–	9.13×10^{-3}	7.89×10^{-4}	1.04×10^{-2}	–

Table XVII. Comparison of error figures for BCS, GA, CG and SVD-based approach.

Observations

- In questo caso ricostruzioni migliori ottenute mediante BCS per i casi $Noiseless$ e $SNR = 20\,dB$, ricostuzioni invece più pulite ottenute mediante GA per i casi con maggiore rumore, ma con errore interno sempre inferiore per le ricostruzioni ottenute mediante BCS rispetto alle ricostruzioni con GA.

RESULTS: $\varepsilon_r = 3.0$

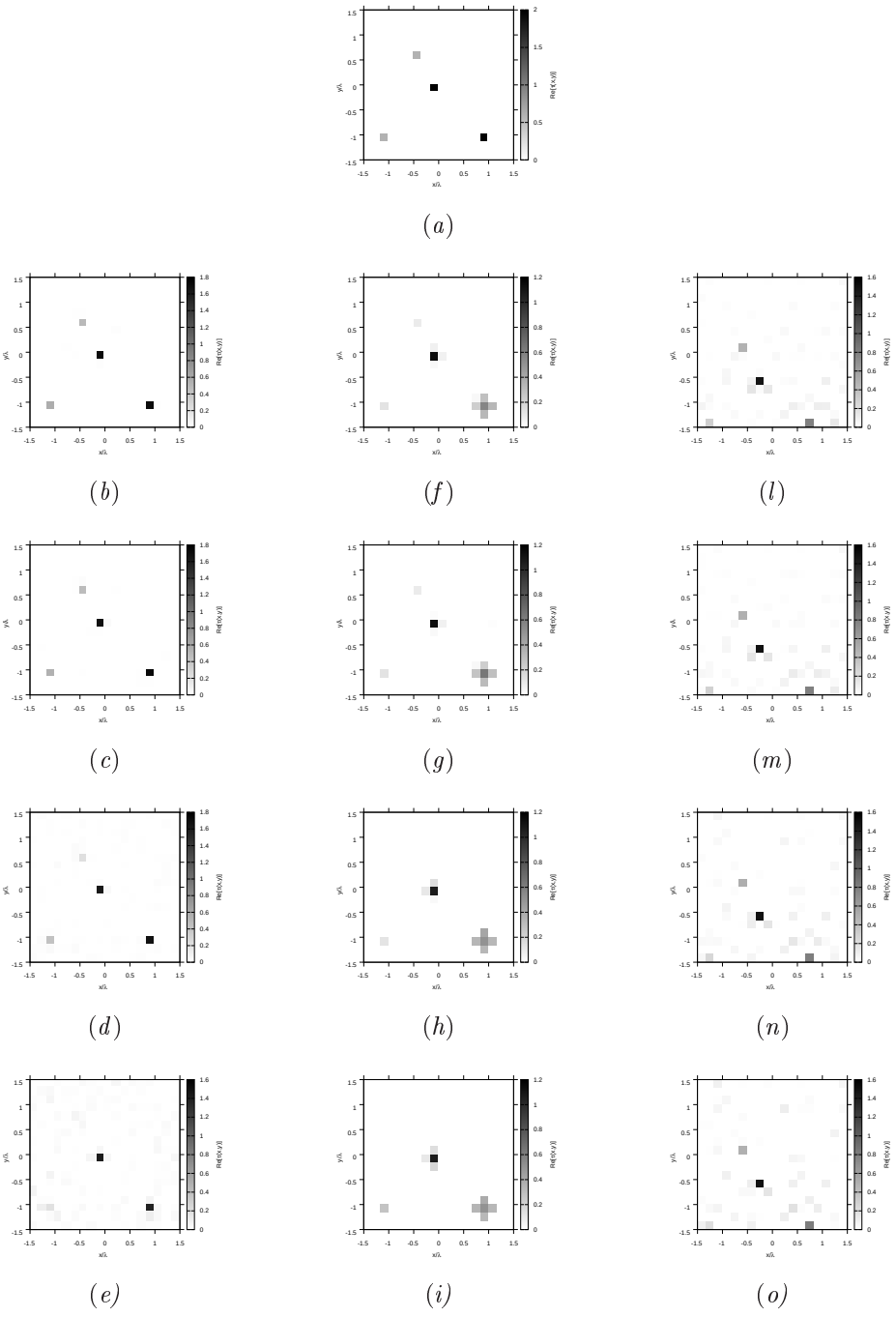

Figure 101. Actual object (a), (b)-(e) BCS reconstructed $(g)(i)$ GA-reconstructed, and (l)-(o) CG reconstructed object for $(b)(f)(l)$ Noiseless case, $(c)(g)(m)$ $SNR = 20$ [dB] , $(d)(h)(n)$ $SNR = 10$ [dB] , $(e)(i)(o)$ $SNR = 5$ [dB].

RESULTS: $\varepsilon_r = 3.0$

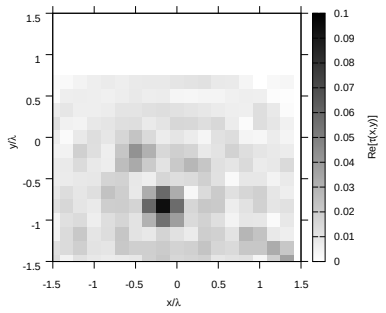

Figure 102. Actual object - Born approximation SVD-based approach reconstructed (Noiseless case)

SNR	Noiseless				20 [dB]			
	BCS	GA	CG	SVD	BCS	GA	CG	SVD
ξ_{tot}	3.64×10^{-3}	8.55×10^{-3}	1.10×10^{-2}	2.31×10^{-2}	4.37×10^{-3}	8.13×10^{-3}	1.08×10^{-2}	–
ξ_{int}	6.61×10^{-2}	0.3425	0.1242	0.4857	7.44×10^{-2}	0.3377	0.1155	–
ξ_{ext}	2.67×10^{-4}	4.38×10^{-3}	1.03×10^{-2}	1.48×10^{-2}	7.64×10^{-4}	4.01×10^{-3}	1.02×10^{-2}	–

SNR	10 [dB]				5 [dB]			
	BCS	GA	CG	SVD	BCS	GA	CG	SVD
ξ_{tot}	1.06×10^{-2}	9.90×10^{-3}	1.11×10^{-2}	–	2.06×10^{-2}	1.01×10^{-2}	1.17×10^{-2}	–
ξ_{int}	0.1416	0.3695	0.1136	–	0.2488	0.3450	0.1167	–
ξ_{ext}	4.75×10^{-3}	5.41×10^{-3}	1.04×10^{-2}	–	1.12×10^{-2}	5.87×10^{-3}	1.11×10^{-2}	–

Table XVIII. Comparison of error figures for BCS, GA, CG and SVD-based approach.

Observations

- In questo caso ricostruzioni migliori ottenute mediante BCS per i casi $Noiseless$ e $SNR = 20\,dB$, ricostuzioni invece più pulite ottenute mediante GA per i casi con maggiore rumore, ma con errore interno sempre inferiore per le ricostruzioni ottenute mediante BCS rispetto alle ricostruzioni con GA.

6 TEST CASE: Low Number of Views - Square Cylinder

Goal: compare the performances of BCS, GA and CG

- Number of Views: V
- Number of Measurements: M
- Number of Cells for the Inversion: N
- Number of Cells for the Direct solver: D
- Side of the investigation domain: L

Test Case Description

Direct solver:

- Square domain divided in $\sqrt{D} \times \sqrt{D}$ cells
- Domain side: $L = 3\lambda$
- $D = 1296$ (discretization for the direct solver: $< \lambda/10$)

Investigation domain:

- Square domain divided in $\sqrt{N} \times \sqrt{N}$ cells
- $L = 3\lambda$
- $2ka = 2 \times \frac{2\pi}{\lambda} \times \frac{L\sqrt{2}}{2} = 6\pi\sqrt{2} = 26.65$
- $\#DOF = \frac{(2ka)^2}{2} = \frac{(2\times\frac{2\pi}{\lambda}\times\frac{L\sqrt{2}}{2})^2}{2} = 4\pi^2\left(\frac{L}{\lambda}\right)^2 = 4\pi^2 \times 9 \approx 355.3$
- N scelto in modo da essere vicino a $\#DOF$: $N = 324$ (18×18)

Measurement domain:

- Measurement points taken on a circle of radius $\rho = 3\lambda$
- Full-aspect measurements
- $M \approx 2ka \rightarrow M = 27$

Sources:

- Plane waves
- $V = 4$
- Amplitude $A = 1$
- Frequency: 300 MHz $(\lambda = 1)$

Object:

- Square cylinder of side $\frac{\lambda}{6} = 0.1667$
- $\varepsilon_r \in \{1.5, 2.0, 2.5, 3.0\}$
- $\sigma = 0$ [S/m]

BCS parameters:

- Initial estimate of the noise: $n_0 = 1.0 \times 10^{-3}$
- Convergenze parameter: $\tau = 1.0 \times 10^{-8}$

CG parameters:

- Iterations: 200
- Peso stato: 0
- Peso dati: 1

GA parameters:

- Iterations: 10000
- Tournament Selection: $TRUE$
- Prob. Crossover: 0.8
- Prob. Mutation: 0.4
- Prob. Bit Muation: 0.05
- Prob. New Generation: 0.01
- Elitism: $TRUE$
- Crossover Child: 1
- Population: 200
- Convergence Threshold: 0.001

RESULTS: $\varepsilon_r = 1.5$

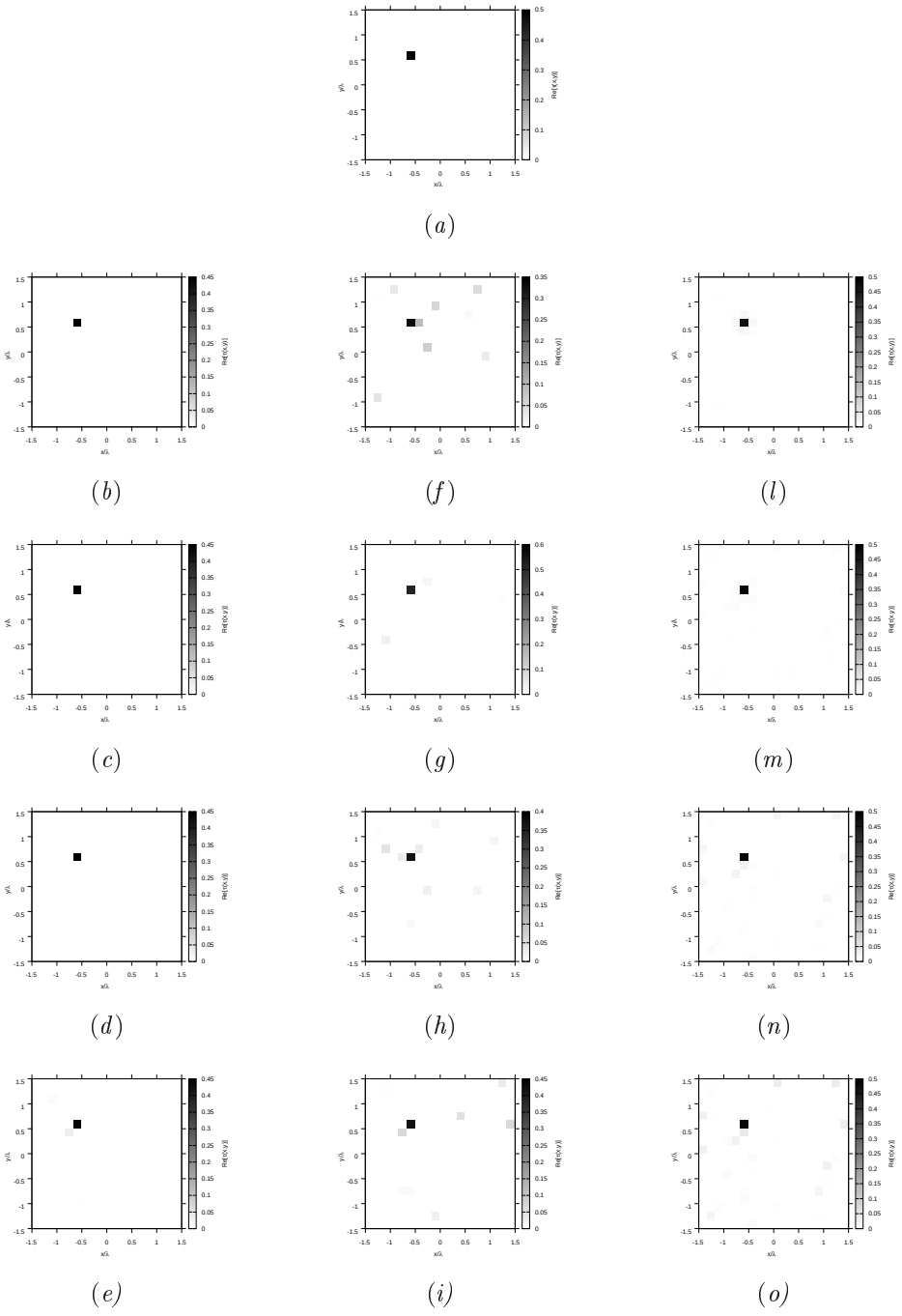

Figure 103. Actual object (a), (b)-(e) BCS reconstructed $(g)(i)$ GA-reconstructed, and (l)-(o) CG reconstructed object for $(b)(f)(l)$ Noiseless case, $(c)(g)(m)$ $SNR = 20$ [dB] , $(d)(h)(n)$ $SNR = 10$ [dB] , $(e)(i)(o)$ $SNR = 5$ [dB].

RESULTS: $\varepsilon_r = 2.0$

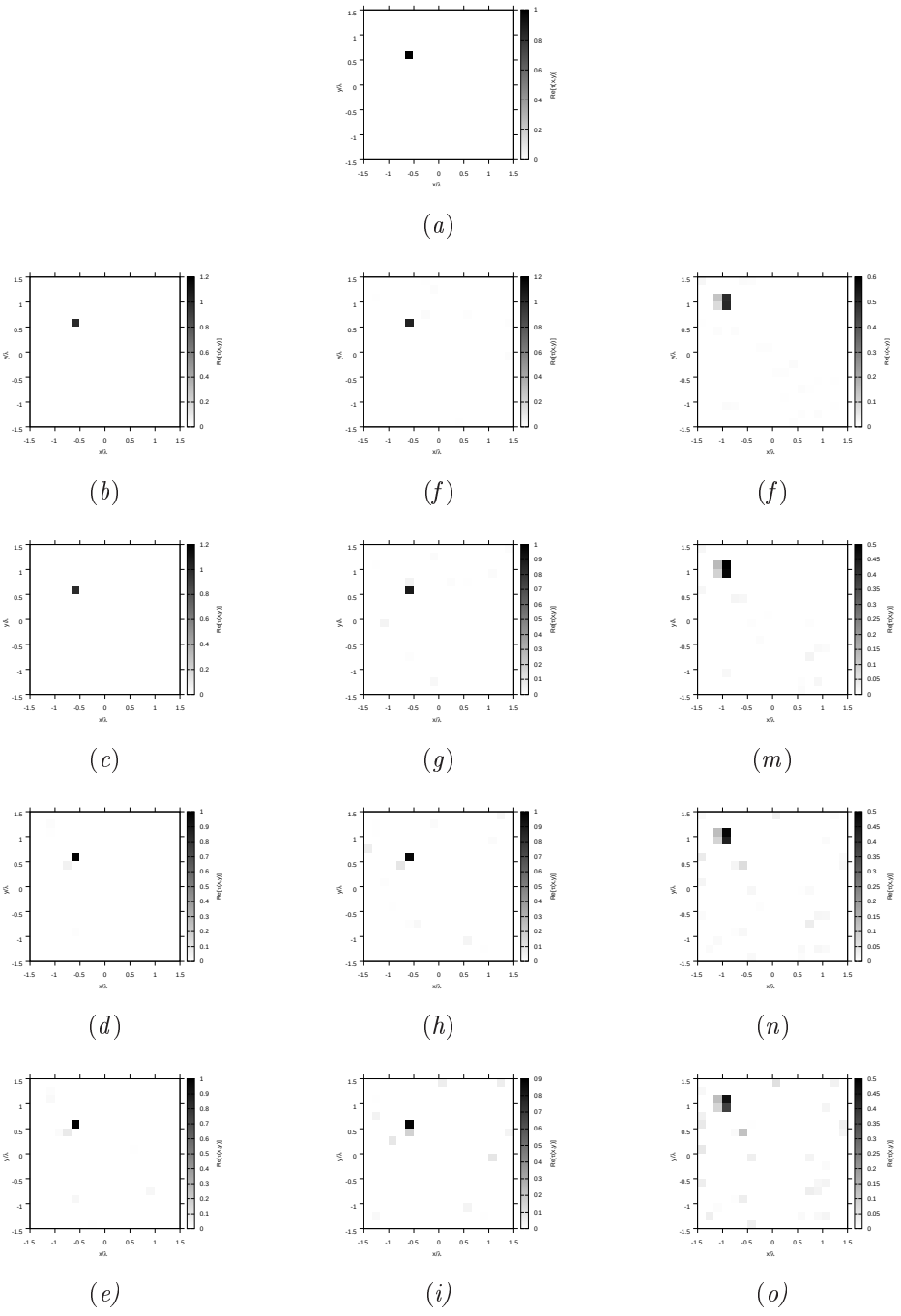

(a)

(b) (f) (f)

(c) (g) (m)

(d) (h) (n)

(e) (i) (o)

Figure 104. Actual object (a), (b)-(e) BCS reconstructed $(g)(i)$ GA-reconstructed, and (l)-(o) CG reconstructed object for $(b)(f)(l)$ Noiseless case, $(c)(g)(m)$ $SNR = 20$ [dB] , $(d)(h)(n)$ $SNR = 10$ [dB] , $(e)(i)(o)$ $SNR = 5$ [dB].

RESULTS: $\varepsilon_r = 2.5$

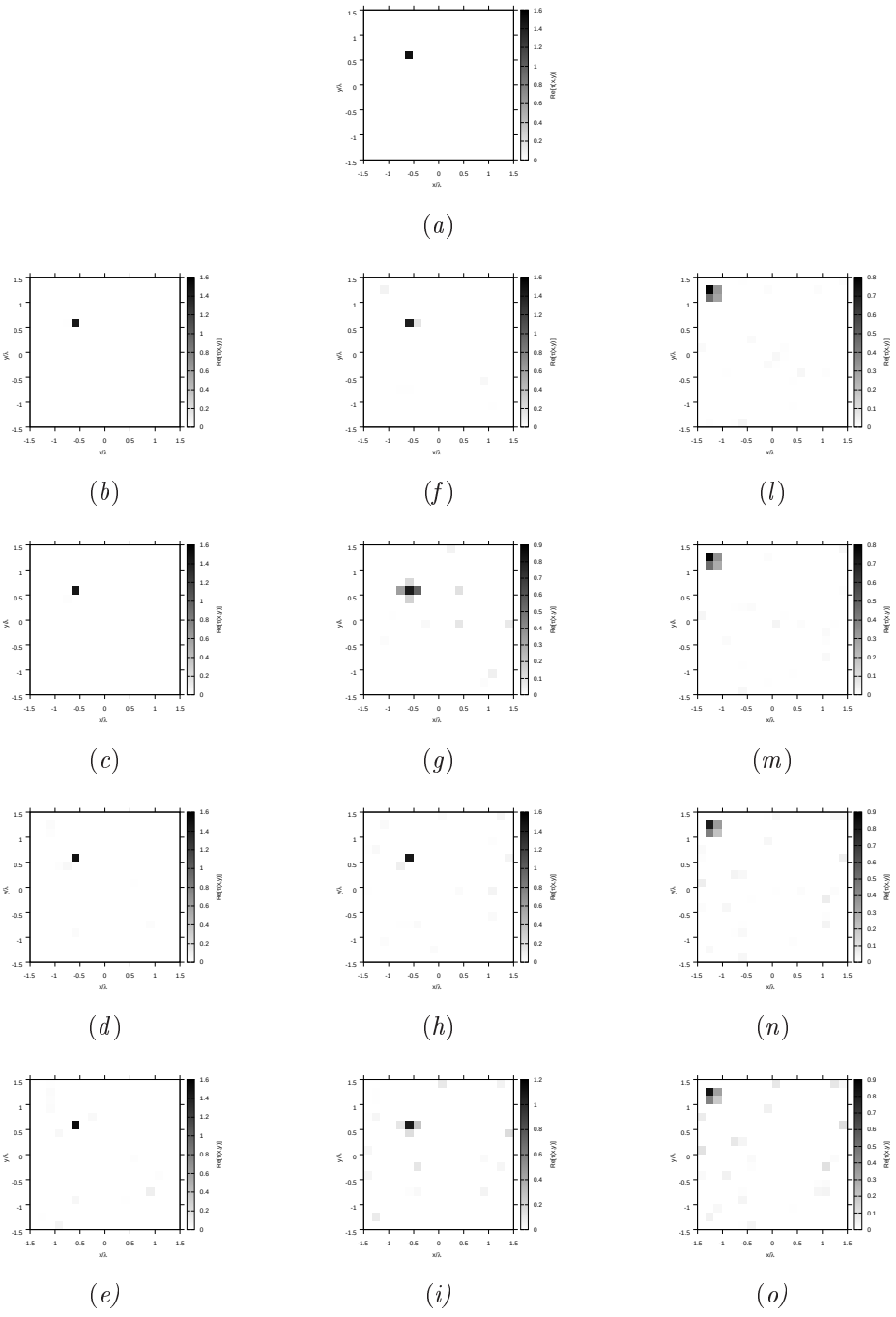

Figure 105. Actual object (a), (b)-(e) BCS reconstructed $(g)(i)$ GA-reconstructed, and (l)-(o) CG reconstructed object for $(b)(f)(l)$ Noiseless case, $(c)(g)(m)$ $SNR = 20$ [dB] , $(d)(h)(n)$ $SNR = 10$ [dB] , $(e)(i)(o)$ $SNR = 5$ [dB].

RESULTS: $\varepsilon_r = 3.0$

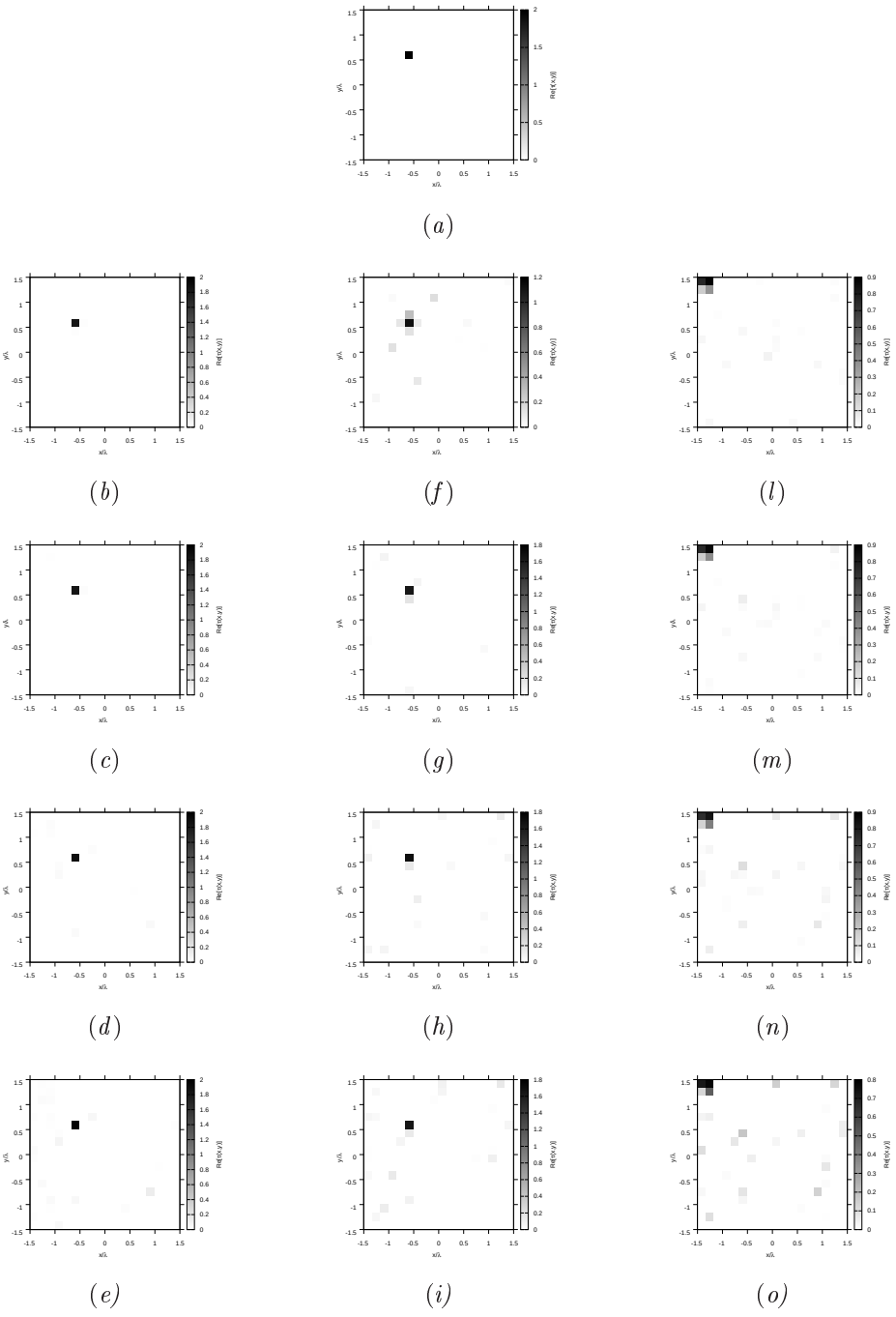

Figure 106. Actual object (a), (b)-(e) BCS reconstructed $(g)(i)$ GA-reconstructed, and (l)-(o) CG reconstructed object for $(b)(f)(l)$ Noiseless case, $(c)(g)(m)$ $SNR = 20$ [dB] , $(d)(h)(n)$ $SNR = 10$ [dB] , $(e)(i)(o)$ $SNR = 5$ [dB].

RESULTS Comparison: $\varepsilon_r = 1.5$

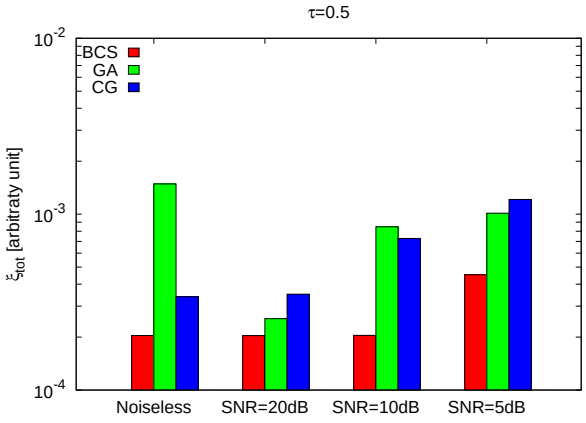

(a)

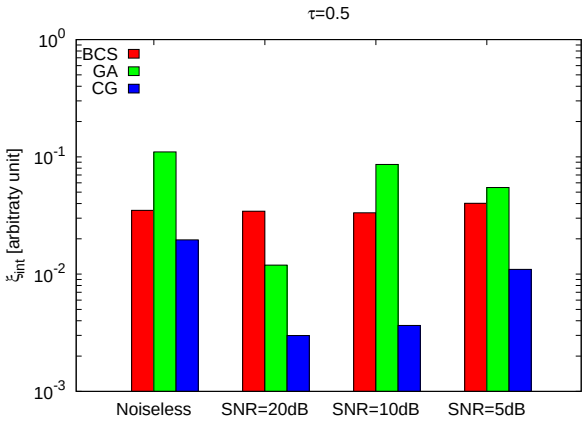

(b)

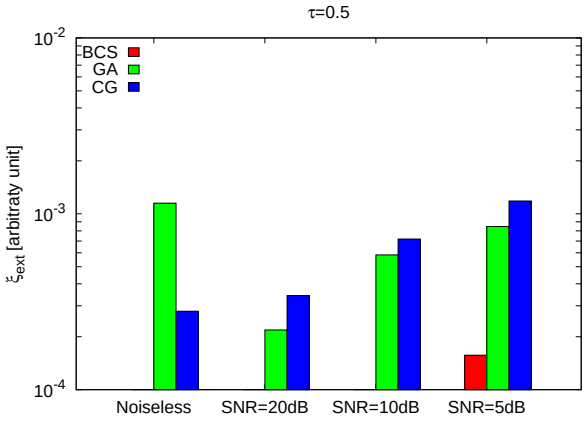

(c)

Figure 107. Behaviour of error figures for different SNR values: (a) total error ξ_{tot}, (b) internal error ξ_{int}, (c) external error ξ_{ext}.

RESULTS Comparison: $\varepsilon_r = 2.0$

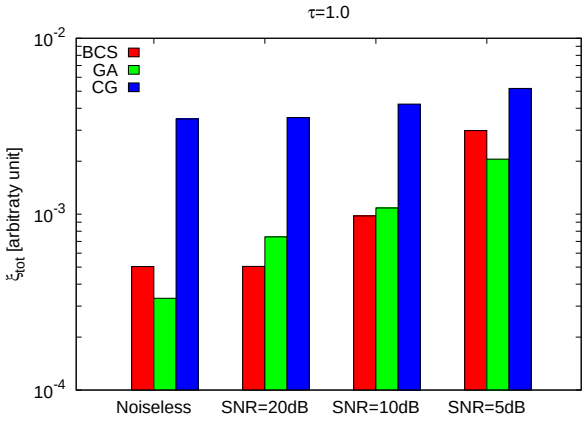

(a)

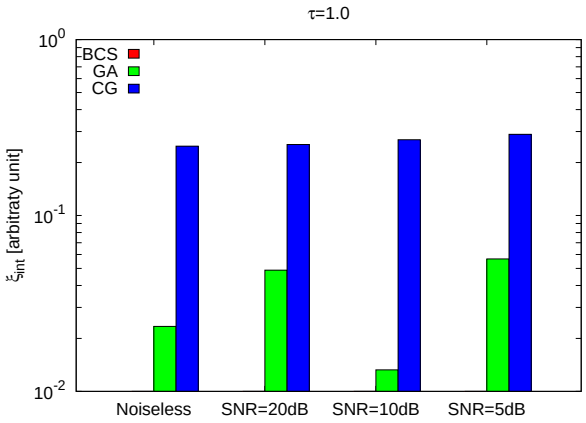

(b)

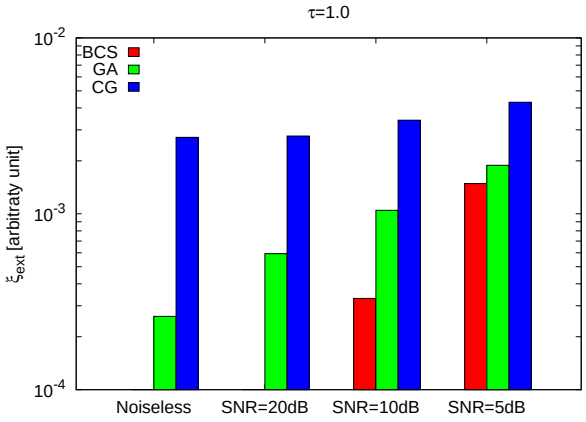

(c)

Figure 108. Behaviour of error figures for different SNR values: (a) total error ξ_{tot}, (b) internal error ξ_{int}, (c) external error ξ_{ext}.

RESULTS Comparison: $\varepsilon_r = 2.5$

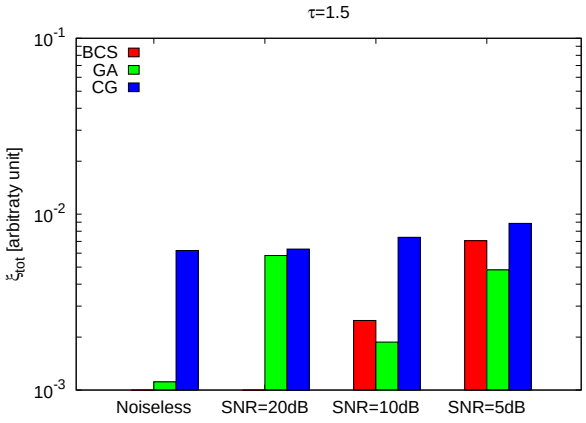

(a)

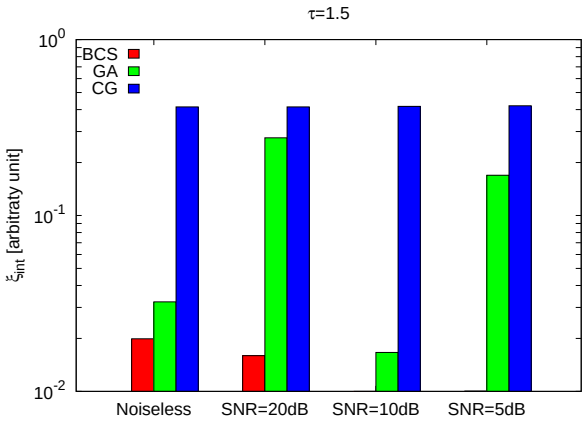

(b)

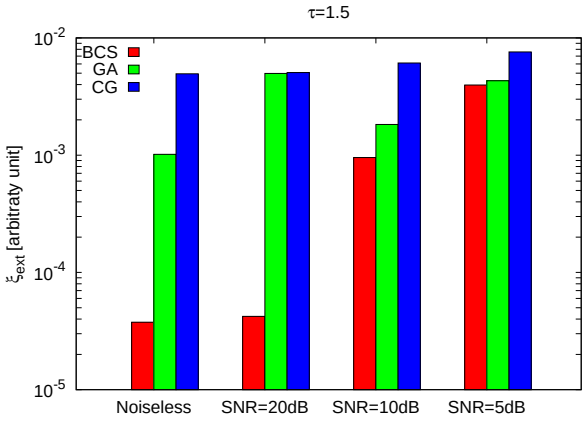

(c)

Figure 109. Behaviour of error figures for different SNR values: (a) total error ξ_{tot}, (b) internal error ξ_{int}, (c) external error ξ_{ext}.

RESULTS Comparison: $\varepsilon_r = 3.0$

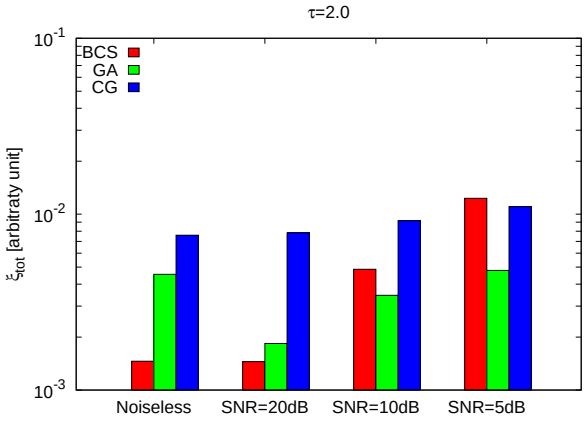

(a)

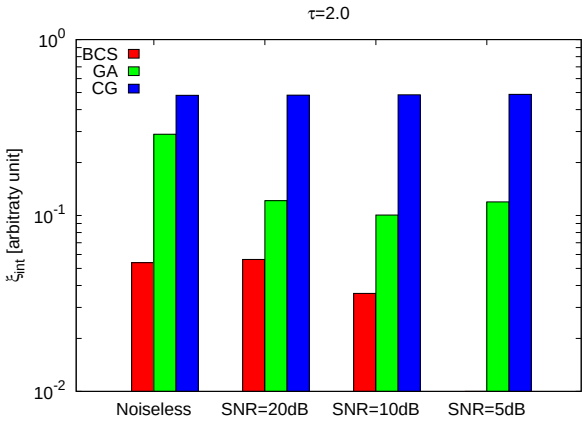

(b)

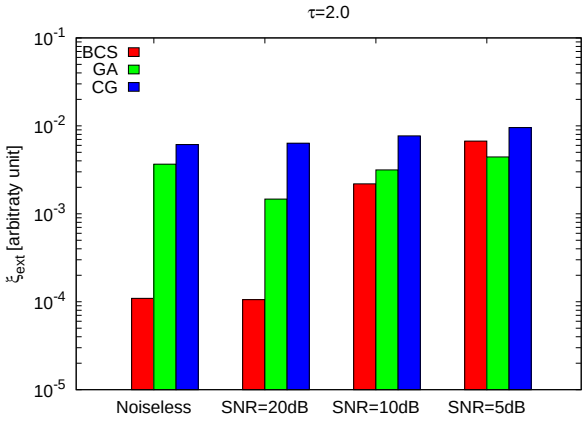

(c)

Figure 110. Behaviour of error figures for different SNR values: (a) total error ξ_{tot}, (b) internal error ξ_{int}, (c) external error ξ_{ext}.

RESULTS Comparison: *Noiseless*

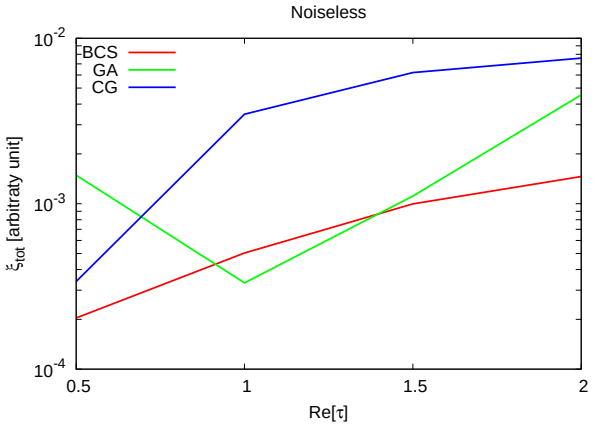

(a)

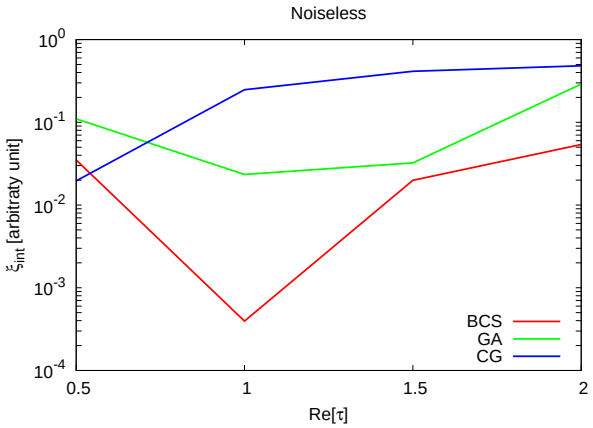

(b)

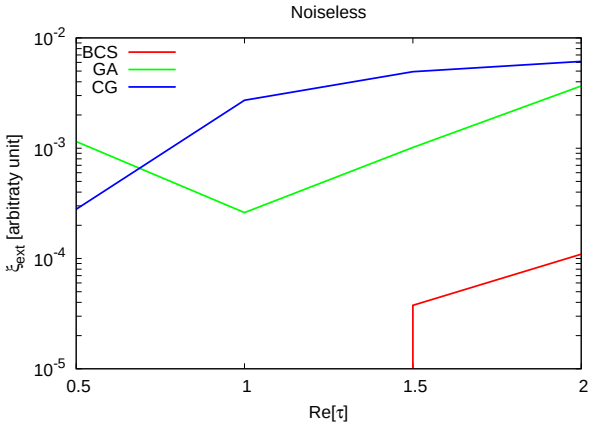

(c)

Figure 111. Behaviour of error figures as a function of ε_r: (a) total error ξ_{tot}, (b) internal error ξ_{int}, (c) external error ξ_{ext}.

RESULTS Comparison: $SNR = 20\,dB$

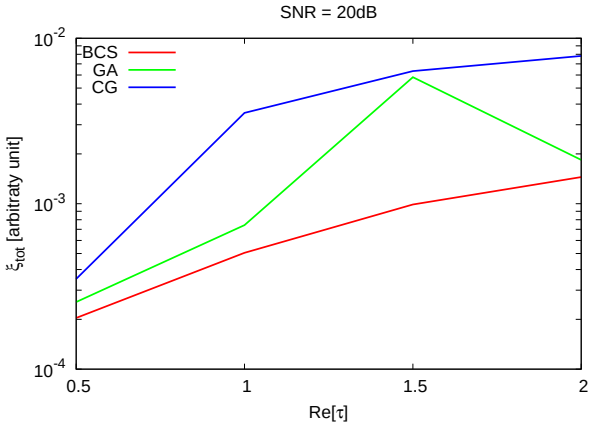

(a)

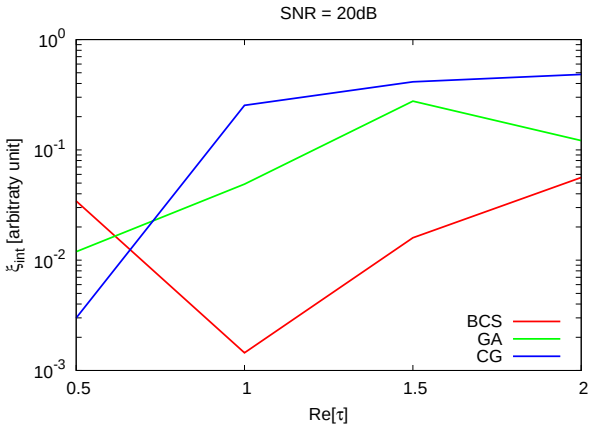

(b)

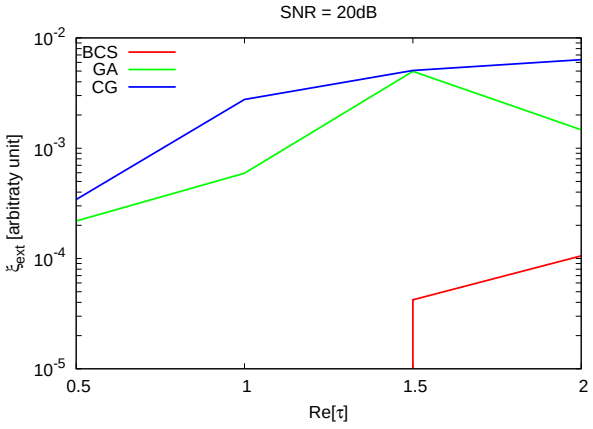

(c)

Figure 112. Behaviour of error figures as a function of ε_r: (a) total error ξ_{tot}, (b) internal error ξ_{int}, (c) external error ξ_{ext}.

RESULTS Comparison: $SNR = 10\,dB$

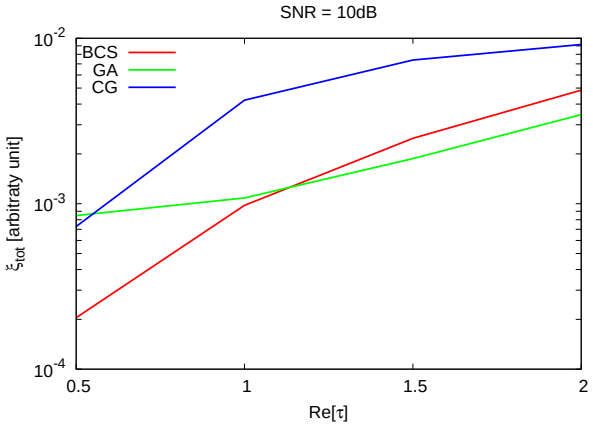

(a)

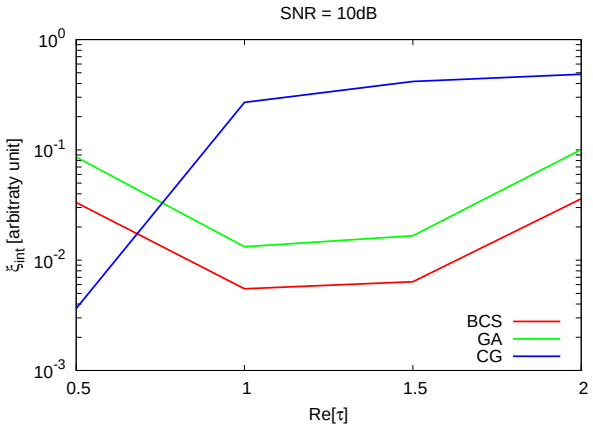

(b)

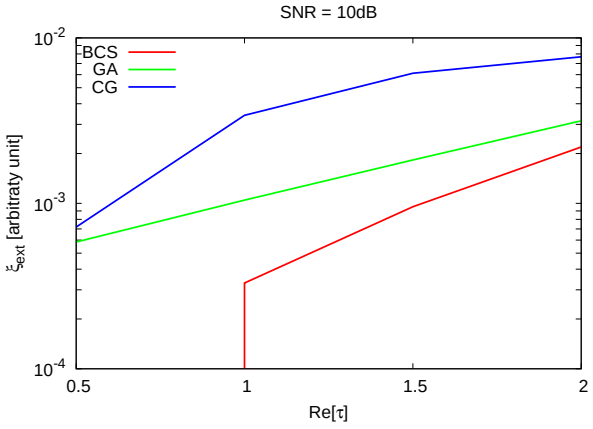

(c)

Figure 113. Behaviour of error figures as a function of ε_r: (a) total error ξ_{tot}, (b) internal error ξ_{int}, (c) external error ξ_{ext}.

RESULTS Comparison: $SNR = 5\,dB$

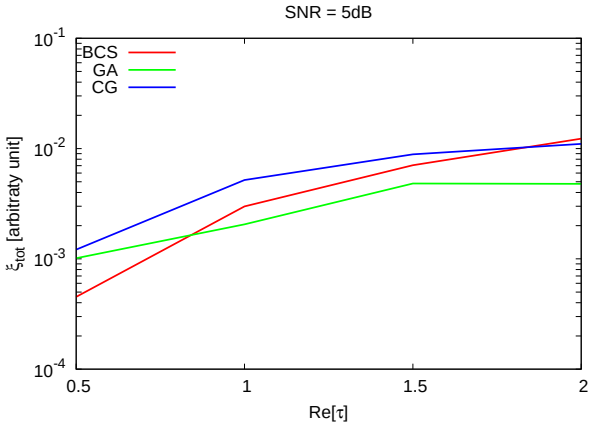

(a)

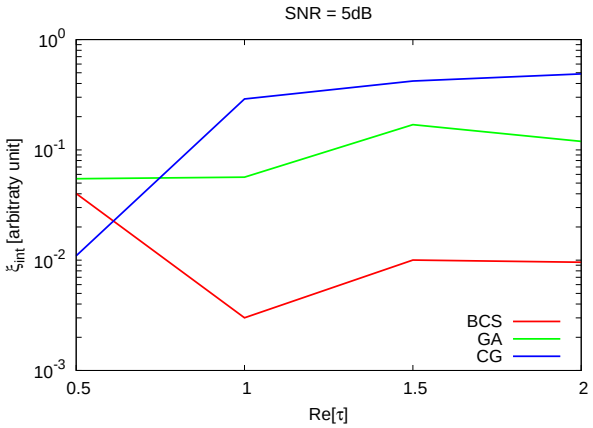

(b)

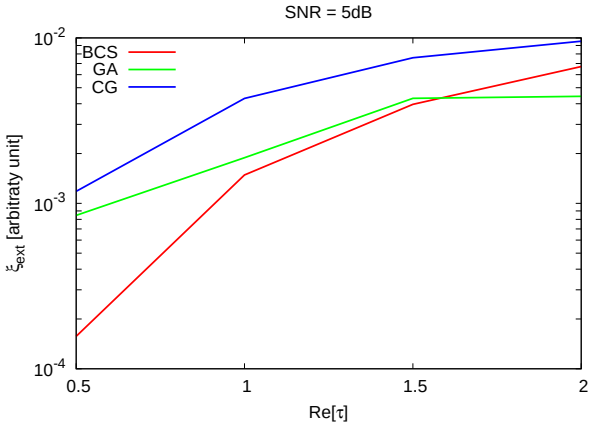

(c)

Figure 114. Behaviour of error figures as a function of ε_r: (a) total error ξ_{tot}, (b) internal error ξ_{int}, (c) external error ξ_{ext}.

7 TEST CASE: Low Number of Views - Two Square Cylinders

Goal: compare the performances of BCS, GA and CG

- Number of Views: V
- Number of Measurements: M
- Number of Cells for the Inversion: N
- Number of Cells for the Direct solver: D
- Side of the investigation domain: L

Test Case Description

Direct solver:

- Square domain divided in $\sqrt{D} \times \sqrt{D}$ cells
- Domain side: $L = 3\lambda$
- $D = 1296$ (discretization for the direct solver: $< \lambda/10$)

Investigation domain:

- Square domain divided in $\sqrt{N} \times \sqrt{N}$ cells
- $L = 3\lambda$
- $2ka = 2 \times \frac{2\pi}{\lambda} \times \frac{L\sqrt{2}}{2} = 6\pi\sqrt{2} = 26.65$
- $\#DOF = \frac{(2ka)^2}{2} = \frac{(2 \times \frac{2\pi}{\lambda} \times \frac{L\sqrt{2}}{2})^2}{2} = 4\pi^2 \left(\frac{L}{\lambda}\right)^2 = 4\pi^2 \times 9 \approx 355.3$
- N scelto in modo da essere vicino a $\#DOF$: $N = 324$ (18×18)

Measurement domain:

- Measurement points taken on a circle of radius $\rho = 3\lambda$
- Full-aspect measurements
- $M \approx 2ka \rightarrow M = 27$

Sources:

- Plane waves
- $V = 4$
- Amplitude $A = 1$
- Frequency: 300 MHz ($\lambda = 1$)

Object:

- Square cylinder of side $\frac{\lambda}{6} = 0.1667$
- $\varepsilon_r \in \{1.5, 2.0, 2.5, 3.0\}$ (one square), $\varepsilon_r = 1.9$ (one square)
- $\sigma = 0$ [S/m]

BCS parameters:

- Initial estimate of the noise: $n_0 = 1.0 \times 10^{-3}$
- Convergenze parameter: $\tau = 1.0 \times 10^{-8}$

CG parameters:

- Iterations: 200
- Peso stato: 0
- Peso dati: 1

GA parameters:

- Iterations: 10000
- Tournament Selection: $TRUE$
- Prob. Crossover: 0.8
- Prob. Mutation: 0.4
- Prob. Bit Muation: 0.05
- Prob. New Generation: 0.01
- Elitism: $TRUE$
- Crossover Child: 1
- Population: 200
- Convergence Threshold: 0.001

RESULTS: $\varepsilon_r = 1.5$

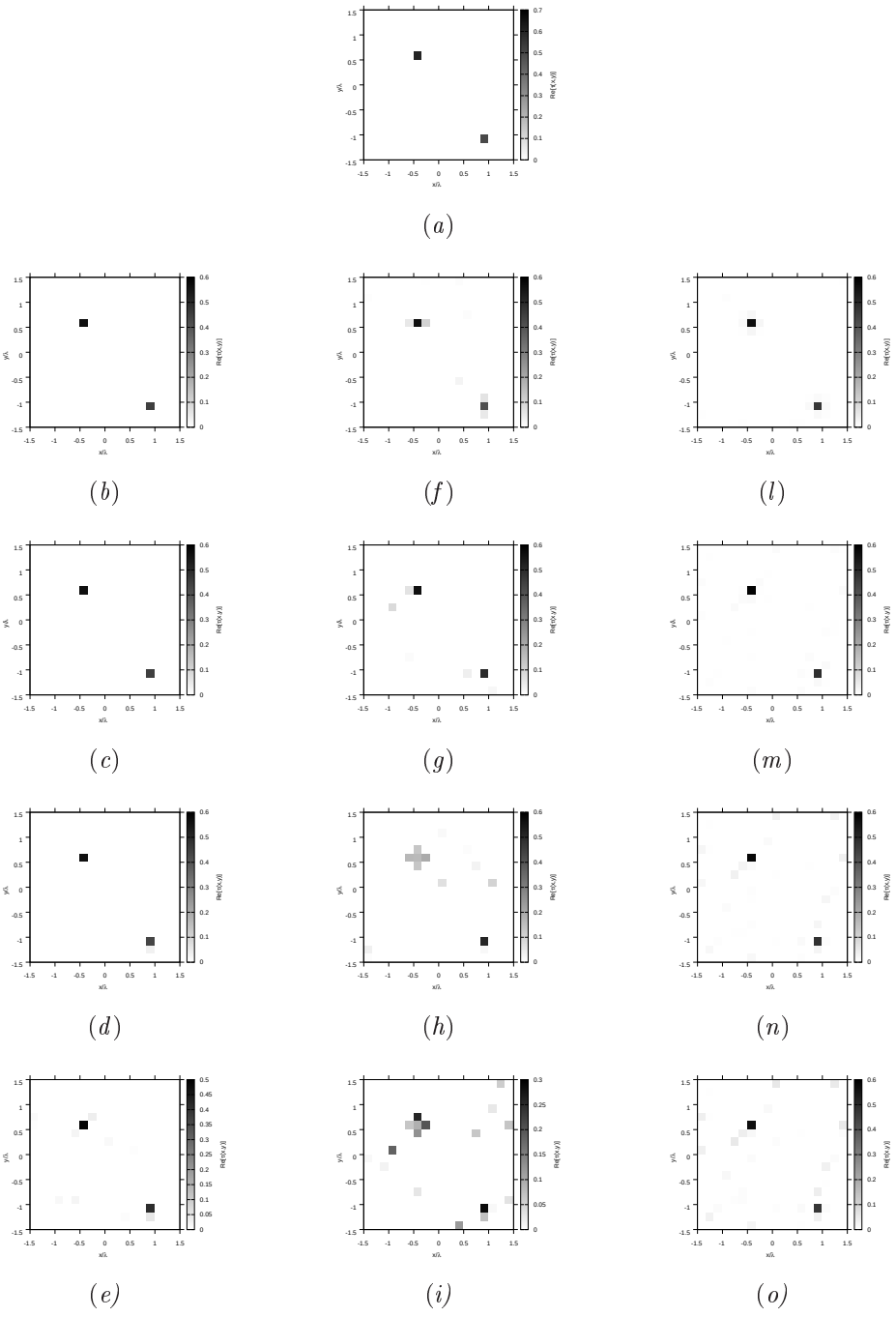

Figure 115. Actual object (a), (b)-(e) BCS reconstructed $(g)(i)$ GA-reconstructed, and (l)-(o) CG reconstructed object for $(b)(f)(l)$ Noiseless case, $(c)(g)(m)$ $SNR = 20$ [dB] , $(d)(h)(n)$ $SNR = 10$ [dB] , $(e)(i)(o)$ $SNR = 5$ [dB].

RESULTS: $\varepsilon_r = 2.0$

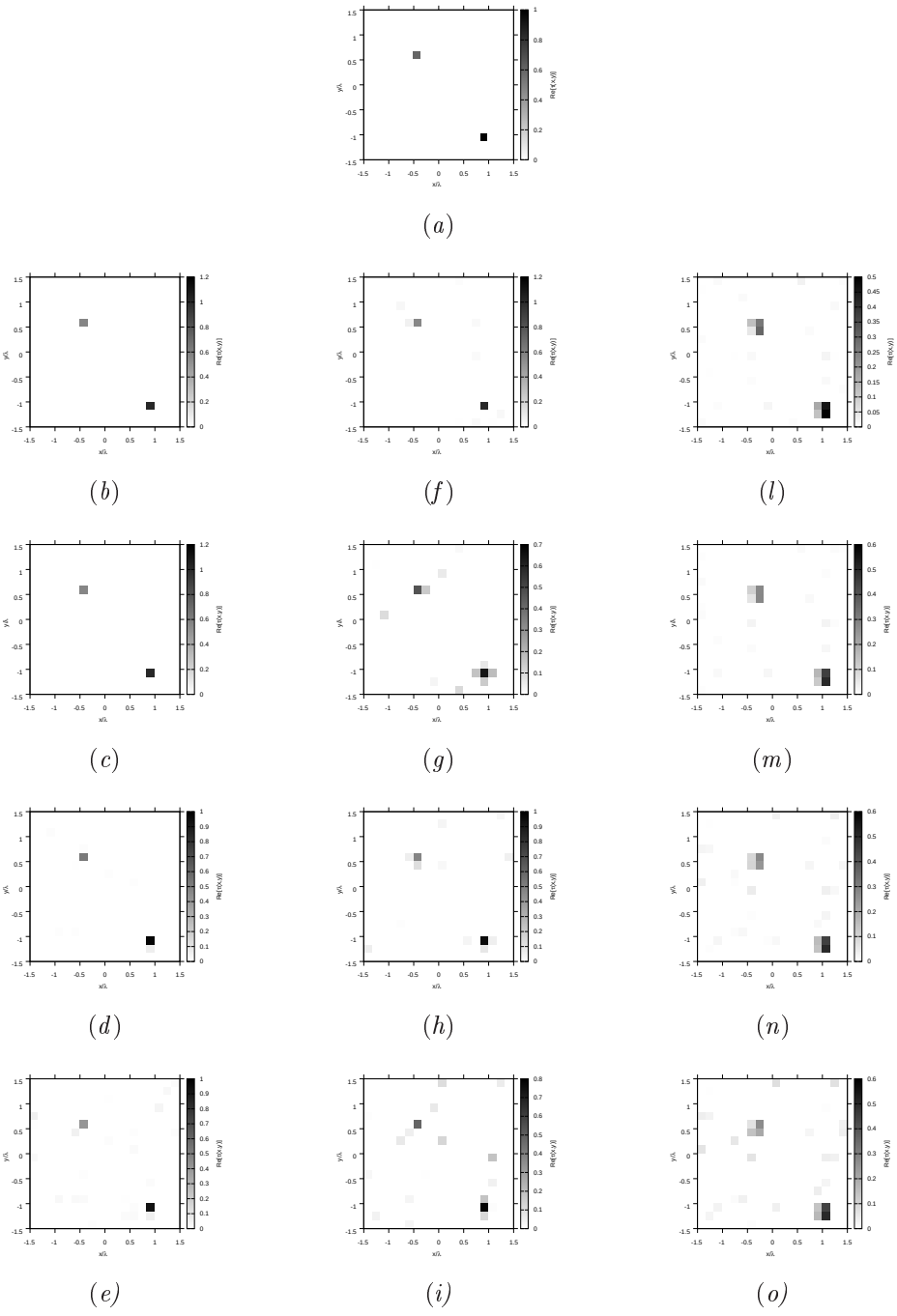

(a)

(b) (f) (l)

(c) (g) (m)

(d) (h) (n)

(e) (i) (o)

Figure 116. Actual object (a), (b)-(e) BCS reconstructed $(g)(i)$ GA-reconstructed, and (l)-(o) CG reconstructed object for $(b)(f)(l)$ Noiseless case, $(c)(g)(m)$ $SNR = 20$ [dB] , $(d)(h)(n)$ $SNR = 10$ [dB] , $(e)(i)(o)$ $SNR = 5$ [dB].

RESULTS: $\varepsilon_r = 2.5$

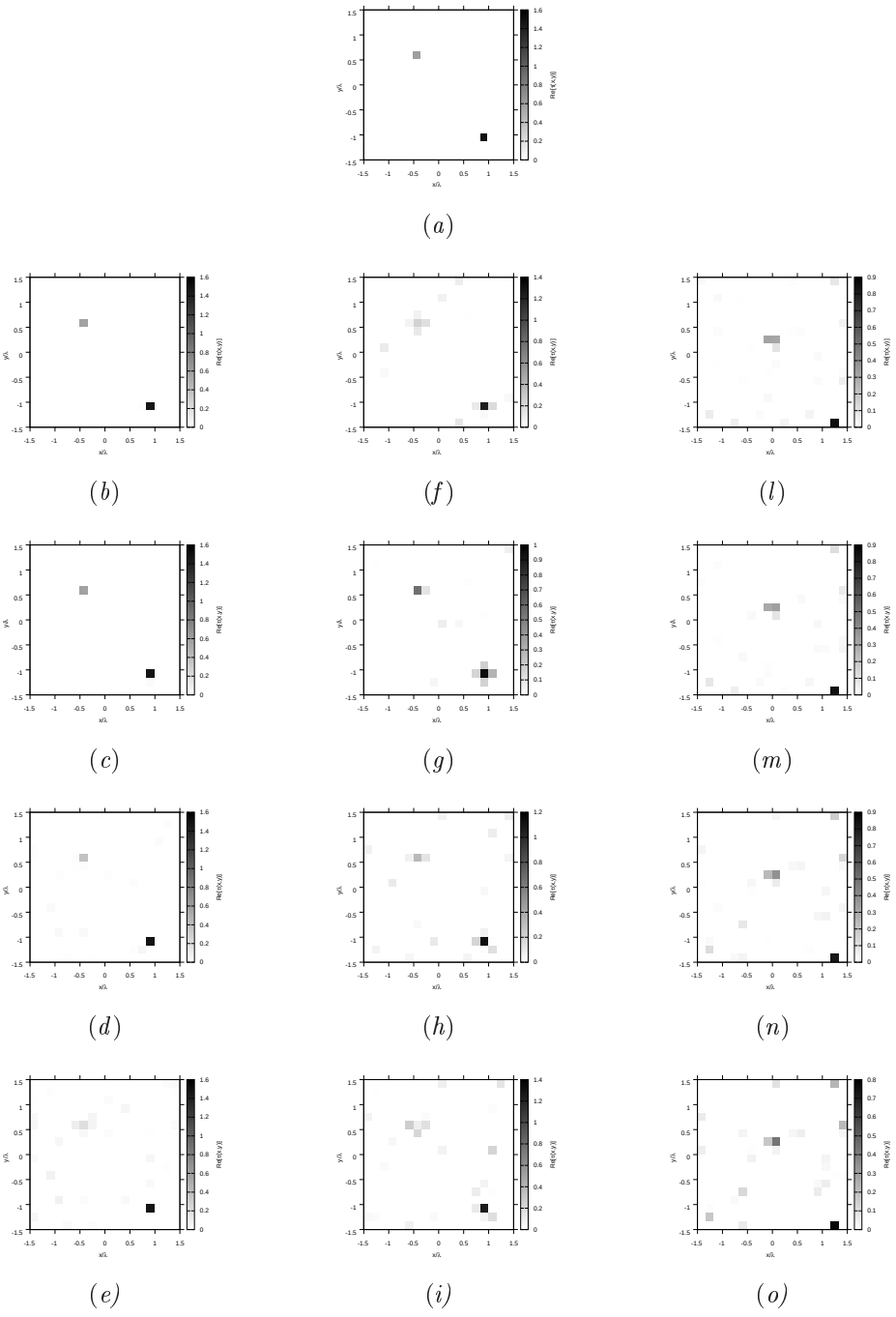

Figure 117. Actual object (a), (b)-(e) BCS reconstructed $(g)(i)$ GA-reconstructed, and (l)-(o) CG reconstructed object for $(b)(f)(l)$ Noiseless case, $(c)(g)(m)$ $SNR = 20$ [dB] , $(d)(h)(n)$ $SNR = 10$ [dB] , $(e)(i)(o)$ $SNR = 5$ [dB].

RESULTS: $\varepsilon_r = 3.0$

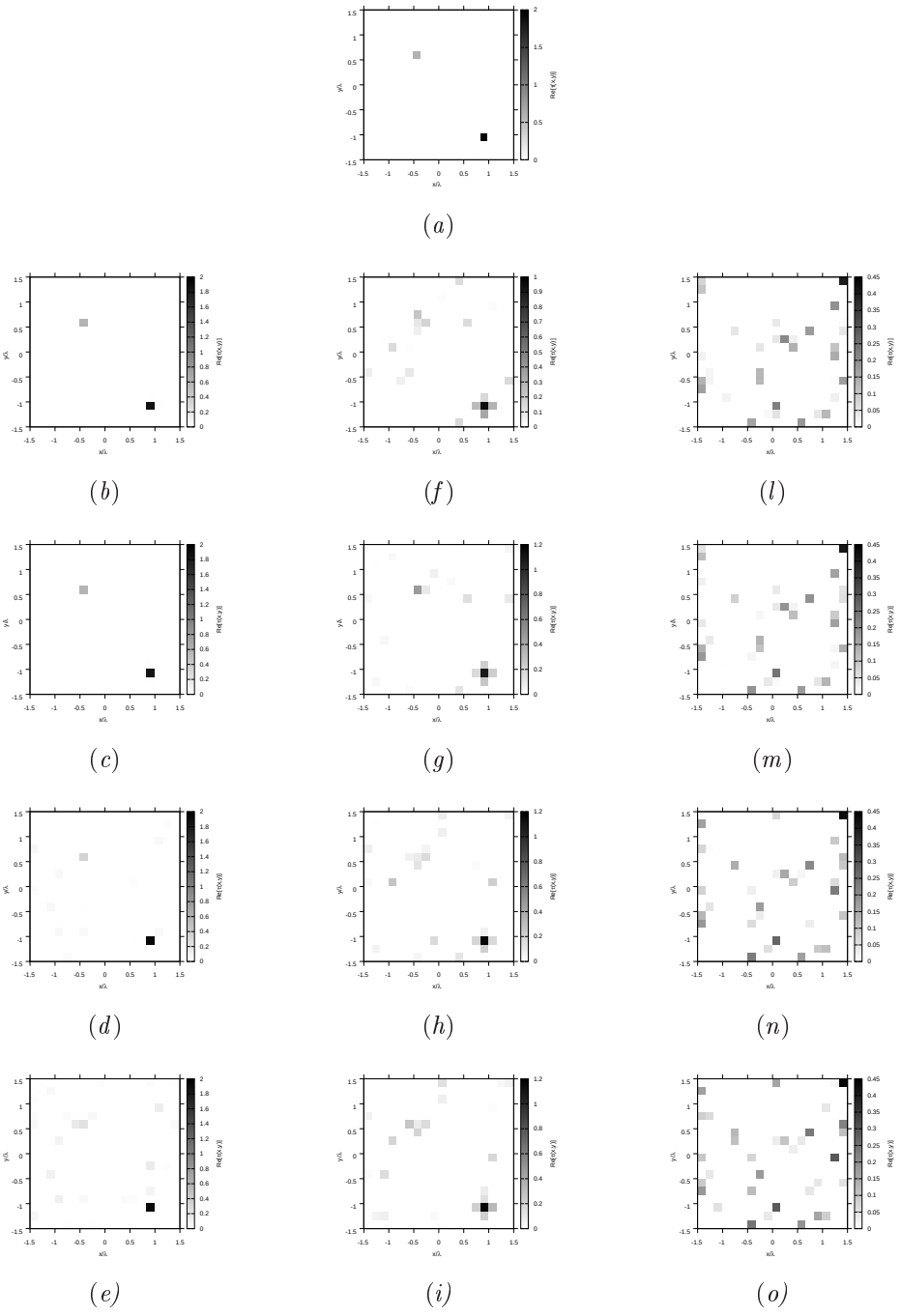

Figure 118. Actual object (a), (b)-(e) BCS reconstructed $(g)(i)$ GA-reconstructed, and (l)-(o) CG reconstructed object for $(b)(f)(l)$ Noiseless case, $(c)(g)(m)$ $SNR = 20$ [dB] , $(d)(h)(n)$ $SNR = 10$ [dB] , $(e)(i)(o)$ $SNR = 5$ [dB].

RESULTS Comparison: $\varepsilon_r = 1.5$

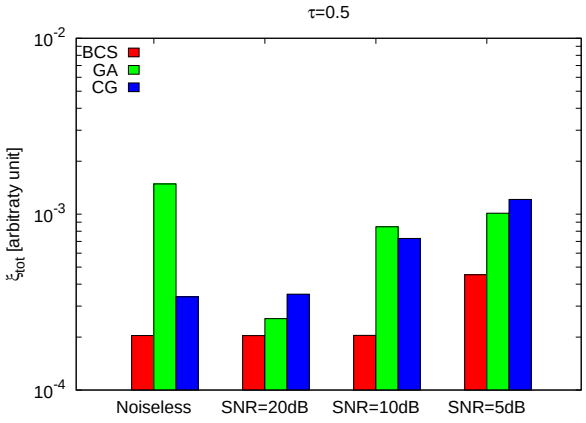

(a)

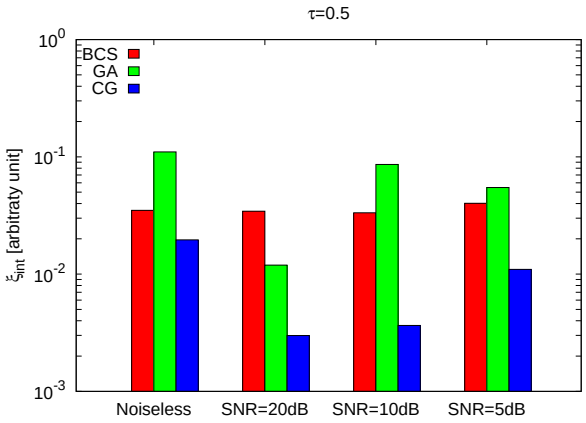

(b)

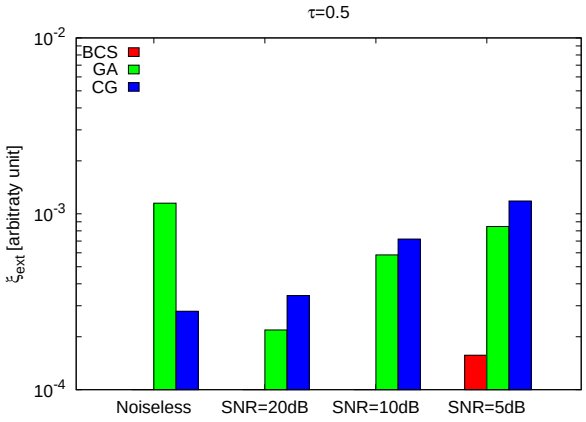

(c)

Figure 119. Behaviour of error figures for different SNR values: (a) total error ξ_{tot}, (b) internal error ξ_{int}, (c) external error ξ_{ext}.

RESULTS Comparison: $\varepsilon_r = 2.0$

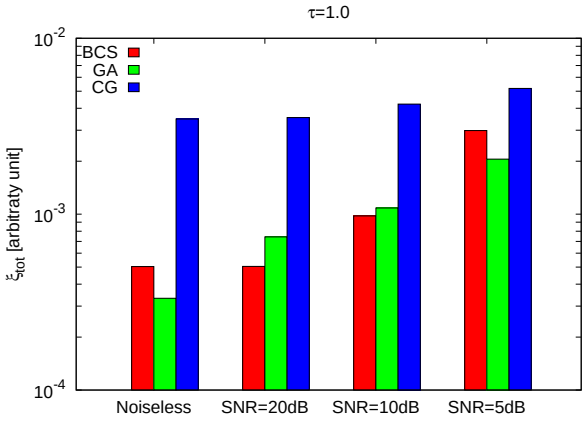

(a)

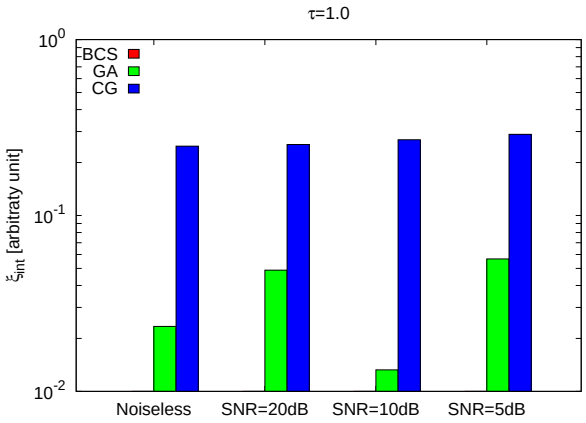

(b)

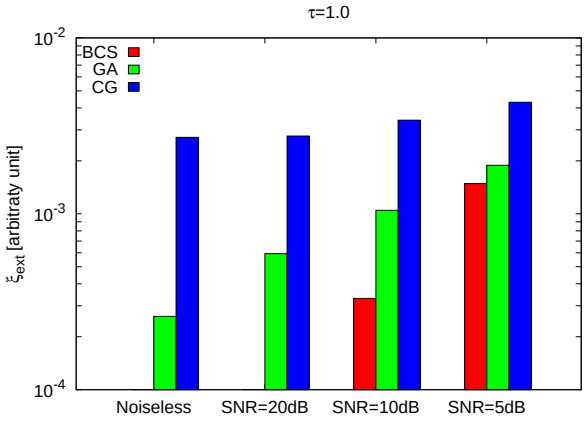

(c)

Figure 120. Behaviour of error figures for different SNR values: (a) total error ξ_{tot}, (b) internal error ξ_{int}, (c) external error ξ_{ext}.

RESULTS Comparison: $\varepsilon_r = 2.5$

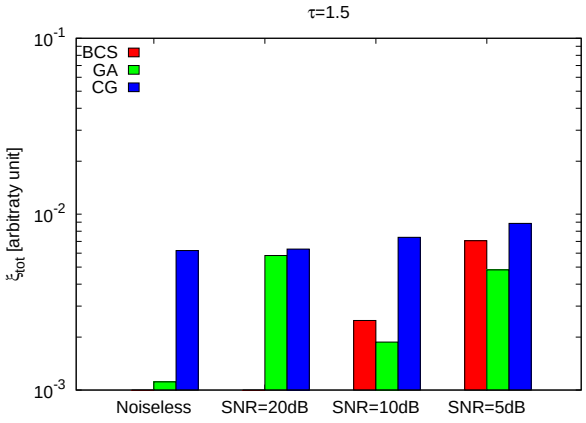

(a)

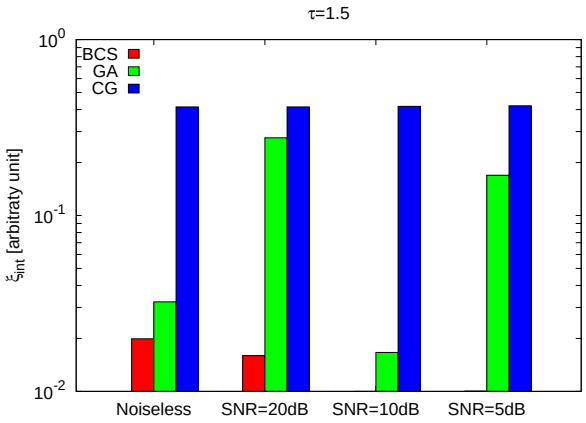

(b)

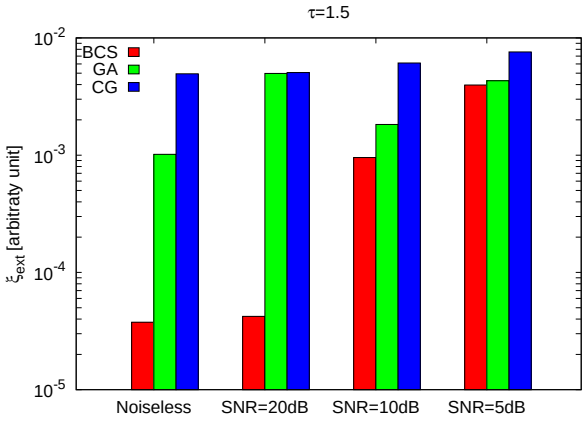

(c)

Figure 121. Behaviour of error figures for different SNR values: (a) total error ξ_{tot}, (b) internal error ξ_{int}, (c) external error ξ_{ext}.

RESULTS Comparison: $\varepsilon_r = 3.0$

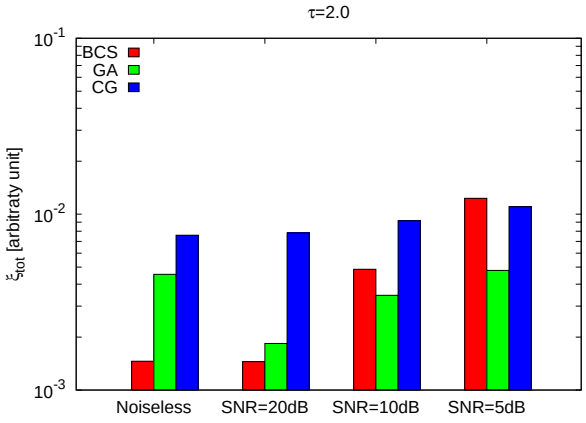

(a)

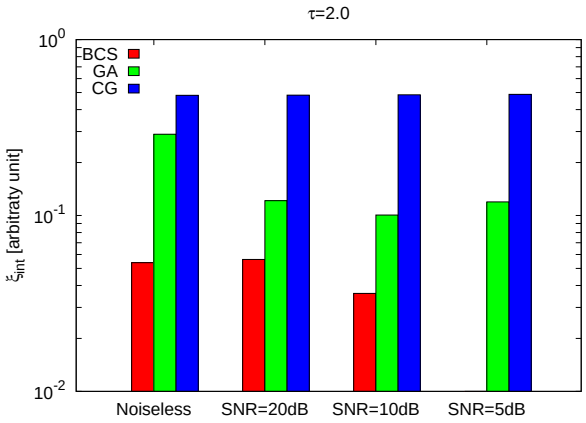

(b)

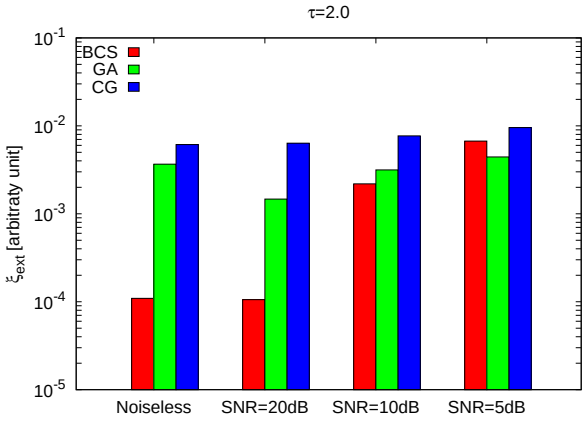

(c)

Figure 122. Behaviour of error figures for different SNR values: (a) total error ξ_{tot}, (b) internal error ξ_{int}, (c) external error ξ_{ext}.

RESULTS Comparison: *Noiseless*

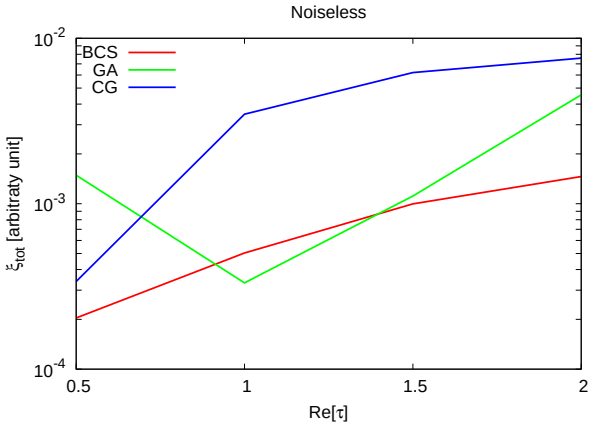

(a)

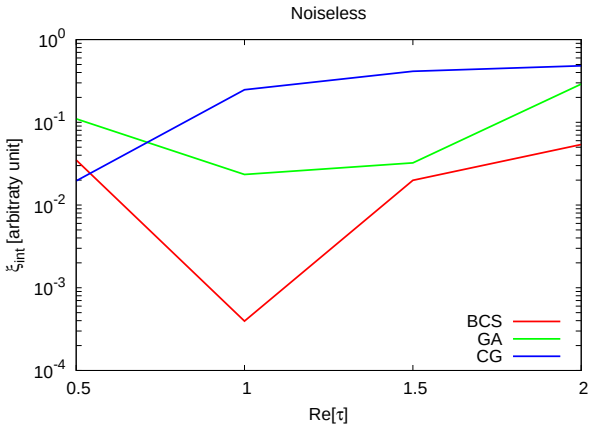

(b)

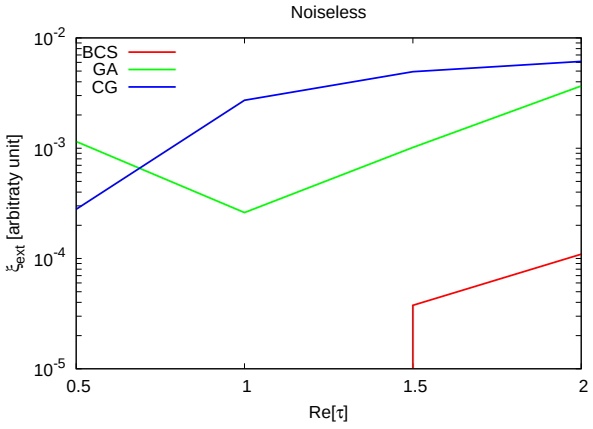

(c)

Figure 123. Behaviour of error figures as a function of ε_r: (a) total error ξ_{tot}, (b) internal error ξ_{int}, (c) external error ξ_{ext}.

RESULTS Comparison: $SNR = 20\,dB$

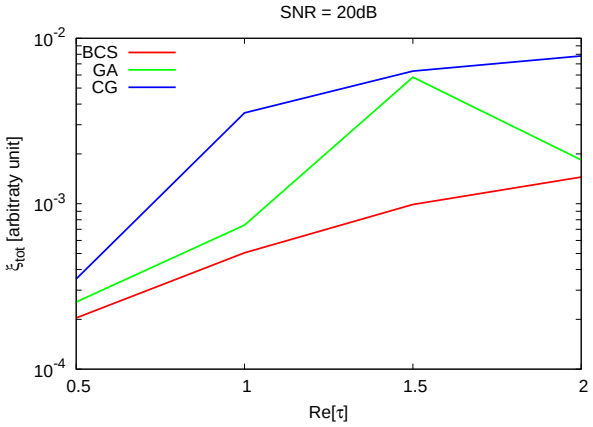

(a)

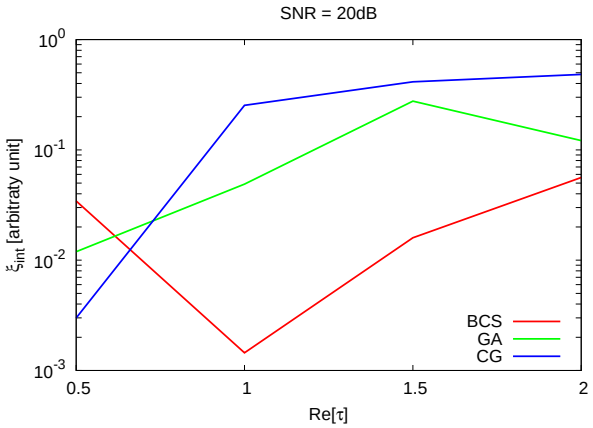

(b)

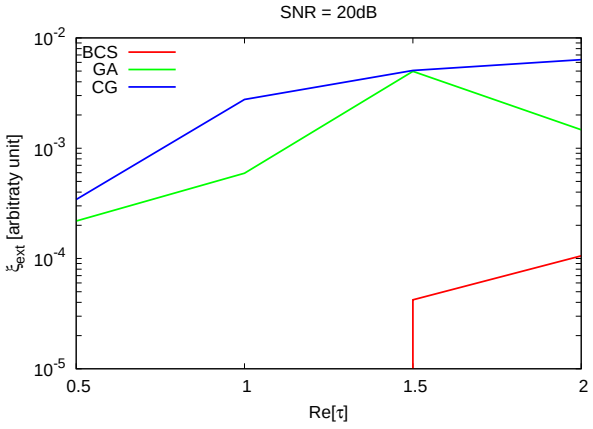

(c)

Figure 124. Behaviour of error figures as a function of ε_r: (a) total error ξ_{tot}, (b) internal error ξ_{int}, (c) external error ξ_{ext}.

RESULTS Comparison: $SNR = 10\,dB$

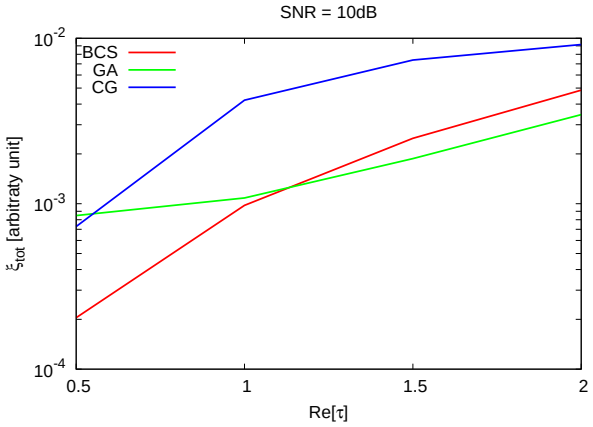

(a)

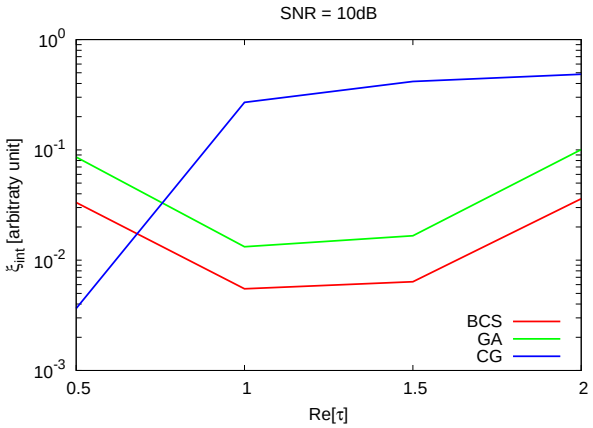

(b)

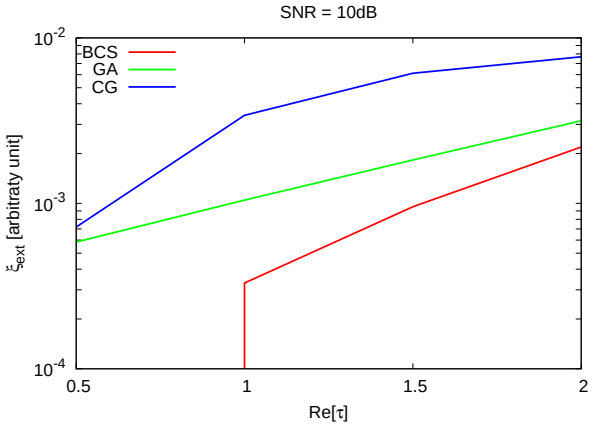

(c)

Figure 125. Behaviour of error figures as a function of ε_r: (a) total error ξ_{tot}, (b) internal error ξ_{int}, (c) external error ξ_{ext}.

RESULTS Comparison: $SNR = 5\,dB$

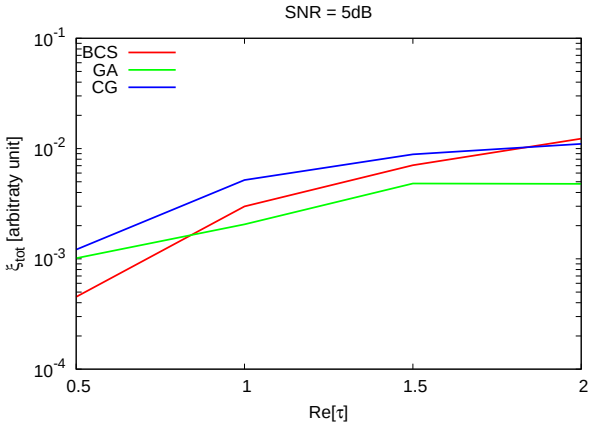

(a)

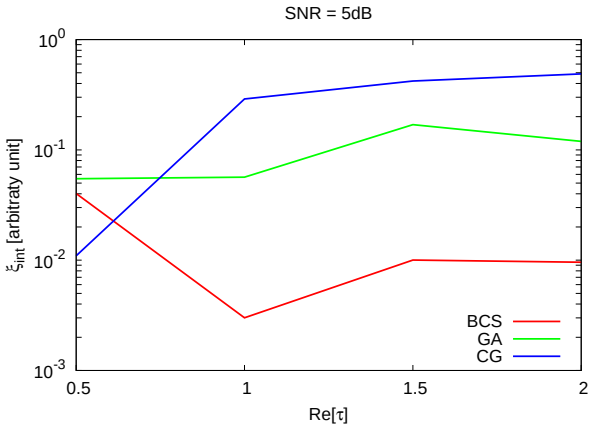

(b)

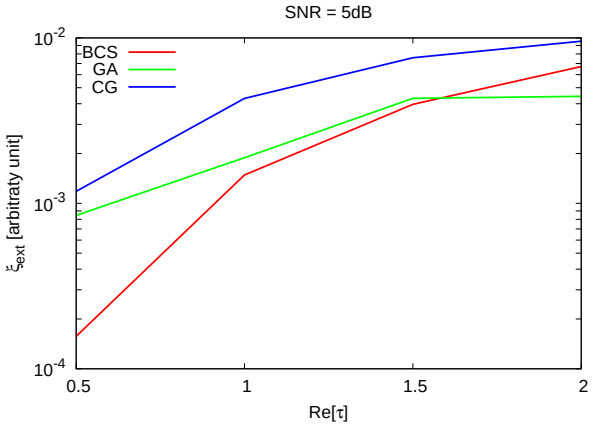

(c)

Figure 126. Behaviour of error figures as a function of ε_r: (a) total error ξ_{tot}, (b) internal error ξ_{int}, (c) external error ξ_{ext}.

8 TEST CASE: Low Number of Views - Square Cylinders

Goal: compare the performances of BCS, GA and CG

- Number of Views: V
- Number of Measurements: M
- Number of Cells for the Inversion: N
- Number of Cells for the Direct solver: D
- Side of the investigation domain: L

Test Case Description

Direct solver:

- Square domain divided in $\sqrt{D} \times \sqrt{D}$ cells
- Domain side: $L = 3\lambda$
- $D = 1296$ (discretization for the direct solver: $< \lambda/10$)

Investigation domain:

- Square domain divided in $\sqrt{N} \times \sqrt{N}$ cells
- $L = 3\lambda$
- $2ka = 2 \times \frac{2\pi}{\lambda} \times \frac{L\sqrt{2}}{2} = 6\pi\sqrt{2} = 26.65$
- $\#DOF = \frac{(2ka)^2}{2} = \frac{(2\times\frac{2\pi}{\lambda}\times\frac{L\sqrt{2}}{2})^2}{2} = 4\pi^2\left(\frac{L}{\lambda}\right)^2 = 4\pi^2 \times 9 \approx 355.3$
- N scelto in modo da essere vicino a $\#DOF$: $N = 324$ (18×18)

Measurement domain:

- Measurement points taken on a circle of radius $\rho = 3\lambda$
- Full-aspect measurements
- $M \approx 2ka \rightarrow M = 27$

Sources:

- Plane waves
- $V = 4$
- Amplitude $A = 1$
- Frequency: 300 MHz $(\lambda = 1)$

Object:

- Square cylinder of side $\frac{\lambda}{6} = 0.1667$
- $\varepsilon_r \in \{1.5, 2.0, 2.5, 3.0\}$
- $\sigma = 0$ [S/m]

BCS parameters:

- Initial estimate of the noise: $n_0 = 1.0 \times 10^{-3}$
- Convergenze parameter: $\tau = 1.0 \times 10^{-8}$

CG parameters:

- Iterations: 200
- Peso stato: 0
- Peso dati: 1

GA parameters:

- Iterations: 10000
- Tournament Selection: $TRUE$
- Prob. Crossover: 0.8
- Prob. Mutation: 0.4
- Prob. Bit Muation: 0.05
- Prob. New Generation: 0.01
- Elitism: $TRUE$
- Crossover Child: 1
- Population: 200
- Convergence Threshold: 0.001

RESULTS: $\varepsilon_r = 1.5$

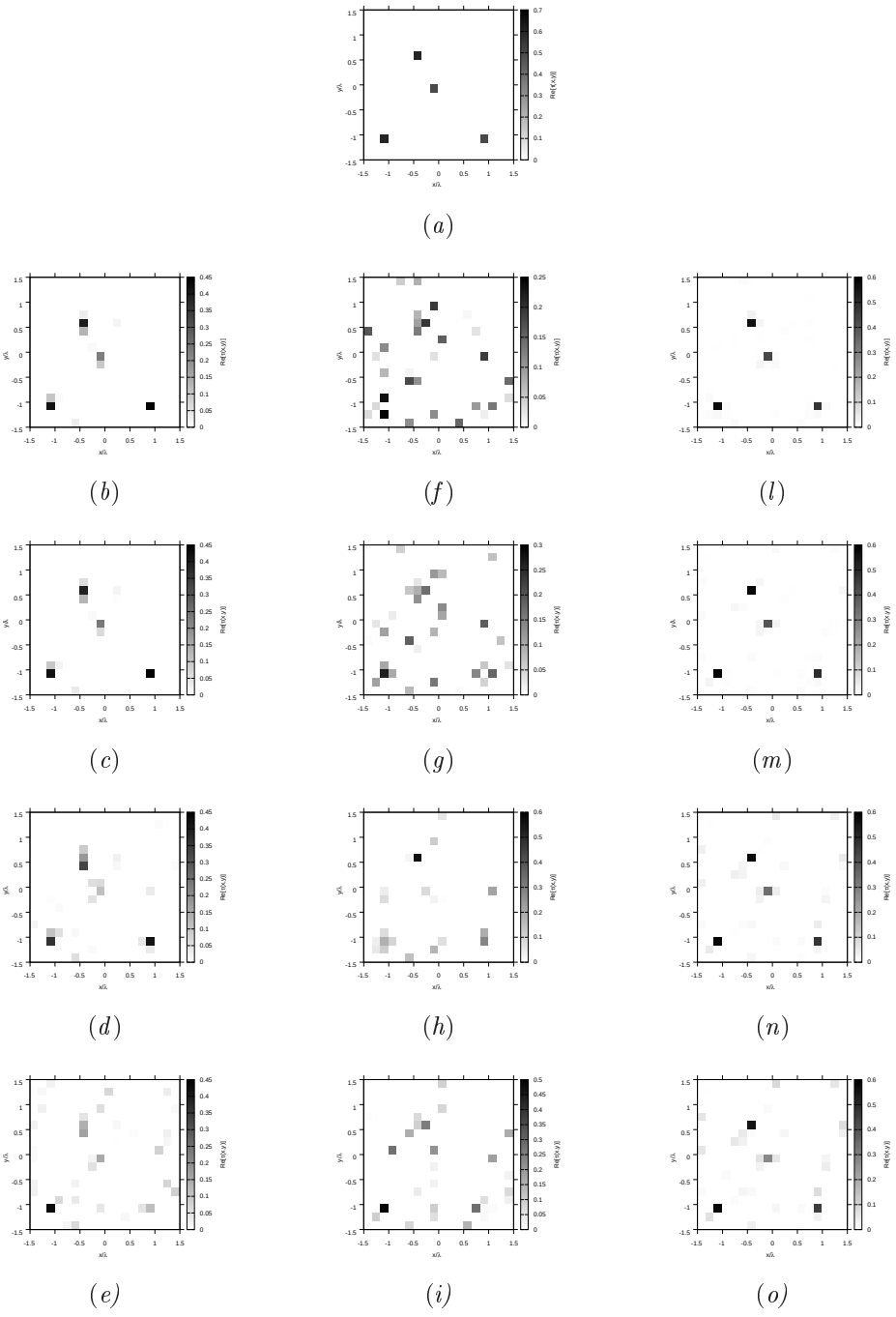

(a)

(b) (f) (l)

(c) (g) (m)

(d) (h) (n)

(e) (i) (o)

Figure 127. Actual object (a), (b)-(e) BCS reconstructed $(g)(i)$ GA-reconstructed, and (l)-(o) CG reconstructed object for $(b)(f)(l)$ Noiseless case, $(c)(g)(m)$ $SNR = 20$ [dB] , $(d)(h)(n)$ $SNR = 10$ [dB] , $(e)(i)(o)$ $SNR = 5$ [dB].

RESULTS: $\varepsilon_r = 2.0$

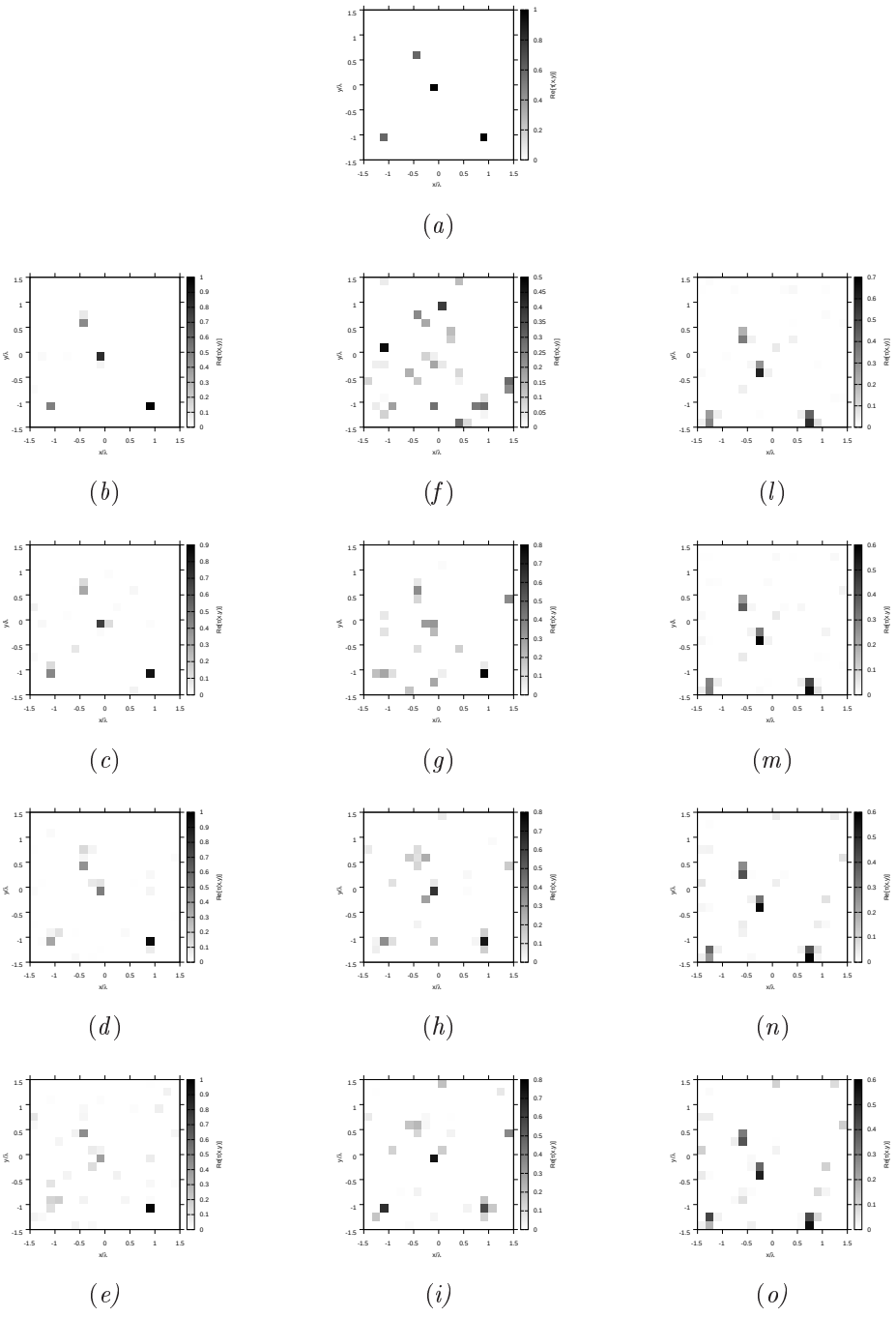

(a)

(b) (f) (l)

(c) (g) (m)

(d) (h) (n)

(e) (i) (o)

Figure 128. Actual object (a), (b)-(e) BCS reconstructed $(g)(i)$ GA-reconstructed, and (l)-(o) CG reconstructed object for $(b)(f)(l)$ Noiseless case, $(c)(g)(m)$ $SNR = 20$ [dB] , $(d)(h)(n)$ $SNR = 10$ [dB] , $(e)(i)(o)$ $SNR = 5$ [dB].

RESULTS: $\varepsilon_r = 2.5$

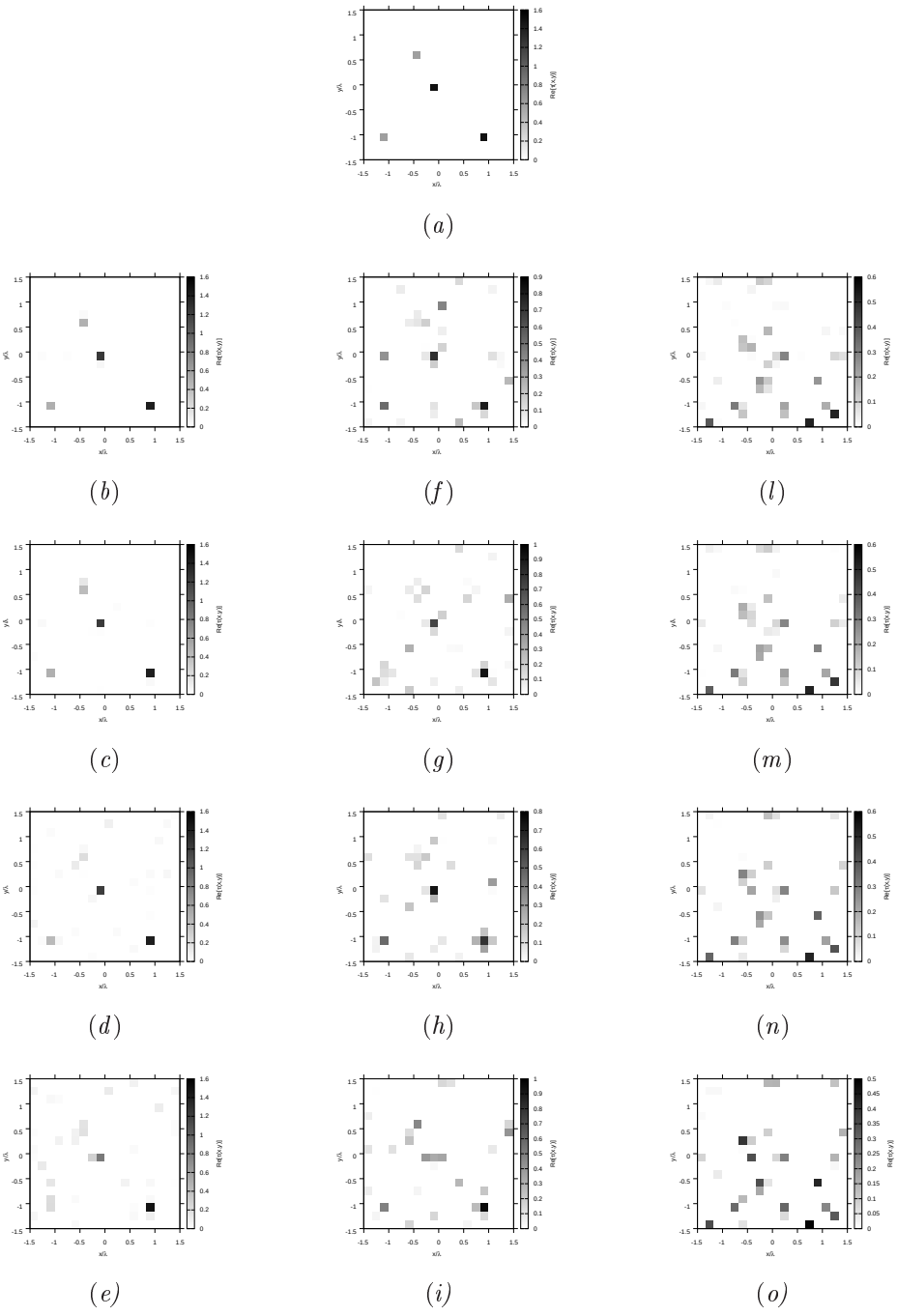

(a)

(b) (f) (l)

(c) (g) (m)

(d) (h) (n)

(e) (i) (o)

Figure 129. Actual object (a), (b)-(e) BCS reconstructed $(g)(i)$ GA-reconstructed, and (l)-(o) CG reconstructed object for $(b)(f)(l)$ Noiseless case, $(c)(g)(m)$ $SNR = 20$ [dB] , $(d)(h)(n)$ $SNR = 10$ [dB] , $(e)(i)(o)$ $SNR = 5$ [dB].

RESULTS: $\varepsilon_r = 3.0$

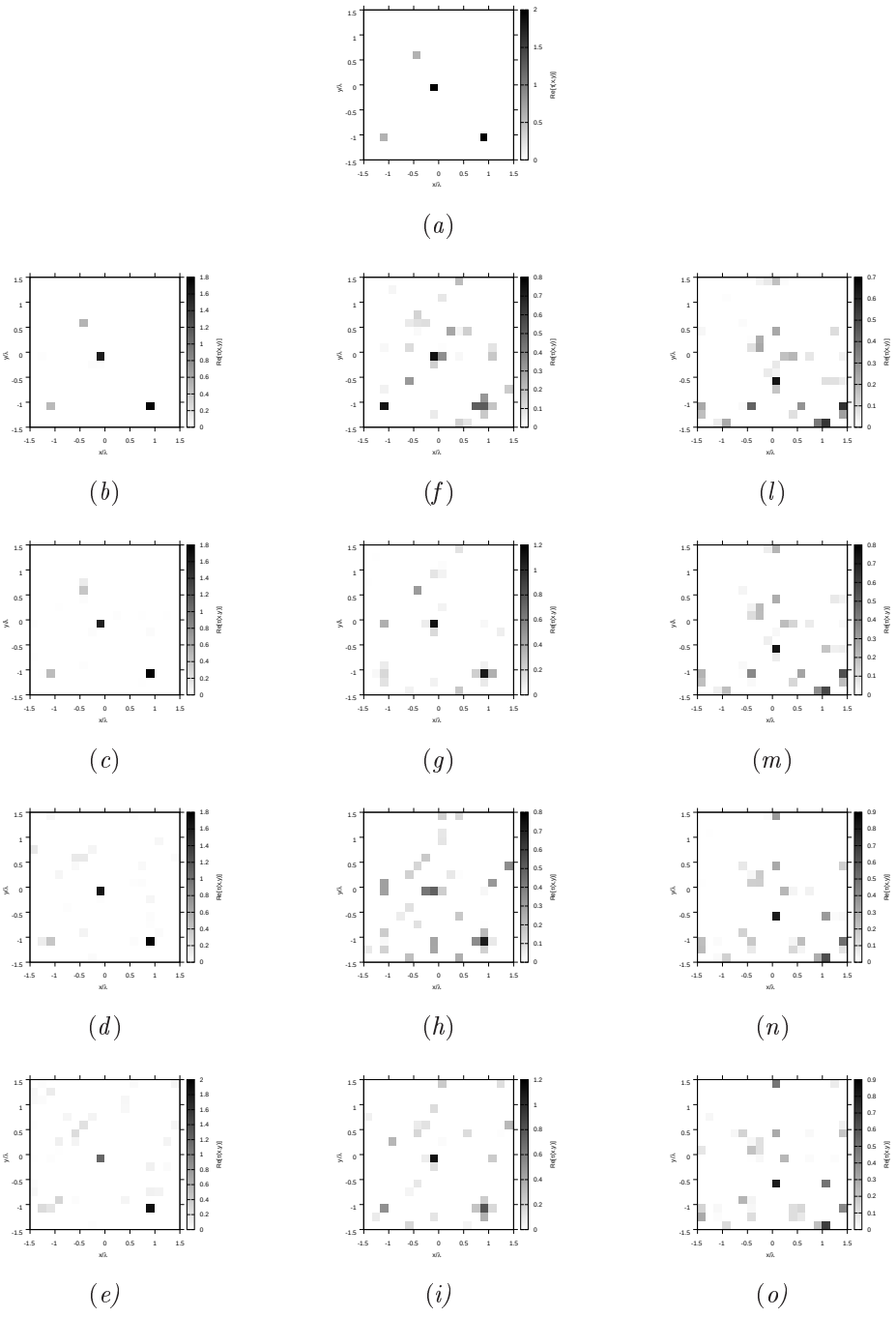

(a)

(b) (f) (l)

(c) (g) (m)

(d) (h) (n)

(e) (i) (o)

Figure 130. Actual object (a), (b)-(e) BCS reconstructed $(g)(i)$ GA-reconstructed, and (l)-(o) CG reconstructed object for $(b)(f)(l)$ Noiseless case, $(c)(g)(m)$ $SNR = 20$ [dB] , $(d)(h)(n)$ $SNR = 10$ [dB] , $(e)(i)(o)$ $SNR = 5$ [dB].

RESULTS Comparison: $\varepsilon_r = 1.5$

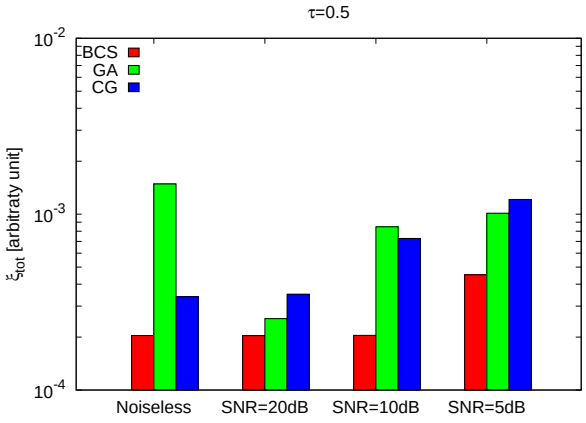

(a)

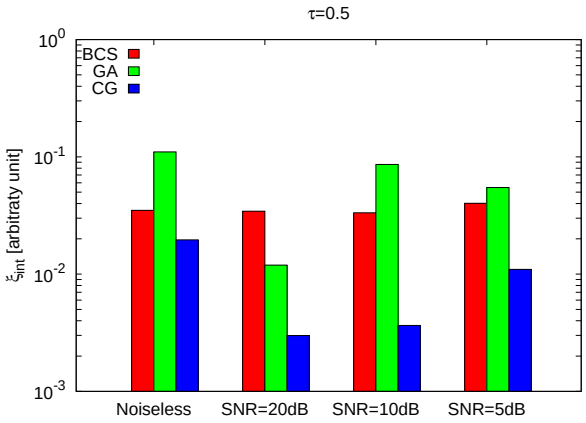

(b)

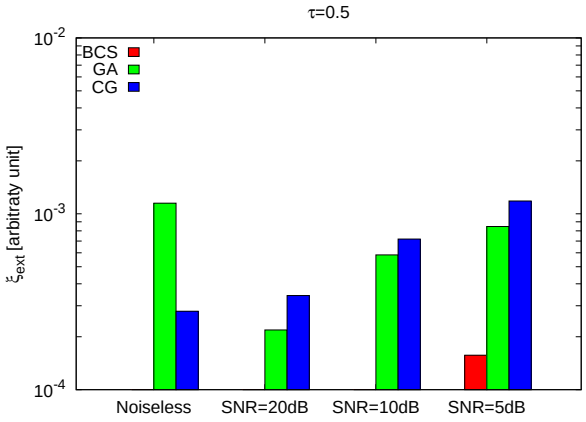

(c)

Figure 131. Behaviour of error figures for different SNR values: (a) total error ξ_{tot}, (b) internal error ξ_{int}, (c) external error ξ_{ext}.

RESULTS Comparison: $\varepsilon_r = 2.0$

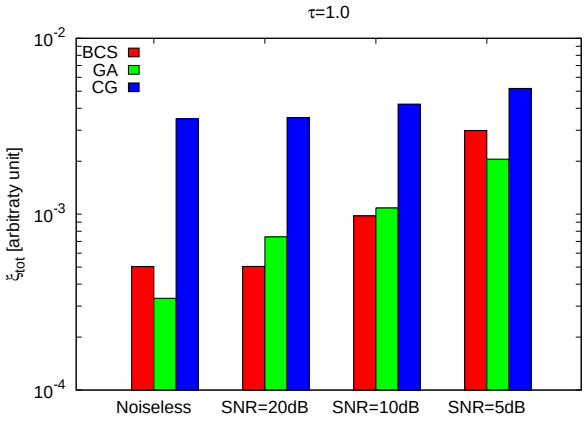

(a)

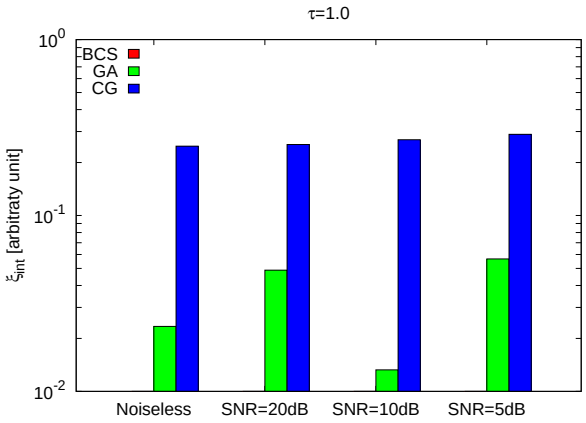

(b)

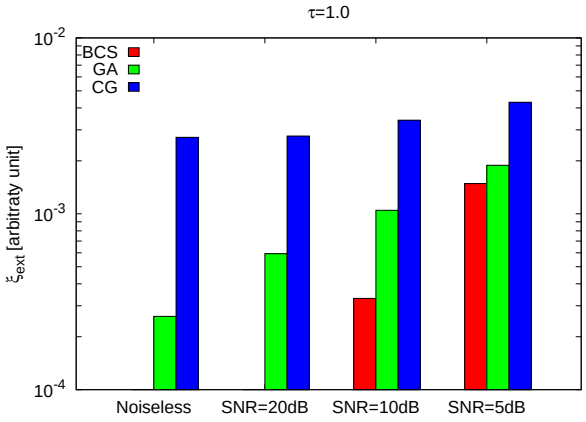

(c)

Figure 132. Behaviour of error figures for different SNR values: (a) total error ξ_{tot}, (b) internal error ξ_{int}, (c) external error ξ_{ext}.

RESULTS Comparison: $\varepsilon_r = 2.5$

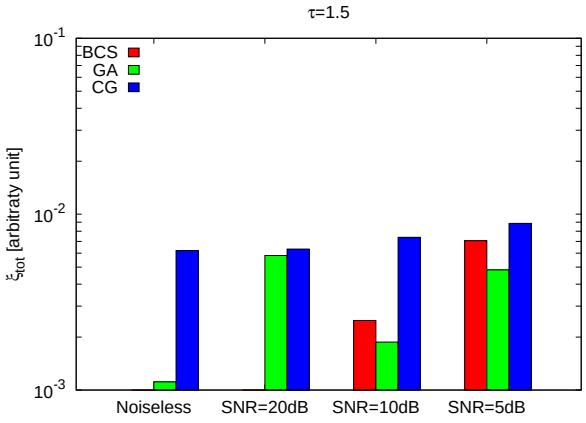

(a)

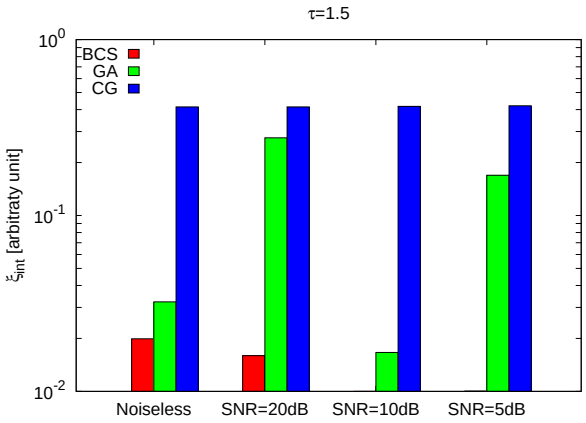

(b)

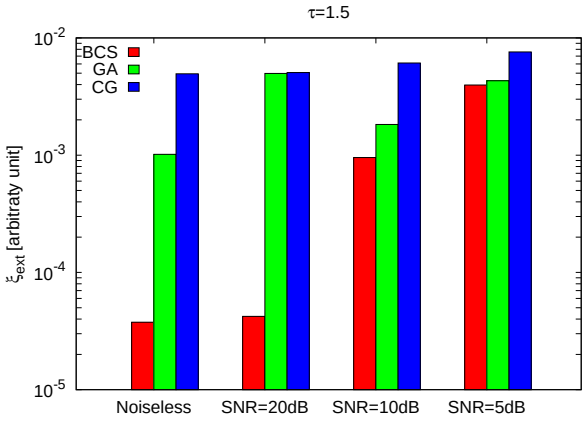

(c)

Figure 133. Behaviour of error figures for different SNR values: (a) total error ξ_{tot}, (b) internal error ξ_{int}, (c) external error ξ_{ext}.

RESULTS Comparison: $\varepsilon_r = 3.0$

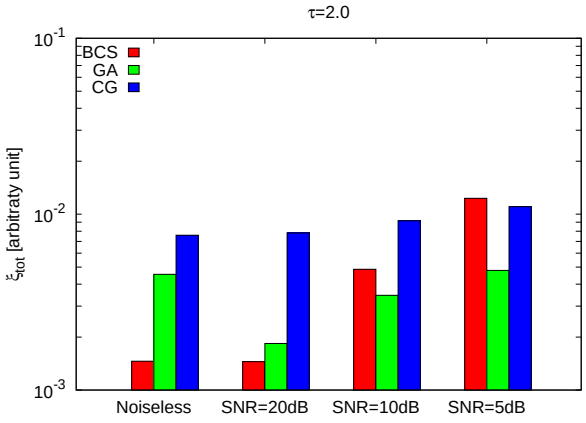

(a)

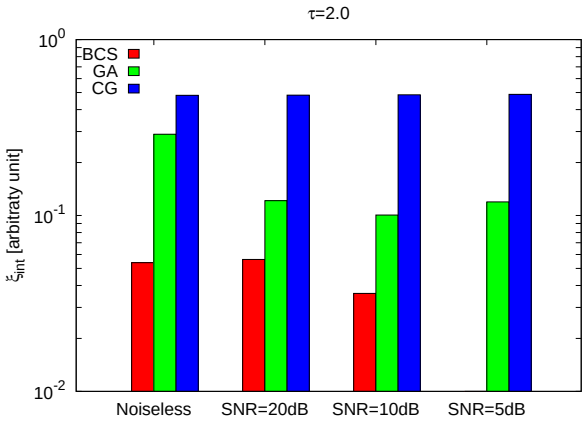

(b)

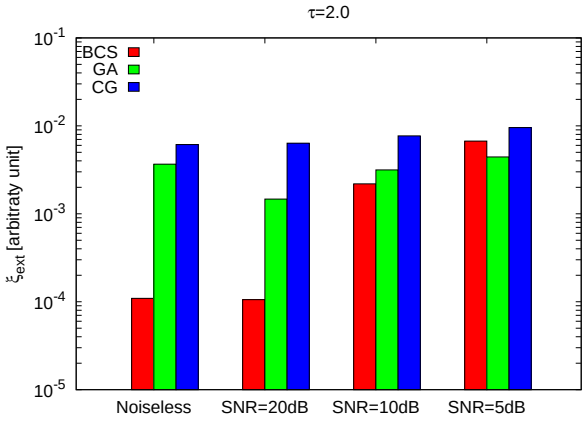

(c)

Figure 134. Behaviour of error figures for different SNR values: (a) total error ξ_{tot}, (b) internal error ξ_{int}, (c) external error ξ_{ext}.

RESULTS Comparison: *Noiseless*

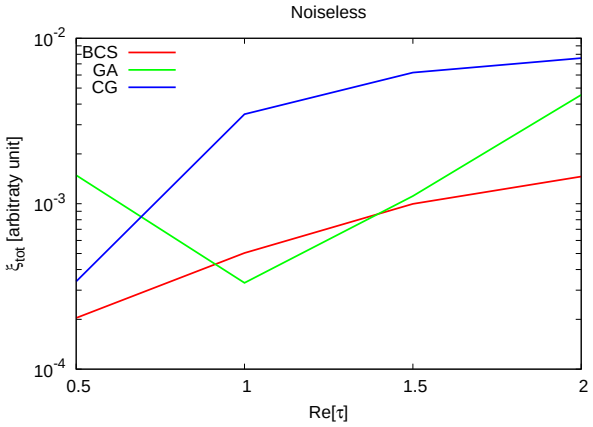

(a)

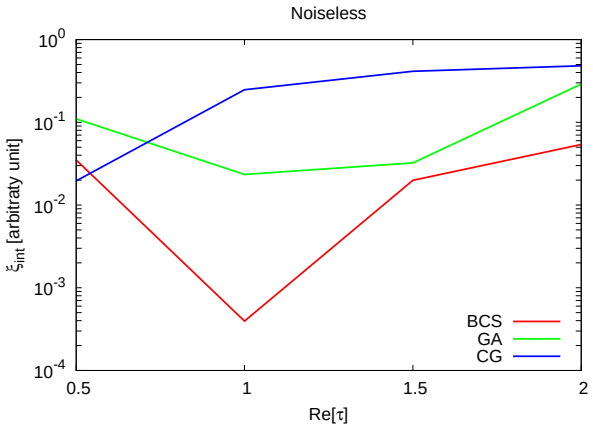

(b)

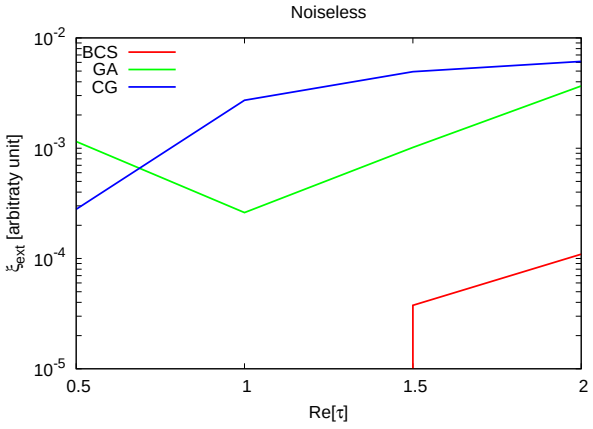

(c)

Figure 135. Behaviour of error figures as a function of ε_r: (a) total error ξ_{tot}, (b) internal error ξ_{int}, (c) external error ξ_{ext}.

RESULTS Comparison: $SNR = 20\,dB$

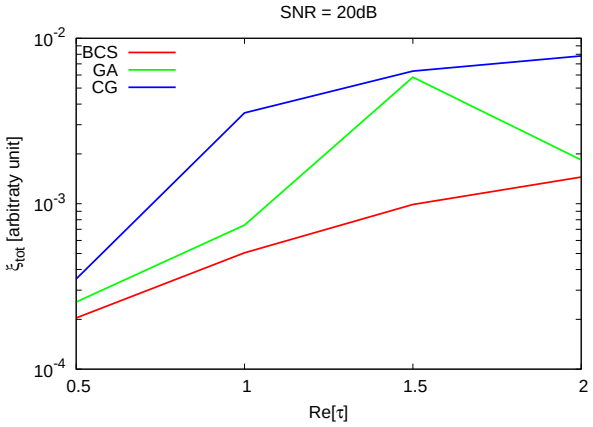

(a)

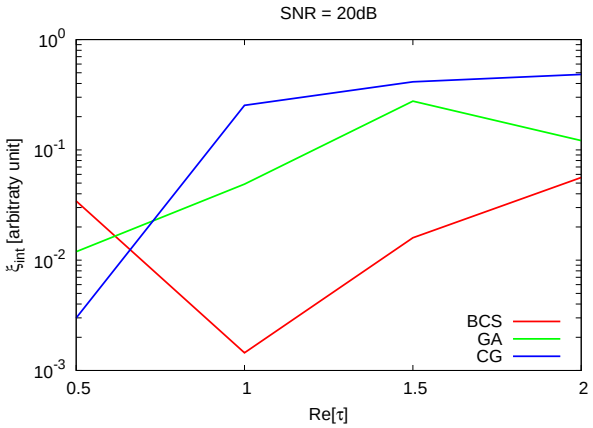

(b)

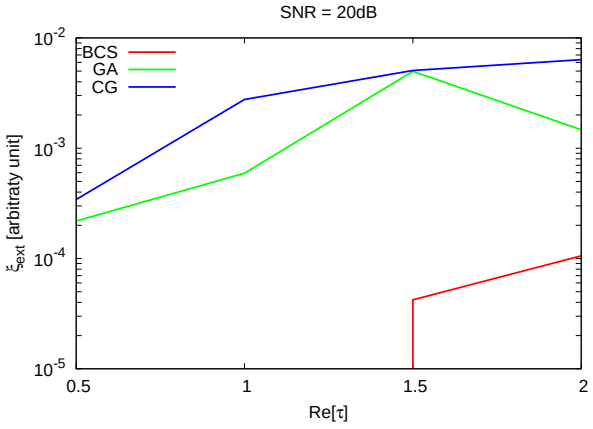

(c)

Figure 136. Behaviour of error figures as a function of ε_r: (a) total error ξ_{tot}, (b) internal error ξ_{int}, (c) external error ξ_{ext}.

RESULTS Comparison: $SNR = 10\,dB$

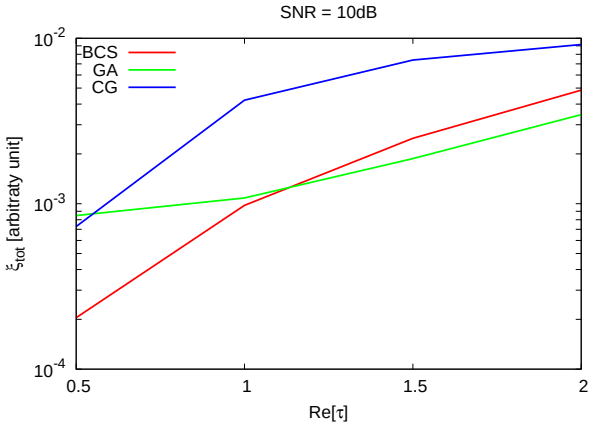

(a)

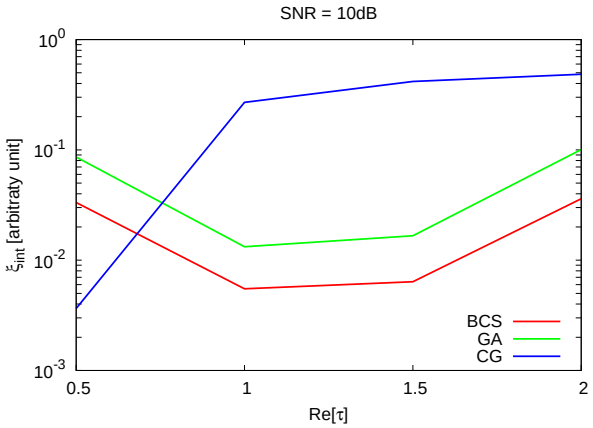

(b)

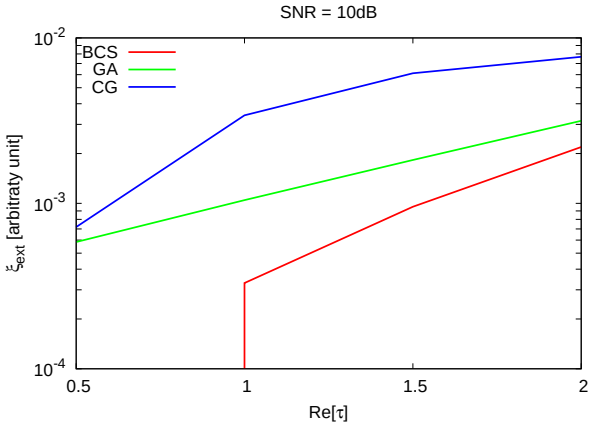

(c)

Figure 137. Behaviour of error figures as a function of ε_r: (a) total error ξ_{tot}, (b) internal error ξ_{int}, (c) external error ξ_{ext}.

RESULTS Comparison: $SNR = 5\,dB$

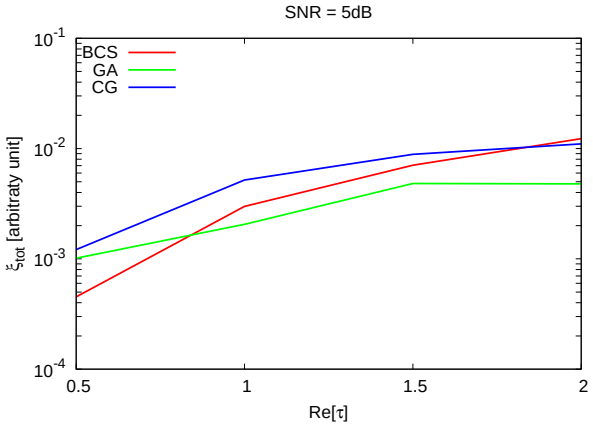

(a)

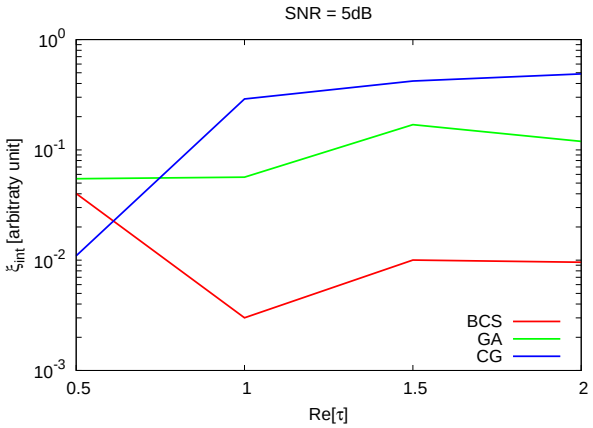

(b)

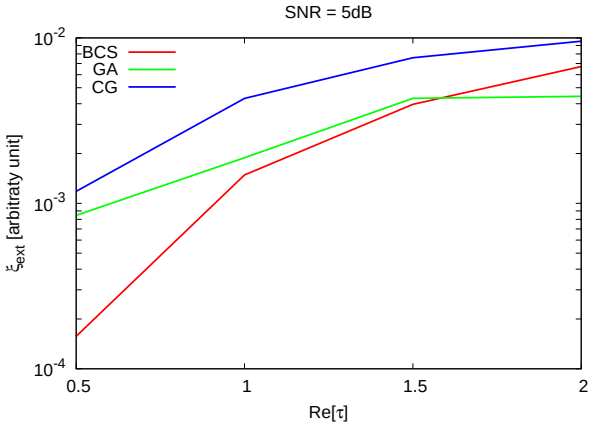

(c)

Figure 138. Behaviour of error figures as a function of ε_r: (a) total error ξ_{tot}, (b) internal error ξ_{int}, (c) external error ξ_{ext}.

References

[1] E. J. Candes and M. B. Wakin, "An introduction to compressive sampling", *IEEE Signal Processing Magazine*, vol. 25, no. 2, pp. 21-30, March 2008.

[2] S. Ji, Y. Xue, and L. Carin, "Bayesian compressive sampling", *IEEE Trans. on Signal Processing*, vol. 56, no. 6, pp. 2346-2356, June 2008.

[3] R. F. Harrington, *Field computation by moment methods*, New York: IEEE Press, 1993.

[4] J. H. Richmond, "Scattering by a dielectric cylinder of arbitrary cross shape", *IEEE Trans. Antennas Propagat.*, vol. AP-13, no. 3, pp. 334-341, May 1965.

[5] M. Slaney, A. C. Kak, and L. E. Larsen, "Limitations of imaging with first-order diffraction tomography", *IEEE Trans. on Microwave Theory and Techniques*, vol. MTT-32, no. 8, pp. 860-874, Aug. 1984.

[6] L. Poli, G. Oliveri, and A. Massa, "Imaging sparse metallic cylinders through a Local Shape Function Bayesian Compressive Sensing approach," Journal of Optical Society of America A, vol. 30, no. 6, pp. 1261-1272, 2013.

[7] F. Viani, L. Poli, G. Oliveri, F. Robol, and A. Massa, "Sparse scatterers imaging through approximated multitask compressive sensing strategies," Microwave Opt. Technol. Lett., vol. 55, no. 7, pp. 1553-1558, Jul. 2013.

[8] L. Poli, G. Oliveri, P. Rocca, and A. Massa, "Bayesian compressive sensing approaches for the reconstruction of two-dimensional sparse scatterers under TE illumination," IEEE Trans. Geosci. Remote Sensing, vol. 51, no. 5, pp. 2920-2936, May. 2013.

[9] L. Poli, G. Oliveri, and A. Massa, "Microwave imaging within the first-order Born approximation by means of the contrast-field Bayesian compressive sensing," IEEE Trans. Antennas Propag., vol. 60, no. 6, pp. 2865-2879, Jun. 2012.

[10] G. Oliveri, P. Rocca, and A. Massa, "A bayesian compressive sampling-based inversion for imaging sparse scatterers," IEEE Trans. Geosci. Remote Sensing, vol. 49, no. 10, pp. 3993-4006, Oct. 2011.

[11] G. Oliveri, L. Poli, P. Rocca, and A. Massa, "Bayesian compressive optical imaging within the Rytov approximation," Optics Letters, vol. 37, no. 10, pp. 1760-1762, 2012.

[12] L. Poli, G. Oliveri, F. Viani, and A. Massa, "MT-BCS-based microwave imaging approach through minimum-norm current expansion," IEEE Trans. Antennas Propag., in press. doi:10.1109/TAP.2013.2265254

[13] S. C. Hagness, E. C. Fear, and A. Massa, "Guest Editorial: Special Cluster on Microwave Medical Imaging", IEEE Antennas Wireless Propag. Lett., vol. 11, pp. 1592-1597, 2012.

[14] G. Oliveri, Y. Zhong, X. Chen, and A. Massa, "Multi-resolution subspace-based optimization method for inverse scattering," Journal of Optical Society of America A, vol. 28, no. 10, pp. 2057-2069, Oct. 2011.

[15] A. Randazzo, G. Oliveri, A. Massa, and M. Pastorino, "Electromagnetic inversion with the multiscaling inexact-Newton method - Experimental validation," Microwave Opt. Technol. Lett., vol. 53, no. 12, pp. 2834-2838, Dec. 2011.

[16] G. Oliveri, L. Lizzi, M. Pastorino, and A. Massa, "A nested multi-scaling inexact-Newton iterative approach for microwave imaging," IEEE Trans. Antennas Propag., vol. 60, no. 2, pp. 971-983, Feb. 2012.

[17] G. Oliveri, A. Randazzo, M. Pastorino, and A. Massa, "Electromagnetic imaging within the contrast-source formulation by means of the multiscaling inexact Newton method," Journal of Optical Society of America A, vol. 29, no. 6, pp. 945-958, 2012.

[18] M. Benedetti, D. Lesselier, M. Lambert, and A. Massa, "Multiple shapes reconstruction by means of multi-region level sets," IEEE Trans. Geosci. Remote Sensing, vol. 48, no. 5, pp. 2330-2342, May 2010.

[19] M. Benedetti, D. Lesselier, M. Lambert, and A. Massa, "A multi-resolution technique based on shape optimization for the reconstruction of homogeneous dielectric objects," Inverse Problems, vol. 25, no. 1, pp. 1-26, Jan. 2009.

[20] M. Donelli, D. Franceschini, P. Rocca, and A. Massa, "Three-dimensional microwave imaging problems solved through an efficient multi-scaling particle swarm optimization," IEEE Trans. Geosci. Remote Sensing, vol. 47, no. 5, pp. 1467-1481, May 2009.

[21] M. Benedetti, G. Franceschini, R. Azaro, and A. Massa, "A numerical assessment of the reconstruction effectiveness of the integrated GA-based multicrack strategy," IEEE Antennas Wireless Propag. Lett., vol. 6, pp. 271-274, 2007.

[22] P. Rocca, M. Carlin, G. Oliveri, and A. Massa, "Interval analysis as applied to inverse scattering," IEEE International Symposium on Antennas Propag. (APS/URSI 2013), Chicago, Illinois, USA, Jul. 8-14, 2012.

[23] L. Manica, P. Rocca, M. Salucci, M. Carlin, and A. Massa, "Scattering data inversion through interval analysis under Rytov approximation," 7th European Conference on Antennas Propag. (EuCAP 2013), Gothenburg, Sweden, Apr. 8-12, 2013.

[24] P. Rocca, M. Carlin, and A. Massa, "Imaging weak scatterers by means of an innovative inverse scattering technique based on the interval analysis," 6th European Conference on Antennas Propag. (EuCAP 2012), Prague, Czech Republic, Mar. 26-30, 2012.

[25] G. Oliveri and A. Massa, "Bayesian compressive sampling for pattern synthesis with maximally sparse non-uniform linear arrays," IEEE Trans. Antennas Propag., vol. 59, no. 2, pp. 467-481, Feb. 2011.

[26] G. Oliveri, M. Carlin, and A. Massa, "Complex-weight sparse linear array synthesis by Bayesian Compressive Sampling," IEEE Trans. Antennas Propag., vol. 60, no. 5, pp. 2309-2326, May 2012.

[27] G. Oliveri, P. Rocca, and A. Massa, "Reliable Diagnosis of Large Linear Arrays - A Bayesian Compressive Sensing Approach," IEEE Trans. Antennas Propag., vol. 60, no. 10, pp. 4627-4636, Oct. 2012.

[28] F. Viani, G. Oliveri, and A. Massa, "Compressive sensing pattern matching techniques for synthesizing planar sparse arrays" IEEE Trans. Antennas Propag., in press. doi:10.1109/TAP.2013.2267195

[29] M. Carlin, P. Rocca, G. Oliveri, F. Viani, and A. Massa, "Directions-of-Arrival Estimation through Bayesian Compressive Sensing strategies," IEEE Trans. Antennas Propag., in press.

[30] M. Carlin, P. Rocca, "A Bayesian compressive sensing strategy for direction-of-arrival estimation," 6th European Conference on Antennas Propag. (EuCAP 2012), Prague, Czech Republic, pp. 1508-1509, 26-30 Mar. 2012.

[31] M. Carlin, P. Rocca, G. Oliveri, and A. Massa, "Bayesian compressive sensing as applied to directions-of-arrival estimation in planar arrays", Journal of Electrical and Computer Engineering, Special Issue on "Advances in Radar Technologies", in press.